HEXACOORDINATE SILICON COMPLEXES AS CATHODIC COLORANTS

by

Derek Micheal Peloquin

A dissertation submitted to the faculty of
the University of North Carolina at Charlotte
in partial fulfillment of the requirements
for the degree of Doctor of Philosophy in
Nanoscale Science

Charlotte

2016

Approved by:

Dr. Thomas A. Schmedake

Dr. Bernadette T. Donovan–Merkert

Dr. Daniel Rabinovich

Dr. Michael G. Walter

Dr. Brigid Mullany

ABSTRACT

DEREK MICHEAL PELOQUIN. Hexacoordinate silicon complexes as cathodic colorants. (Under the direction of DR. THOMAS ANDREW SCHMEDAKE.)

Electrochemical and spectroelectrochemical characterization of hexacoordinate polypyridine silicon complexes show that they are fitting candidates for electrochromic applications. Tris(bipyridine)silicon(IV), $[Si(bpy)_3]^{+4}$, is colorless in acetonitrile as the hexafluorophosphate salt, with two overlapping peaks at 327 and 341 nm. Successive reduction by up to three electrons turns the solution green, as the intensity of the 327/341 nm peaks decrease and two new peaks emerge, one around 390 nm and a very broad transition centered around 800 nm. Each reduction is fully reversible and entirely based on the bipyridine ligands, and full conversion to each charged state is realized at the proper potential. Tris(4,4'–di–*tert*–butyl–2,2'–bipyridine)silicon(IV), $[Si(4dtbbpy)_3]^{+4}$, and tris(5,5'–dimethyl–2,2'–bipyridine)silicon(IV), $[Si(5dmbpy)_3]^{+4}$, are similar with initial overlapping peaks at 321/334 nm and 340/356 nm, respectively for the two complexes. These peaks disappear on reduction and a sharp peak at 391 nm and a broad peak at 807 nm both emerge for $[Si(4dtbbpy)_3]^{n}$, whereas these peaks are at 413 and 830 nm for $[Si(5dmbpy)_3]^{n}$. The complexes are both colorless in solution as the +4 species then green upon reduction. Bis(4'–tolylterpyridine)silicon(IV), $[Si(ttpy)_2]^{+4}$, is slightly yellow in acetonitrile as the hexafluorophosphate salt, with a sharp peak at 302 nm and two overlapping peaks at 378 and 407 nm. Reduction by two electrons turns the solution blue with emergence of a broad peak centered around 653 nm, and reduction by a further two electrons turn the solution reddish–purple with a peak at 514 nm that tails out into the infrared.

DEDICATION

This dissertation is firstmost dedicated to God, the Virgin Mary, and all the saints, especially St. Joan of Arc, my patron, and St. Thomas Aquinas, patron of students and universities. Secondly, it is dedicated to the lovely Meghan Elizabeth Teresa Peloquin, without whom finishing my research would have been much more of a struggle.

ACKNOWLEDGMENTS

The author gratefully extends his appreciation to Dr. Thomas Schmedake for the many years of guidance and mentoring and recruiting him to the University. Also to his parents, Catherine and Donald, as well as the rest of his family and friends, for their loving support. He must also express his appreciation to all of the UNC Charlotte undergraduates that helped perform this work: Domelia Dewitt, Phuong Tran, Thuydung Le, John Pope, Tavis Lamb, Paula Hang, Peichu Wei, Cody Auclair, Jake Lee, Ziahaw Thor, and Kendra Majka. Contributions to this work were also provided by Shreya Patel of North Carolina School of Science and Mathematics, Joycelyn Swain, Sha'Mere Herder, and Dr. Godfrey Mbah of Johnson C. Smith University, and Elliott Locke of North Carolina State University. Dr. Michael Murphy is thanked for use of his lab space and spectrometer while Dr. Jon Merkert and Edi Yapi are responsible for the electrochemistry in collaboration with Dr. Bernadette Donovan–Merkert. Dr. Merkert is also thanked with Dr. Cliff Carlin for handling instrumentation issues, Paul Bainbridge and Dewey Williams for handling of waste and chemicals, and Caroline Kennedy, Robin Burns, Lisa Carlin, Nancy Queen, and Nikki Redman for front office support. Extreme gratitude is extended to the members of his committee, Dr. Bernadette Donovan–Merkert, Dr. Michael Walter, and Dr. Brigid Mullany, and especially to Dr. Daniel Rabinovich for his additional mentoring and support. For funding support, the author and T.A.S. acknowledge the Graduate Assistant Support Plan, the UNC Charlotte Faculty Research Grant Program, and the NSF REU Site program in partnership with the ASSURE program of the DoD under NSF Grant No. CHE1460867. This NSF grant supported Domelia over the summer of 2015 and Elliott over the summer of 2012.

TABLE OF CONTENTS

LIST OF TABLES

LIST OF FIGURES

LIST OF SCHEMES

LIST OF ABBREVIATIONS

acac	acetylacetonato
apip	4–{[2–(methylamino)phenyl]imino}–2–pentanone
a.u.	arbitrary units
B3LYP	Becke 3–parameter, Lee, Yang, and Parr basis set
baquin	*N*–8–quinolinylbenzamide
binolato	1,1’–binaphthalene–2,2’–diolato
BMI	1–butyl–3–methylimidazolium
BP86	Becke 88, Perdew 86 basis set
bp	1,1’–biphenyl–2,2’–diolato
bpy	2,2’–bipyridine
bq	1,2–benzoquinone–4,5–diolato
Brbpy	5–bromo–2,2’–bipyridine
Br_2bpy	5,5’–dibromo–2,2’–bipyridine
Brcat	4,5–dibromocathecholato
Brpy	3–bromopyridine
Br_2py	2,5–dibromopyridine
Bu	butyl
Bz	benzyl
cat	catecholato
CCDC	Cambridge Crystallographic Data Centre
CD	circular dichroism
CE	counter electrode

Cltpy	4’–chloro–2,2’:6’,2”–terpyridine
COD	1,5–cyclooctadiene
COSMO	conductor–like screening model
Cp*	pentamethylcyclopentadienyl
CP/MAS	cross polarization magic–angle spinning
CSD	Cambridge Structural Database
CV	cyclic voltammetry
dcm	dichloromethyl
dcms	dichloro(methyl)silyl
DFT	density functional theory
bpydhb	2,2’–bipyridine dihydrobromide
diba	*N*,*N*’–diisopropylbenzamidine
Dipic	pyridine–2,6–dicarboxylate
DMAP	4–(*N*,*N*–dimethylamino)pyridine
DMSO	dimethylsulfoxide
DNA	deoxyribonucleic acid
4dpbpy	4,4’–diphenyl–2,2’–bipyridine
5dpbpy	5,5’–diphenyl–2,2’–bipyridine
dpcatH	1–H–1,10–phenanthroline–5,6–diolato
dped	*N*,*N*’–diphenylethylenediamine
dppz	dipyrido[3,2–a:2’,3’–c]phenazine
DSC	differential scanning calorimetry
5dvbpy	5,5’–divinyl–2,2’–bipyridine

EA	elemental analysis
EC	electrochromic
ed	1,2–ethylenediolato
EDTA	ethylenediaminetetraacetic acid
EL	electroluminescent
EPA	Environmental Protection Agency
epy	4–ethylpyridine
e.r.	enantiomeric resolution
Et	ethyl
Fc	ferrocene
GC–MS	gas chromatography coupled with mass spectrometry
GPT	glass pressure tube
H_d	heat of decomposition
HOMO	highest occupied molecular orbital
HV	heptyl viologen
Icat	4–iodocatecholato
imp	2–(iminomethyl)–phenolato
^{i}Pr	isopropyl
LUMO	lowest unoccupied molecular orbital
lut	lutidine
4dmbpy	4,4’–dimethyl–2,2’–bipyridine
4dmobpy	4,4’–dimethoxy–2,2’–bipyridine
5dmbpy	5,5’–dimethyl–2,2’–bipyridine

mcat	4–methylcatecholato
Me	methyl
MLCT	metal–to–ligand charge transfer
mquin	2–methyl–8–oxyquinolato
MV	methyl viologen
NA	not available
ncat	4,5–dinitrocatecholato
NMR	nuclear magnetic resonance
OLED	organic light–emitting diode
OPS	octa(phenyl)silsesquioxane
OTf	trifluoromethanesulfonato
pc	phthalocyanine
PC	propylene carbonate
PEDOT	poly(3,4–ethylene dioxythiophene)
Pent	pentyl
Ph	phenyl
$PhBP^{Ph}_3$	phenyltris(diphenylphosphinomethyl)borate
phen	1,10–phenanthroline
phn	9,10–phenanthrenediolato
phpy	4–phenylpyridine
pic	picoline
pip	4–[(2–phenolato)imino]–2–pentanone
PL	photoluminescent

PPy	polypyrrole
Pr	propyl
PSF	pear–shaped flask
P(VDF–*co*–HFP)	poly(vinylidene fluoride–*co*–hexafluoropropylene)
PXV	poly(hexyl viologen)
py	pyridine
pyre	pyrene–4,5–diolato
pybox	2,6–bis(2–oxazolinyl)pyridine
pyS	pyridine–2–thiolato
Q_E	heat of explosion
qin	1–[(8–quinolinylimino)methyl]–2–naphthalenolato
qip	2–[(8–quinolinylimino)methyl]–phenolato
quin	8–oxyquinolato
quinS	8–thioquinolato
RBF	round bottom flask
RDX	hexahydro–1,3,5–trinitro–1,3,5–triazine
RE	reference electrode
R.T.	room temperature
SEM	scanning electron microscopy
SOMO	singly occupied molecular orbital
SPS	poly(styrene sulfonate)
%T	percent transmittance
TBA	tetra–*N*–butylammonium

4dtbbpy	4,4'–di–*tert*–butyl–2,2'–bipyridine
4tbpy	4–*tert*–butylpyridine
tcm	trichloromethyl
tcs	trichlorosilyl
tcsm	(trichlorosilyl)dichloromethyl
tfbm	α,α–bis(trifluoromethyl)benzenemethanolato
TFSI	bis(trifluoromethylsulfonyl)imide
THF	tetrahydrofuran
T_m	melting temperature
TMEDA	*N*,*N*,*N'*,*N'*–tetramethylethylenediamine
tol	toluene/tolyl
tpip	4–[(2–thiophenolato)imino]–2–pentanone
tpy	2,2':6',2"–terpyridine
ttpy	4'–*p*–tolyl–2,2':6',2"–terpyridine
TPP	tetraphenylporphyrin
Ts	substrate temperature
TZ2P	triple zeta double polarization
VACP/MAS	variable amplitude cross polarization magic–angle spinning
VBV	vinyl benzyl viologen
vpy	4–vinylpyridine
WE	working electrode
ZORA	zeroth order regular approximation

CHAPTER 1: HEXACOORDINATE SILICON COMPLEXES WITH PYRIDINE–CONTAINING LIGANDS[1]

1.1. Introduction

The chemistry of hexacoordinate silicon complexes containing one or more pyridine–like ligands is covered in this chapter. Pyridine–containing ligands are excellent ligands for stabilizing hexacoordinate silicon complexes, and over 100 hexacoordinate silicon complexes containing at least one pyridine–like ligand have been deposited with the Cambridge Structural Database (CSD). This chapter presents advances in the literature since the year 2000 and covers complexes with pyridines, substituted pyridines, pyridine–2–thiolates, oxyquinolates, thioquinolates, iminoquinolates, bipyridines, phenanthrolines, and terpyridines (FIGURE 1). These ligands are particularly significant for a number of reasons. Firstly, multidentate pyridine–containing ligands are particularly good at stabilizing hexacoordinate silicon compounds, and a wide variety of complexes have been isolated and structurally characterized (TABLES 1-4). Secondly, despite the hydrolytic susceptibility of the Si–N bond in tetrahedral silicon complexes, some of these complexes are quite resistant to hydrolysis and are even stable in aqueous solutions. Thirdly, the noninnocence of pyridine–containing ligands provides opportunities to explore the ligand–localized redox activity of these complexes. And lastly, the complexes can act as d–electron free analogs of ubiquitous transition metal coordination complexes in applications where MLCT bands are not needed or are undesired.

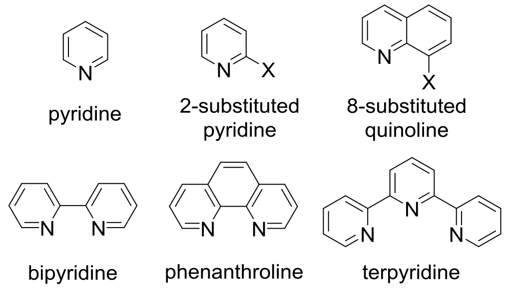

FIGURE 1: Types of pyridine–containing ligands observed in hexacoordinate silicon complexes.

Much of the early (pre–2000) coordination chemistry of hexacoordinate silicon complexes with pyridyl–containing ligands has been extensively reviewed in a number of comprehensive reviews, and several more recent reviews have covered other significant areas of hexacoordinate silicon chemistry.[2-11] This chapter covers the literature since 2000 on the subject of hexacoordinate silicon with pyridine–containing ligands and discusses emerging applications in fluorescence, high–energy materials, biology, and electrochromism, athough electrochromism is discussed more fully in later chapters. It also includes data and references on all of the structurally characterized hexacoordinate silicon complexes with one or more pyridine–containing ligand that have ever been deposited with the Cambridge Structural Database. The chapter is organized according to ligand type starting with monodentate pyridine and substituted pyridines along with bidentate 2–substituted pyridines. The next section discusses complexes with quinoline–type ligands. Finally, complexes with polypyridine ligands (bipyridine, phenanthroline, and terpyridine) are discussed.

Chapter 2 will then focus on the specifics of electrochromism and materials that are being studied for electrochromic applications. This especially includes the author's contribution in the form of the spectroelectrochemical characterization of tris(bipyridine)silicon(IV) hexafluorophosphate. Chapter 3 will then present the synthesis and characterization of other novel bipyridine– and terpyridine–type silicon complexes done by the author and coworkers. Chapter 4 will describe the fundamentals of electrochromic devices and the author's progress towards polymerizable silicon complexes. Finally, Chapter 5 will seek to discuss conclusions of this dissertation and potential future directions of this work.

1.2. Pyridine–type Ligands

1.2.1. Complexes with Pyridine

Silicon tetrahalides are very Lewis acidic and readily form adducts through direct combination with pyridine. Crystal structures of 43 hexacoordinate silicon complexes containing at least one monodentate pyridine or substituted pyridine ligand are currently contained in the CSD (TABLE 1). For unsubstituted pyridine the range of Si–N bond lengths is quite small, 1.93-2.02 Å, with the shortest bond length reported for *trans*–tetrafluorobis(pyridine)silicon[12] and the longest bond in the pentafluoro(pyridine)silicate anion.[13] Significantly, all of the di–substituted complexes exist solely in the trans orientation. However, several tetra–substituted complexes demonstrate the ability of the silicon center to accommodate pyridine ligands separated by only 90°. The greater basicity of the 4–dimethylaminopyridine ligand (DMAP) is apparent in the shorter Si–N bond lengths (1.90-1.92), which are just outside the range of all other hexacoordinate pyridine–silicon complexes. The DMAP ligand was also shown to coordinate to the electrophilic silicon center of $[PhBP^{Ph}{}_3]RuH(\eta^3\text{–}H_2SiRR')$ (R,R′ = Ph, Me or Ph, Ph) to form the corresponding hexacoordinate complexes $[PhBP^{Ph}{}_3]Ru(\mu\text{–}H)_3SiRR'(DMAP)$.[14]

TABLE 1: Hexacoordinate silicon complexes containing one or more monodentate pyridine or substituted pyridine ligand that have been deposited with the Cambridge Structural Database.

CSD entry ID and reference number	Chemical formula	Si–N bond lengths (Å)	^{29}Si NMR shift (ppm)
GAMZIF[14]	[(PhBP$^{Ph}{}_3$)Ru(μ-H)$_3$SiPh$_2$(DMAP)]·tol	1.90 (Si–N)	31 (C$_6$D$_6$)
HIJNET[15]	*trans*-[SiH$_2$(3-pic)$_4$]Cl$_2$·4CHCl$_3$	1.97 (Si–N)	N/A
HUFSEG[16]	*trans*-[SiH$_2$(4-pic)$_4$]Br$_2$·6CHCl$_3$	1.96 (Si–N)	N/A
HUFSIK[17]	*trans*-[SiH$_2$(4-pic)$_4$]Cl$_2$·6CHCl$_3$	1.96 (Si–N)	N/A
HUFYUC[18]	*trans*-[SiH$_2$(3-pic)$_4$]Br$_2$·4CHCl$_3$	1.97-1.99 (Si–N)	N/A
JEPCOW[19]	*trans*-[SiCl$_4$(py)$_2$]	1.98 (Si–N)	N/A
KOPLOQ[20]	*trans*-[SiCl$_4$(4-pic)$_2$]	1.98 (Si–N)	N/A
KOPNEI[20]	*trans*-[SiBrCl$_3$(4-pic)$_2$]	1.97 (Si–N)	N/A
KOPQAH[20]	*trans*-[SiBr$_2$Cl$_2$(4-pic)$_2$]	1.98 (Si–N)	N/A
KOPQEL[20]	*trans*-[SiBr$_3$Cl(4-pic)$_2$]	1.98	N/A
KOPQIP[20]	*trans*-[SiBr$_4$(4-pic)$_2$]	1.98	N/A
KOPQOV[21]	*trans*-[SiCl$_2$(4-pic)$_4$](I$_3$)$_2$·CHCl$_3$	1.97	N/A
NENTEH[22]	*trans*-[SiBr$_2$(DMAP)$_4$)]Br$_2$·6CHCl$_3$	1.90-1.92	N/A
NIYZUR[23]	*trans*-[SiCl$_2$H$_2$(DMAP)$_2$]·2CHCl$_3$	1.93	-151.9 (CP/MAS)
NIZBAA[23]	*trans*-[SiCl$_2$H$_2$(Brpy)$_2$]	1.97	-145.2 (CP/MAS)
NIZBEE[23]	*trans*-[SiCl$_2$H$_2$(vpy)$_2$]	1.96	-146.2 (CP/MAS)
NIZBII[23]	*trans*-[SiH$_2$(epy)$_4$]Cl$_2$·6CHCl$_3$	1.96	N/A
NIZBOO[23]	*trans*-[SiCl$_2$H$_2$(4tbpy)$_2$]	1.96	-149.5 (CP/MAS)
NIZBUU[23]	*trans*-[SiCl$_2$H$_2$(epy)$_2$]	1.96	-152.2 (CP/MAS)
NIZCEF[23]	*trans*-[SiCl$_2$H$_2$(4-pic)$_2$]	1.97	-148.8 (CP/MAS)
QEFBOS[24]	*trans*-[SiH$_2$(3,4-lut)$_4$]Br$_2$·6CHCl$_3$	1.98-1.99	N/A
QESDOH[25]	*trans*-[SiBr$_4$(py)$_2$]	1.98	N/A
QESDUN[25]	*trans*-[SiBr$_4$(3,5-lut)$_2$]	2.00	N/A
SOBXOW[26]	*trans*-[SiCl$_2$H$_2$(py)$_2$]	1.97	N/A
SOBYOX[26]	*trans*-[SiCl$_2$H$_2$(3-pic)$_2$]	1.97	N/A
SOBYUD[26]	*trans*-[SiH$_2$(py)$_4$]Cl$_2$·4CHCl$_3$	1.96-1.97	N/A
SUQVEG[27]	*trans*-[SiCl$_3$H(4tbpy)$_2$]	1.97-1.98	-170.0 (CP/MAS)
SUQVIK[27]	*trans*-[SiCl$_2$HMe(4-pic)$_2$]	2.00-2.02	-135.6 (CP/MAS)
SUQVOQ[27]	*trans*-[SiCl$_3$H(phpy)$_2$]	1.98	-165.6 (CP/MAS)
SUQVUW[27]	*trans*-[SiCl$_2$HMe(DMAP)$_2$]	1.98	-141.3 (CP/MAS)
TFPYSI[12]	*trans*-[SiF$_4$(py)$_2$]	1.93	N/A
TOKFUV[28]	*trans*-[SiCl$_3$H(Brpy)$_2$]·0.5Brpy	1.98-1.99	-165.7 (CP/MAS)
UZOLUR[29]	*trans*-[SiCl$_3$(OSiCl$_3$)(py)$_2$]	1.95-1.97	-180.5 (CP/MAS)
XALMEC[30]	*trans*-[SiH$_2$(3,4-lut)$_4$]Cl$_2$·6CHCl$_3$	1.97	-21.8 (CDCl$_3$)
XALMIG[30]	*trans*-[SiCl$_2$H$_2$(2,4-lut)$_2$]	2.02	N/A
XALMOM[30]	*trans*-[SiBr$_2$HMe(3,5-lut)$_2$]	2.03	-140.8 (solid state)
XATBAV[31]	*trans*-[SiCl$_4$(3,4-lut)$_2$]	1.99	N/A
XATBEZ[31]	*trans*-[SiBrCl$_3$(3,4-lut)$_2$]	1.98	N/A
XATBID[31]	*trans*-[SiBr$_2$Cl$_2$(3,4-lut)$_2$]	1.99	N/A
XATBOJ[31]	*trans*-[SiBr$_3$Cl(3,4-lut)$_2$]	1.99	N/A
XATBUP[31]	*trans*-[SiBr$_4$(3,4-lut)$_2$]	1.99	N/A
XAXRUJ[32]	*trans*-[SiH$_2$(3,5-lut)$_4$]Br$_2$·2MeCN	1.97-1.98	N/A
YUKPUR[13]	*trans*-[MnF$_2$(py)$_4$][SiF$_5$(py)]	2.02	N/A

The reactivity of hexacoordinate pyridine complexes has inspired a few potential applications. Besgubenko and coworkers explored the possibility of using *trans*–

dichlorotetrakis(DMAP)silicon(IV) chloride as an alternative to carbodiimides as a dehydrating agent for amide bond formation, but found it inferior to the analogous *N*–methylimidazole complex due to the latter's greater hydrolytic stability.[33] Likewise, Churakov and coworkers demonstrated that Si(pyridine)$_2$F$_4$ along with other SiF$_4$ adducts serve as potential precursors to fluorosilatranes.[34-35]

Goldvaser has explored the reversible complexation of trifluorosilanes with pyridines for potential molecular self–assembly.[36-38] They report NMR evidence of complexation at low temperatures for phenyltrifluorosilane with pyridine and 4–methoxypyridine to form the hexacoordinate species. Complexation with pyridine and 4–methoxypyridine was observed at room temperature with the more electron deficient trifluoro(pentafluorophenyl)silane. Extensive multinuclear evidence indicates exclusive formation of the *trans*–pyridine isomers.

Pyridine ligands have also been used as axial ligands in silicon porphyrins and phthalocyanines. Cissell and coworkers synthesized two silicon(IV) tetraphenylporphyrins, Si(TPP)(pyridine)$_2$ and Si(TPP)Cl$_2$.[39-40] Similar chemistry also afforded the phthalocyanine analogs, Si(pc)(pyridine)$_2$ and Si(pc)Cl$_2$.[41] As seen in FIGURE 2, the TPP ligand in Si(TTP)Cl$_2$ possesses a fully oxidized -2 oxidation state (18 electrons), while the TPP ligand in the pyridine–coordinated analog possesses a -4 oxidation state (20 electrons). The latter is synthesized by reducing Si(TPP)Cl$_2$ with two equiv. of Na/Hg in THF followed by precipitation and then dissolution in pyridine. Si(TPP)Cl$_2$ has a fluorescence yield of 2.7% and a lifetime of 1.8 ns, while the reduced pyridine analog has a fluorescence yield ≤ 0.04% and a lifetime of 2.4 ps. The significantly shortened lifetime was attributed to the ruffled structure adopted by the antiaromatic 20 electron porphyrin system and the introduction of low–energy singlet states lying below the emissive state (Q–state).

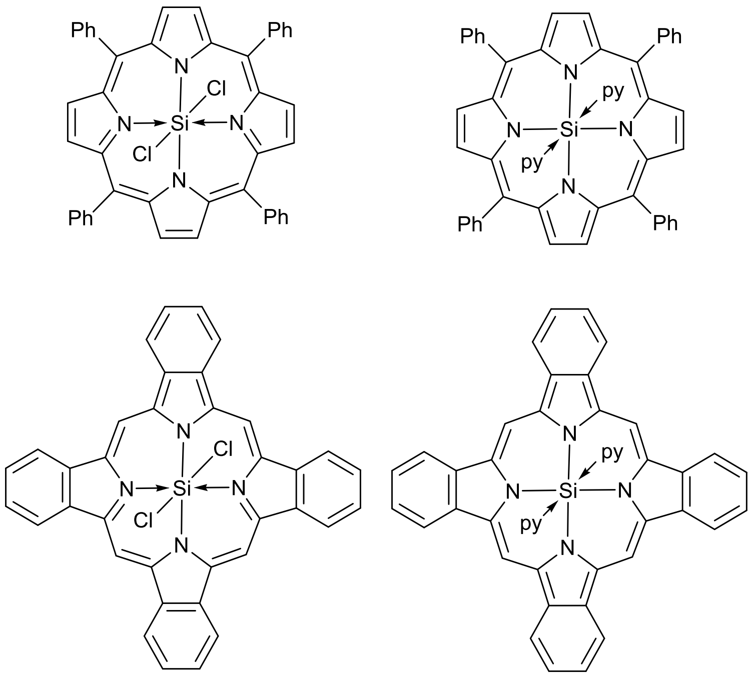

FIGURE 2: Structures of (top left) $Si(TPP)Cl_2$, (top right) $Si(TPP)(py)_2$, (bottom left) $Si(pc)Cl_2$, and (bottom right) $Si(pc)(py)_2$.[39-41]

1.2.2. Complexes with Pyridine–2–thiolate

The ambidentate pyridine–2–thiolato (pyS, FIGURE 3) ligand has been used to obtain a range of stable, hexacoordinate silicon complexes (TABLE 2).

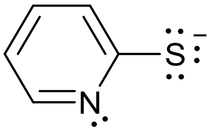

FIGURE 3: Pyridine–2–thiolate ligand with explicit lone pairs.

TABLE 2: Hexacoordinate silicon complexes containing one or more pyridine–2–thiolate ligand that have been deposited with the Cambridge Structural Database.

CSD entry ID and reference number	Chemical formula	Si–X bond lengths (Å)	^{29}Si NMR shift (ppm)
POVTOL[42]	*cis*-$[Si(pyS)_2(pyS\text{-}\kappa S)_2]$	1.94-1.95 (Si–N), 2.29-2.34 (Si–S)	-165 ($CDCl_3$)
QIKTEL[43]	*cis*-$[SiCl_2(pyS)_2]$	1.95 (Si–N), 2.27 (Si–S)	-182.2-(-177.4) (VACP/MAS)
QIKTIP[43]	*cis*-$[SiClPh(pyS)_2]$	1.95-1.97 (Si–N), 2.30-2.42 (Si–S)	-156.9-(-153.4), -152.9-(-149.0) (VACP/MAS)
QIKTOV[43]	*cis*-$[Si(N_3)Ph(pyS)_2]$	1.91-1.95 (Si–N), 2.31-2.42 (Si–S)	-156.2 (VACP/MAS)
QIKTUB[43]	*cis*-$[Si(NCO)Ph(pyS)_2]$	1.91-1.94 (Si–N), 2.31-2.44 (Si–S)	-165.5 (VACP/MAS)
QIKVAJ[43]	*cis*-$[Si(NCS)Ph(pyS)_2]$	1.90-1.94 (Si–N), 2.30-2.39 (Si–S)	-170.3 (VACP/MAS)
QIKVEN[43]	*cis*-$[SiClMe(pyS)_2]$	1.92-1.95 (Si–N), 2.34-2.41 (Si–S)	-150.1-(-149.4) (VACP/MAS)

The reaction of two equiv. of 2–mercaptopyridine and trimethylamine with $SiCl_4$, $MeSiCl_3$, or $PhSiCl_3$ provided the corresponding hexacoordinate complex, $Si(pyS)_2RCl$, **1** (FIGURE 4).[43] The chlorophenyl$(pyS)_2$silicon complex could be used as precursor to synthesize several other $Si(pyS)_2PhX$ complexes, **2**, while the dichloro$(pyS)_2$silicon complex can react with two additional equiv. of 2–mercaptopyridine and base to form complex **3**.[42] All of the pyridine–2–thiolate complexes exhibit a Si–N bond length similar to the monodentate pyridine ligands (1.9-2.0 Å); however, unlike with the monodentate pyridine ligands, there is not a clear preference for the pyridine ligands to occupy trans positions. The type **2** complexes of $Si(pyS)_2PhX$ can adopt four isomeric structures (**2A-2D**, FIGURE 4).

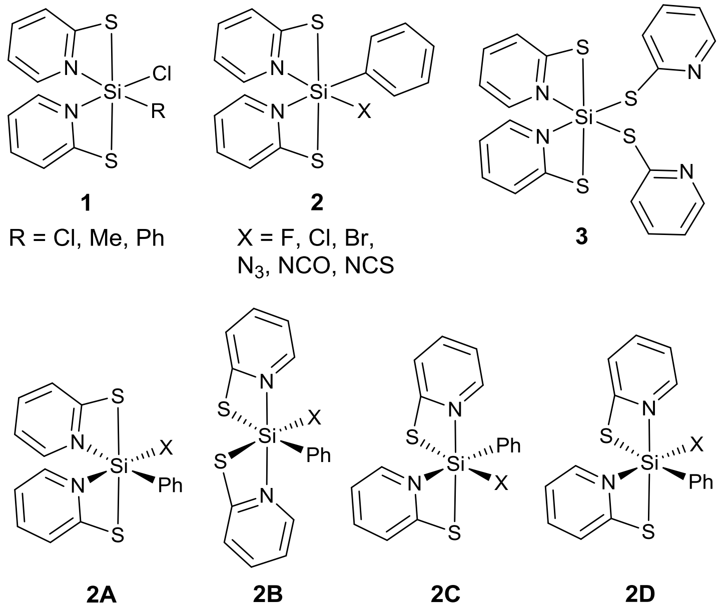

FIGURE 4: Hexacoordinate silicon complexes **1-3** with pyridine–2–thiolato ligands and the stereochemical isomers of compounds **2 (2A-2D)**.[42-43]

For all of the species, where X = F, Cl, Br, N_3, NCO, NCS, calculations predict structure **2C** to be the most stable configuration with **2A** only slightly less stable (ZORA-BP86/TZ2P with COSMO simulating solvation in CH_2Cl_2). This calculation was consistent with NMR experiments at -70 ˚C indicating that each of the six $Si(pyS)_2PhX$ complexes exist as a mixture of two diastereomers, with the **2C** isomer dominant. Furthermore, $Si(pyS)_2PhCl$ co–crystallized as a mixture of **2A** and **2C** geometries. Their calculations predict that the **2A** isomer would be the most stable for $Si(pyS)_2PhI$, but this complex was instead isolated as the ionic compound $Si(pyS)_2Ph^+I^-$. All of the $Si(pyS)_2PhX$ complexes maintain a hexacoordinate silicon center in solution at room temperature with $\delta(^{29}Si)$ = -148 to -168 ppm (CD_2Cl_2). By comparison, even at -70 ˚C, $Si(pyS)_2PhI$ exhibits a peak $\delta(^{29}Si)$ = -77 ppm, which is consistent with a pentacoordinate silicon ionic compound, $[Si(pyS)_2Ph]I$.

Compound **3**, Si(pyS)$_4$, provides an interesting model for analysis since it contains the ligand in both binding modes as bidentate *N,S*–pyridine–2–thiolate and as monodentate *S*–pyridine–2–thiolate. The Si–S bond lengths are only slightly shorter for the monodentate ligand (2.24 Å and 2.25 Å) versus the bidentate ligand (2.34 Å and 2.29 Å), indicating that the stability provided by the chelating effect outweighs the stress of forming a four–membered ring. Also, the N–C–S angles of the bidentate ligands are only 109˚. This significant deviation from the 118˚ N–C–S angles in the monodentate ligands is interpreted by the authors as further evidence of chelation. Research with the ambidentate pyridine–2–thiolate ligand is ongoing, and the authors claim to be exploring the use of these complexes as starting materials for heteronuclear complexes with other metals.

1.3. Quinolate–type Ligands

The bidentate ligands derived from 8–hydroxyquinoline (8–oxyquinolate, quin, FIGURE 5) or 8–mercaptoquinoline (8–thioquinolate, quinS, FIGURE 5) play a very significant role in main group chemistry as exemplified by Al(quin)$_3$, a widely–used emitting material for organic light–emitting diodes (OLEDs). In recent years, there has been a lot of progress with these ligands in expanding the field of stable hexacoordinate silicon complexes. A wide variety of hexacoordinate silicon complexes with these ligands have been structurally characterized (TABLE 3).

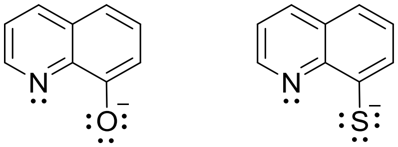

FIGURE 5: (left) 8–oxyquinolate and (right) 8–thioquinolate ligands with explicit lone pairs.

TABLE 3: Hexacoordinate silicon complexes containing one or more quinolate–type ligands that have been deposited with the Cambridge Structural Database.

CSD entry ID and reference number	Chemical formula	Si–X bond lengths (Å)	N–Si–X bond angles (˚)	^{29}Si NMR shift (ppm)
CELFUU[44]	$[SiClMe(quin)_2]$	2.01-2.02 (Si–N), 1.76-1.77 (Si–O)	83.4-83.6 (N–Si–O)	N/A
IHAFAY[45]	$[SiPh_2(quin)_2]$	2.10-2.11 (Si–N), 1.77 (Si–O)	81.6-81.7 (N–Si–O)	N/A
ODAQIV[46]	$[Si(\eta^2\text{–Pent})(quin)_2]$	2.09-2.13 (Si–N), 1.79-1.80 (Si–O)	80.5-81.7 (N–Si–O)	-114.0, -112.0 (CP/MAS), -20.2 ($CDCl_3$), -47.2 (THF-d_8)
ODARES[46]	$[Si(\eta^2\text{–Bu})(quin)_2]\cdot 5THF$	2.06-2.07 (Si–N), 1.80-1.81 (Si–O)	81.4-81.8 (N–Si–O)	-103.3 (CP/MAS), -98.6 ($CDCl_3$), -100.3 (THF-d_8)
ODARIW[46]	$[Si(\eta^2\text{–Pr})(quin)_2]$	2.04 (Si–N), 1.80 (Si–O)	82.5 (N–Si–O)	-129.9 (CP/MAS)
QAXSIS[47]	$[SiMePh(quin)_2]$	2.08-2.10 (Si–N), 1.78-1.79 (Si–O)	81.6-82.1 (N–Si–O)	-27.8 ($CDCl_3$)
QAXTAL[47]	$[Si(quin)_2(dped)]\cdot CHCl_3$	1.95-1.96 (Si–N), 1.79 (Si–O)	84.4-84.8 (N–Si–O)	-152.0 (CP/MAS)
VIQGUY[48]	$[SiPh(quin\text{–}\kappa O)(quin)_2]$ $\cdot 5THF$	1.96-2.03 (Si–N), 1.75-1.80 (Si–O)	83.5-84.2 (N–Si–O)	-147.4 (CP/MAS), -149.8 ($CDCl_3$)
VIQHIN[48]	$[SiPh(mquin\text{–}\kappa O)(mquin)_2]$	2.18-2.26 (Si–N), 1.72-1.73 (Si–O)	80.0-80.2 (N–Si–O)	-114.4 (CP/MAS), -81.6 ($CDCl_3$)
YALFIC[49]	$[SiCl_2(quin)(diba)]$	2.01 (Si–N), 1.74 (Si–O)	84.9 (N–Si–O)	-165.2 (VACP/MAS), -162.4 (CD_2Cl_2)
YALFOI[49]	$[SiBr_2(quin)(diba)]$	1.99 (Si–N), 1.74 (Si–O)	85.2 (N–Si–O)	-200 to -160 (VACP/MAS), -190 (CD_2Cl_2)
YALFUO[49]	$[SiF_2(quin)(diba)]$	2.08 (Si–N), 1.79 (Si–O)	87.9 (N–Si–O)	-170 to -155 (VACP/MAS), -161.4 (CD_2Cl_2)
YALGAV[49]	$[Si(N_3)_2(quin)(diba)]$	2.00 (Si–N), 1.76 (Si–O)	84.4 (N–Si–O)	-169.4 (VACP/MAS), -167.5 (CD_2Cl_2)
YALGEZ[49]	$[Si(NCO)_2(quin)(diba)]$	2.01 (Si–N), 1.76 (Si–O)	84.4 (N–Si–O)	-184.6 (VACP/MAS), -183.5 (CD_2Cl_2)
YALGOJ[49]	$[Si(OTf)_2(quin)(diba)]$	1.96 (Si–N), 1.72 (Si–O)	86.0-86.3 (N–Si–O)	-171.0 (VACP/MAS), -171.2 (CD_2Cl_2)
YALGUP[49]	$[Si(cat)(quin)(diba)]$	2.00 (Si–N), 1.78 (Si–O)	84.2 (N–Si–O)	-145.9 (VACP/MAS), -146.6 (CD_2Cl_2)
YODFUU[50]	$[SiPh(quin)(pip)]$	2.09 (Si–N), 1.76 (Si–O)	82.5 (N–Si–O)	-144.6 (VACP/MAS), -147.2 (CD_2Cl_2)
YODGEF[50]	$[SiPh(quin)(apip)]$	2.09 (Si–N), 1.77 (Si–O)	82.0 (N–Si–O)	-146.9 (VACP/MAS), -144.0 (CD_2Cl_2)
YODGOP[50]	$[SiPh(quin)(tpip)]$	2.03-2.04 (Si–N), 1.75-1.76 (Si–O)	83.2-83.4 (N–Si–O)	-146.4 (VACP/MAS), -141.7 (CD_2Cl_2)
YODGAB[50]	$[SiPh(quinS)(pip)]\cdot 5MeCN$	2.07 (Si–N), 2.27 (Si–S)	84.3 (N–Si–S)	-140.0 (VACP/MAS), -138.8 (CD_2Cl_2)
YODGIJ[50]	$[SiPh(quinS)(apip)]\cdot MeCN$	2.12 (Si–N), 2.30 (Si–S)	82.1 (N–Si–S)	-135.3 (VACP/MAS), -135.8 (CD_2Cl_2)
YODGUV[50]	$[SiPh(quinS)(tpip)]\cdot 5MeCN$	2.03 (Si–N), 2.28 (Si–S)	84.3 (N–Si–S)	-145.4 (VACP/MAS), -141.6 (CD_2Cl_2)

TABLE 3: (continued)

CSD entry ID and reference number	Chemical formula	Si–X bond lengths (Å)	N–Si–X bond angles (˚)	^{29}Si NMR shift (ppm)
COFHUC[51]	$[(baquin)Si(\mu\text{–}baquin)_2(\mu\text{–}O)Si(baquin)]Cl_2\cdot 7CHCl_3$	1.85-1.97 (Si–N), 1.78 (Si–O)	80.6-84.0 (N–Si–N)	N/A
GEZFUO[52]	$[SiF_3(qin)]$	1.94 (Si–N), 1.73 (Si–O)	82.5 (N–Si–N) 92.7, 175.1 (N–Si–O)	N/A
NEZQEP[53]	$[SiCl_2Ph(qip)]\cdot CHCl_3$	1.96-2.00 (Si–N), 1.72 (Si–O)	80.5 (N–Si–N), 92.8, 173.0 (N–Si–O)	-167.1 (DMSO-d_6), -158.4 (CP/MAS)
NEZQIT[53]	$[SiMe(qip)(imp)]Cl\cdot 4CHCl_3$	1.97-2.00 (Si–N), 1.76 (Si–O)	80.9 (N–Si–N), 92.8, 170.2 (N–Si–O)	-168.3 (CP/MAS)

1.3.1. Complexes with Oxyquinolate

The oxyquinolate ligand demonstrates remarkable variety in its coordination geometry with silicon. The first structurally characterized oxyquinolate structure was $Si(quin)_2ClCH_3$, **4** (FIGURE 6), which was obtained by reaction of CH_3SiCl_3 with lithium oxyquinolate.[44] In this structure, the oxygens were located trans to each other as shown in FIGURE 6. A similar geometry was observed with structures **5** and **6**; by comparison, $Si(quin)_2(CH_3)_2$ adopts a tetracoordinate geometry in the solid state.[47] Compound **7** adopted an alternative structure with the quinoline nitrogens trans to each other. A third mode was observed with the centrosymmetric halide complexes **8-Br** and **8-Cl** (SCHEME 1), in which the halogen atoms are trans to each other along with both nitrogen and oxygen atoms (structure inferred from solid state spectroscopic evidence and supported by theoretical calculations). Solid state NMR confirmed a hexacoordinate silicon center for the compounds **5-8**, ^{29}Si NMR (79 MHz, CP/MAS): δ_{iso} = -137.4 ppm (compound **5**), -126.2 ppm (**6**), -152.0 ppm (**7**), -170 ppm (broad due to Si–Br coupling, **8-Br**), and -157.9 ppm (**8-Cl**). The situation changes in solution however. Compound **6** gives only one peak in the ^{29}Si NMR (79 MHz, $CDCl_3$): δ = -27.8 ppm, consistent with a tetrahedral geometry in solution. Although insoluble in $CDCl_3$, compounds **8-Br** and **8-Cl** undergo a conversion to the mer isomer of the cation **9** upon dissolution in DMSO-d_6 likely due to the generation of chloromethylmethylsulfide, colloidal SiO_2, and 8–hydroxyquinoline, ^{29}Si NMR (79 MHz, DMSO-d_6): δ = -151.8 ppm (SCHEME 1).

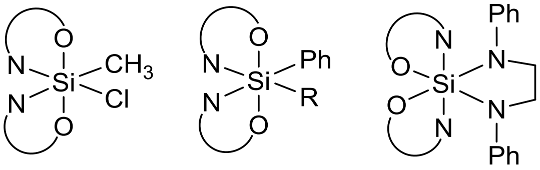

FIGURE 6: Oxyquinolate complexes **4-7**.[44, 47]

SCHEME 1: Conversion of **8-Br** and **8-Cl** into **9** upon dissolution in DMSO-d_6.[47]

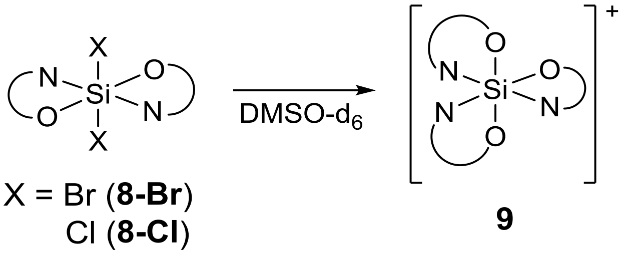

An elegant display of the fine tuning of N → Si coordination was demonstrated with the oxyquinolate ligand and a series of silacycloalkanes (SCHEME 2, compounds **10-13**).[46] Silacycloalkanes exhibit a ring–strain release Lewis acidity dependent on ring size. The silacyclobutane, **10**, would be expected to exhibit the greatest ring–strain release following N → Si complexation. Indeed, compounds **10** and **11**, corresponding to the silacyclobutane and silacyclopentane, adopt hexacoordinate geometries as confirmed by solid state ^{29}Si NMR, -129.9 ppm and -103.3 ppm respectively, and retain the hexacoordinate silicon center in solution, ^{29}Si NMR: -100.3 ppm (THF) and -98.6 ppm

($CDCl_3$) respectively. Compound **12**, the silacyclohexane, possesses a tetrahedral silicon center in solution ^{29}Si NMR: -20.2 ppm ($CDCl_3$, 20 °C). Variable temperature ^{29}Si NMR (THF) was used to explore complexation equilibrium, and ln K vs 1/T plots provided thermodynamic data for formation of the hexacoordinate species **12** ($\Delta H = -23.5$ kJ/mol, $\Delta S = -85.8$ J/mol K) and **13** ($\Delta H = -9.0$ kJ/mol, $\Delta S = -55.7$ J/mol K).

SCHEME 2: Adjusting equilibrium coordination geometry by tuning the ring–strain selease Lewis acidity of the silacycloalkane.[46]

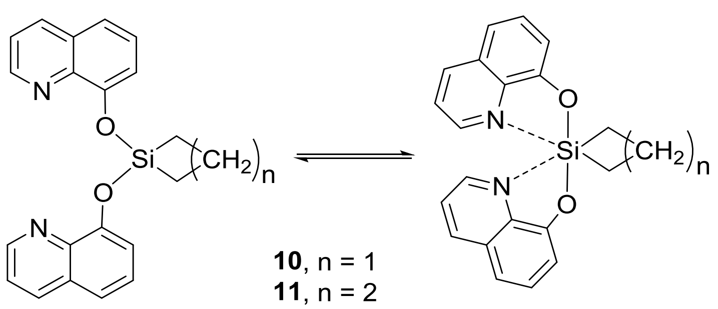

10, n = 1
11, n = 2
12, n = 3
13, n = 4

The trend towards greater Lewis acidity and stronger coordination for smaller rings was also observed in crystallography results. The silacyclobutane and silacyclopentane complexes (**10** and **11**) possessed hexacoordinate silicon centers, with short Si–N bond lengths (Si–N = 2.03 Å, **10** and 2.07 Å, **11**) and oxygens roughly trans to each other (O–Si–O = 164°, **10** and 165°, **11**). The silacycloheptane, **13**, adopted a tetracoordinate geometry with weak Si–N interactions (Si–N = 2.74 Å and 4.02 Å) and O–Si–O bond angle of 99.8°. This geometry could be labeled as a monocapped tetrahedral arrangement due to the preferential orientation but longer distance by one of the two nitrogen atoms. Remarkably, compound **12** was crystallized separately in both the hexacoordinate state and the tetracoordinate state (monocapped tetrahedral). In the hexacoordinate state, **12** exhibited an average Si–N bond length of 2.11 Å and an average O–Si–O bond angle of 162°, while in the tetracoordinate state, **12** exhibited Si–N bond lengths of 2.76 Å and 3.99 Å and an O–Si–O = 99.2°.

The majority of the oxyquinolate complexes have been synthesized through reaction with the deprotonated oxyquinolate with the appropriate chlorosilane or through trans–silylation with 8–trimethylsiloxyquinoline (SCHEME 3).[54] The reaction with 8–trimethylsiloxyquinoline is sufficient for the more Lewis acidic silanes, while the less acidic silanes are usually combined with the deprotonated oxyquinolate reagent. For example, dichlorosilacyclobutane was acidic enough to react with 8–trimethylsiloxyquinoline while the larger dichlorosilacycloalkanes were combined with 8–hydroxyquinoline and trimethylamine.[46]

SCHEME 3: Oxyquinolate complexes synthesized via *trans*–silylation with 8–trimethylsiloxyquinoline.[46, 54]

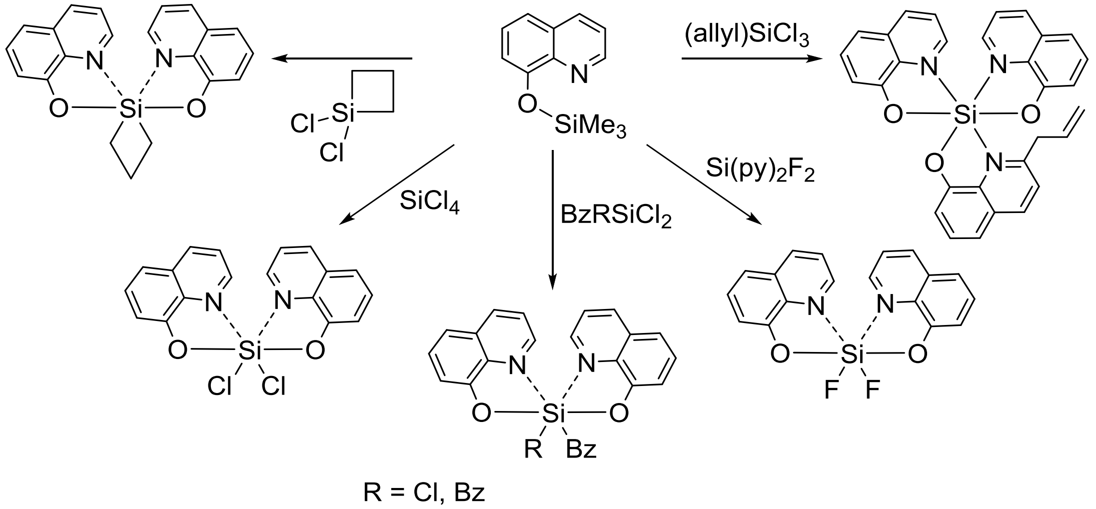

Alternatively, compound **14** has been shown to be a versatile starting point for a variety of hexacoordinate silicon oxyquinolate complexes (SCHEME 4).[49]

SCHEME 4: Oxyquinolate complexes synthesized from **14**.[49]

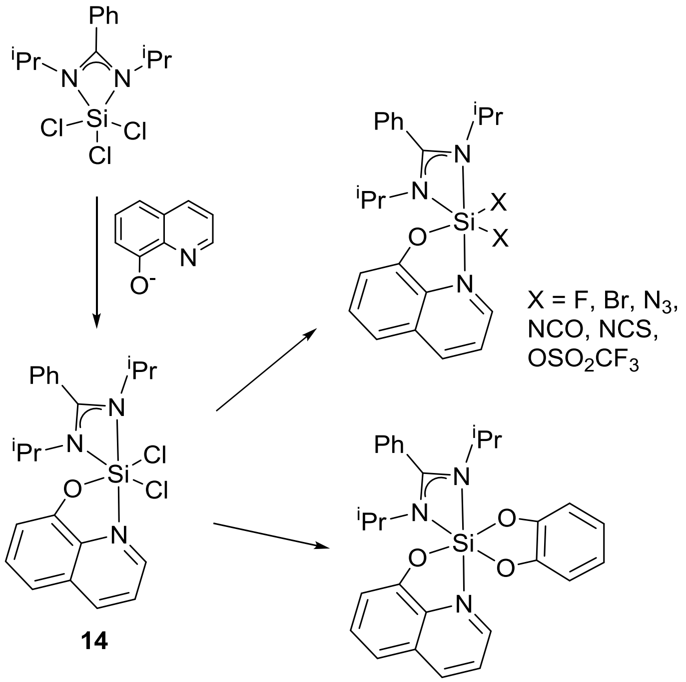

1.3.2. Complexes with Thioquinolate

Hexacoordinate silicon complexes with the thioquinolate ligand are much rarer than the oxyquinolate, but the ligand has been observed to adopt a bidentate *S,N*–coordination mode without much of an effect resulting from the O/S switch. Starting from the pentacoordinate chlorosilane, **15**, Weiss and coworkers synthesized the six variants of **16** (SCHEME 5).[50] In all cases, X–ray crystallography confirmed the adoption of a distorted octahedral structure with a mer arrangement of the O,N,X ligand and the quinoline nitrogen always located trans to the phenyl ring, as shown in SCHEME 5. The Si–N bond to the quinoline nitrogen lies within a narrow range (2.03-2.12 Å) for all 6 structures. ^{29}Si NMR spectra of all 6 species are consistent with hexacoordinate silicon centers in solution δ = -147 to -136 ppm (CD_2Cl_2).

SCHEME 5: Synthesis of oxyquinolate or thioquinolate complex, **16,** with various O,N,X ligands where X = O, NMe, or S.[50]

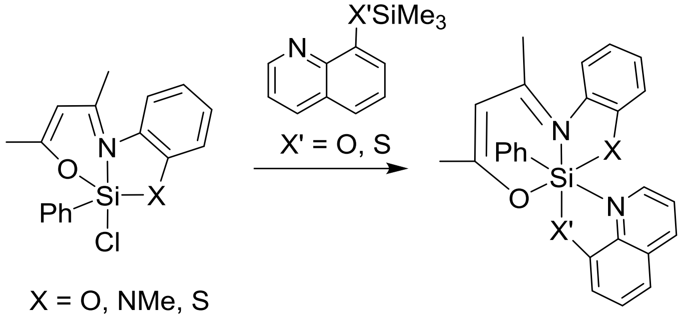

15 **16**

1.3.3. Complexes with (2–N–(Quinoline–8–yl)iminomethylphenolate)

The fluorescence properties and applications of aluminum quinolates suggest that silicon quinolate complexes could be attractive materials for fluorescence applications. A recent report of the fluorescent properties of hexacoordinate silicon complexes with 2–*N*–(quinoline–8–yl)iminomethylphenolate ligands supports this.[52] Compounds **17-19** were synthesized along with their tin analogs (FIGURE 7). All three complexes are fluorescent in the solid state with emission maxima at 563 nm (**17**), 533 nm (**18**), and 532 nm (**19**). They are also fluorescent in solution (DMSO, R.T.) with emission maxima at 499 nm (**17**, quantum yield, $\Phi_F = 0.98$), 518 nm (**18**, $\Phi_F = 0.11$), and 521 nm (**19**, $\Phi_F = 0.01$). With a quantum yield near unity, **17** is particularly interesting and makes a compelling case for future exploration of related Schiff base ligands following this hexacoordinate silicon structure motif.

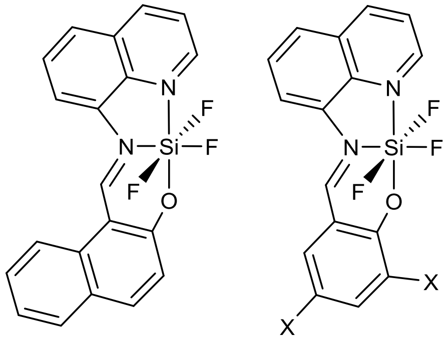

17

18, X = Cl
19, X = Br

FIGURE 7: Compounds **17-19.**[52]

1.4. Polypyridine Ligands

Polypyridine ligands such as bipyridine, phenanthroline, and terpyridine are particularly good at coordinating with silicon to make stable hexacoordinate complexes, and a wide variety of complexes have been structurally characterized (TABLE 4). In some cases, these species are even stable in aqueous solutions providing a wide variety of new opportunities and applications. Polypyridylsilicon(IV) complexes are emerging as potential new materials for biological and electronic applications.

TABLE 4: Hexacoordinate silicon complexes containing one or more bipyridine or phenanthroline ligands that have been deposited with the Cambridge Structural Database.

CSD entry ID and reference number	Chemical formula	Si–N bond lengths (Å)	N–Si–N bond angles (˚)	^{29}Si NMR shift (ppm)
BIPSTI[55]	$[Si(OH)_2(bpy)_2]I_2{\cdot}2H_2O$	1.95, 2.00	80.4	N/A
CLDMSI[56]	$[SiCl_2Me(dcms)(bpy)]{\cdot}0.5MeCN$	2.01-2.03	79.9	N/A
CUMXAL[57]	$[SiF_4(4dmbpy)]$	2.01	78.8	N/A
FUMFAU[58]	*mer*-$[SiCl_3(OSiCl_3)(bpy)]$	1.97	81.0	N/A
KENHUG[59]	*fac*-$[SiCl_3(dcm)(bpy)]$	1.96-1.97	80.7	N/A
KENJAO[59]	*fac*-$[SiCl_3(tcm)(bpy)]$	1.97	80.4	N/A
KENJES[59]	*fac*-$[SiCl_3(tcsm)(bpy)]$	1.97-1.98	81.7	N/A
KOPJOO[60]	$[SiCl_2(bpy)_2]I_2$	1.92-1.94	83.1	-161.0 (CD_3OD)
LAHWUN[37]	*fac*-$[SiF_3(C{\equiv}CPh)(bpy)]$	1.98	79.8	-178.7 ($CDCl_3$)
POGRAG[61]	$[Si(binolato)(bpy)_2](PF_6)_2$	1.91-1.96	82.1-82.5	-156.6 (CD_3CN)
POGREK[61]	$[Si(cat)(bpy)_2](PF_6)_2{\cdot}1.5MeCN$	1.91-1.94	81.9-82.9	-149.1 (CD_3CN)
PYTFSI[62]	$[SiF_4(bpy)]$	1.97-1.98	79.6	N/A
TADRAT[63]	$[Si(N_3)_4(bpy)]$	1.94-1.97	81.2	N/A
UGEPED[64]	$[Si(OMe)_2(bpy)_2]I(I_3)$	1.92-2.00	81.1-81.4	-156.7 (CD_3CN)

TABLE 4: (continued)

CSD entry ID and reference number	Chemical formula	Si–N bond lengths (Å)	N–Si–N bond angles (˚)	^{29}Si NMR shift (ppm)
UGEPIH[64]	$[Si(ed)(bpy)_2]I_2$	1.94-1.95	81.7	-144.1 (CD_3CN)
UGEPON[64]	$[Si(OPh)_2(bpy)_2](I_3)_2$	1.91-1.97	81.4-82.2	-167.4 (CD_3CN)
UGEPUT[64]	$[Si(bp)(bpy)_2](PF_6)_2$	1.91-1.96	81.8-82.1	-155.7 (CD_3CN)
UGEQAA[64]	$[Si(cat)(bpy)_2](PF_6)_2$	1.91-1.93	82.3-82.9	-148.9 (CD_3CN)
YUTLOP[65]	*trans*-$[SiCl_2H_2(bpy)]$	1.96	79.0	-161.0 (CP/MAS)
YUTMEG[65]	$[SiCl_3H(bpy)]$	1.94-1.97	80.9	-169.5 (CP/MAS)
ZIDYIW[66]	$Na[Si(dpcatH)(bpy)_2](ClO_4)_4\cdot 3H_2O$	1.91-1.93	82.2-82.8	-148.2 (CD_3CN)
CIRPEY[67]	$[Si(tfbm)_2(phen)]\cdot 2THF$	2.05-2.09	77.9	N/A
EYOLAF[68]	$[SiF_4(phen)]\cdot MeCN$	1.99	80.6	N/A
GOFSIF[69]	*mer*-$[SiCl_3Et(phen)]$	2.01-2.02	80.0	N/A
KEBXAS[70]	$[Si(phn)(phen)_2](PF_6)_2\cdot 3MeCN$	1.92-1.96	82.7-82.8	N/A
LAHXAU[37]	$[SiF_3(C{\equiv}CPh)(phen)]\cdot CH_2Cl_2$	2.00-2.02	79.7-80.2	-176.6, -166.8 ($CDCl_3$)
NONKUY[71]	$[(Cp^*)Ru(\mu\text{-}\eta^6\text{-}pyre)Si(phen)_2](PF_6)_3\cdot Me_2CO$	1.92-1.94	83.0-83.3	-148.1 ($(CD_3)_2CO$)
POGDEW[61]	$[Si(Icat)(phen)_2](PF_6)_2\cdot 2.25MeCN$	1.92-1.94	82.7-83.9	-149.4 (CD_3CN)
POGRIO[61]	$[Si(Brcat)(phen)_2](PF_6)_2\cdot 2.5MeCN$	1.92-1.94	82.8-83.6	-149.3 (CD_3CN)
POGROU[61]	$[Si(ncat)(phen)_2](PF_6)_2\cdot 3MeCN$	1.92-1.93	83.1-83.6	-149.4 (CD_3CN)
POGRUA[61]	$[Si(bq)(phen)_2](PF_6)_2\cdot 3MeCN$	1.92-1.93	83.5-84.1	-151.7 (CD_3CN)
POGSAH[61]	$[Si(mcat)(phen)_2](PF_6)_2\cdot 2.5MeCN$	1.93	83.0-83.1	-148.7 (CD_3CN)
SINBEW[72]	*cis*-$[SiCl_2(tcs)_2(phen)]\cdot C_6H_6$	1.99-2.01	81.4	N/A
TADQUM[63]	$[Si(N_3)_4(phen)]\cdot MeCN$	1.96-1.98	81.8	N/A
XUTDIA[73]	$[Si(NCO)_4(phen)]\cdot MeCN$	1.98-1.99	81.2	N/A
YUTLUV[65]	$[SiCl_4(phen)]\cdot MeCN$	1.97-1.98	81.8-81.9	-179.7 (CP/MAS)
YUTMAC[65]	*mer*-$[SiCl_3Ph(phen)]$	2.00-2.02	80.1	-153.1 (CP/MAS)
YUTMOQ[65]	*mer*-$[SiCl_3Me(phen)]\cdot THF$	2.00-2.02	80.01	-152.4 (CP/MAS)

1.4.1. Complexes with One Bipyridine or Phenanthroline Ligand

Bipyridine and phenanthroline ligands readily form stable adducts with Lewis acidic silanes. Complex stability generally increases in the order of tetramethylethylenediamine (TMEDA) < pyridine < bipyridine < phenanthroline, and for a given *N*,*N'*–coordinating ligand complex stability increases with Lewis acidity of the silane $SiH_2Cl_2 < SiHCl_3 < SiCl_4$.[65] Most of the early hexacoordinate silicon complexes with one bipyridine or one phenanthroline ligand have been thoroughly covered in earlier reviews of the subject.[2, 5-6] Since 2000, there have been several new developments of note. Portius and coworkers have extended the $Si(bpy)X_4$ and $Si(phen)X_4$ system to include the pseudohalides, $X = N_3^-$ and NCO^-.[63, 73] The isocyanate complexes were formed through reaction of the neutral diimine ligand with $K_2Si(NCO)_6$, and the azide complexes from reaction of the diimine ligand with $Na_2Si(N_3)_6$. Alternatively, $Si(bpy)(N_3)_4$, **20**, can be synthesized from combination of bipyridine with tetraazidosilane (SCHEME 6).

SCHEME 6: Synthesis of $Si(bpy)(N_3)_4$, **20**.[63]

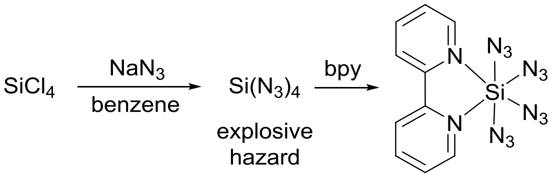

20

Compound **20** or related diimine complexes are of interest as stabilized, high–energy compounds, potentially serving as environmentally preferred replacements of $Pb(N_3)_2$. $Si(N_3)_4$ is an explosive material that is dangerous to handle[74] but upon complexation with bipyridine or phenanthroline it forms the more stable but still high–energy adduct. Compound **20** melts under vacuum at 212 ˚C, and DSC experiments indicate decomposition at an extrapolated onset temperature of 265 ˚C. The heat of decomposition, ΔH_d, was determined to be -2.4 kJ/g, which also provides an estimate for the heat of explosion, Q_E. For comparison with other energetic materials, this places it between NaN_3 (ΔH_d = -0.8 kJ/g) and hexahydro–1,3,5–trinitro–1,3,5–triazine (RDX) (ΔH_d = -4.5 kJ/g).

A recent study by Fester and coworkers uncovered new reactivity modes of phenanthroline complexes of hydridochlorosilanes and chlorosilanes that differed from their bipyridine analogs.[65] Dismutation was observed with the phenanthroline complexes of the hydridochlorosilanes (dichlorosilane and trichlorosilane) as shown in SCHEME 7.

Also, compound **21** was found to convert to the pentacoordinate complex **23** by proceeding through the dismutation product **22** (SCHEME 8). Structures of both **22** and **23** were confirmed with X–ray crystallography.

SCHEME 7: Dismutation reaction of Si(phen)Cl_2H_2.[65]

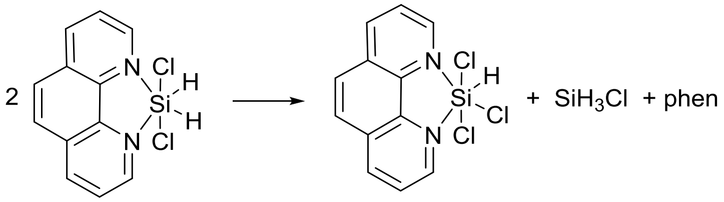

SCHEME 8: Conversion of Si(phen)Cl_2MeH, **21**, to **23**.[65]

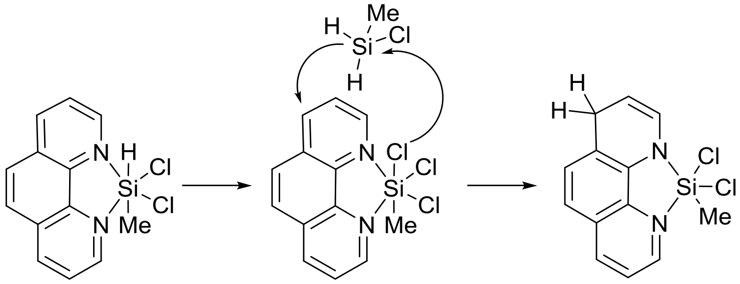

21 **22** **23**

1.4.2. Complexes with Two Bipyridine or Phenanthroline Ligands

The general approach to bis–bipyridine or bis–phenanthroline hexacoordinate silicon complexes is through the corresponding diiodosilane species $[Si(bpy)_2I_2]I_2$, **24a**, or $[Si(phen)_2I_2]I_2$, **24b** (SCHEME 9). Compound **24** is generated by the reaction of SiI_4 with bipyridine or phenanthroline in dichloromethane or chloroform.[75-76] Even with excess ligand, the reaction does not proceed beyond bis–substitution. Compound **24** precipitates out of solution and can be purified by rinsing with dry CH_2Cl_2 or $CHCl_3$ under anaerobic conditions. Reaction with alcohols affords a wide range of products.

They are stable enough to be manipulated in air and in many cases can even be dissolved in water without hydrolysis. Many bis–bipyridylsilicon(IV) and bis–phenanthrolinesilicon(IV) complexes have been characterized structurally, and in all cases, the two bidentate ligands avoid co–planarity and allow the alkoxide ligands to occupy positions cis to each other (TABLE 4).

SCHEME 9: Synthesis of **24a** and **24b**.[75-76]

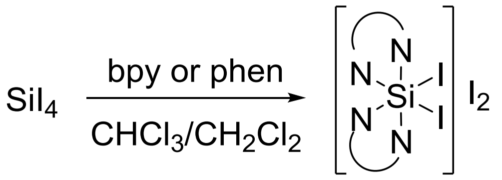

24a NN = bpy
24b NN = phen

Meggers used compounds **24a** and **24b** (SCHEME 10) as precursors to a range of arenediolato complexes **25-31** (FIGURE 8).[61] Reaction of **24a** and **24b** with (*R*)–1,1’–bi–2–naphthol proceeded with high selectivity to **Λ-*(R)*-30a** (10%, 94:6 e.r.) and **Λ-*(R)*-30b** (12%, 95:5 e.r.). All of the species were stable with respect to hydrolysis with no sign of hydrolysis after one week in solution (CD_3CN/D_2O, 1:1, R.T. with daylight).

SCHEME 10: Synthesis of **25a** and **25b**.[61]

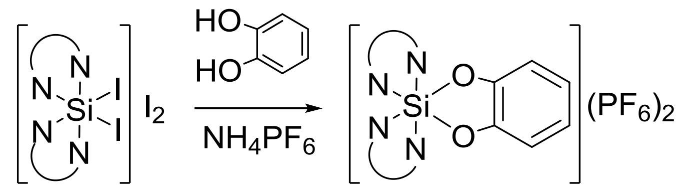

24a NN = bpy
24b NN = phen

25a NN = bpy
25b NN = phen

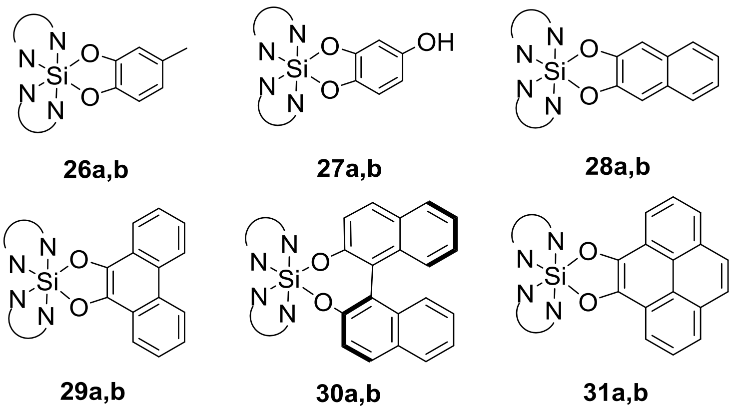

FIGURE 8: Analogous complexes **26-31** formed by the reaction of **24a** or **24b** with the appropriate arenediol.[61]

The reactivity of **24a/b** was greatly reduced with some substituted catechols. Additional bis–phenanthrolinesilicon(IV) complexes were synthesized by subsequent modifications to [Si(phen)$_2$(cat)](PF$_6$)$_2$, **25b** demonstrating the robustness of these species (SCHEME 11).

SCHEME 11: Synthesis of complexes **32-35** through reaction of **25b** with (a) potassium 4–iodylbenzenesulfonate and iodine in glacial acetic acid, (b) *N*–bromosuccinimide in CH$_3$CN, (c) 65% HNO$_3$ in glacial acetic acid, and (d) fuming HNO$_3$ in glacial acetic acid.[61]

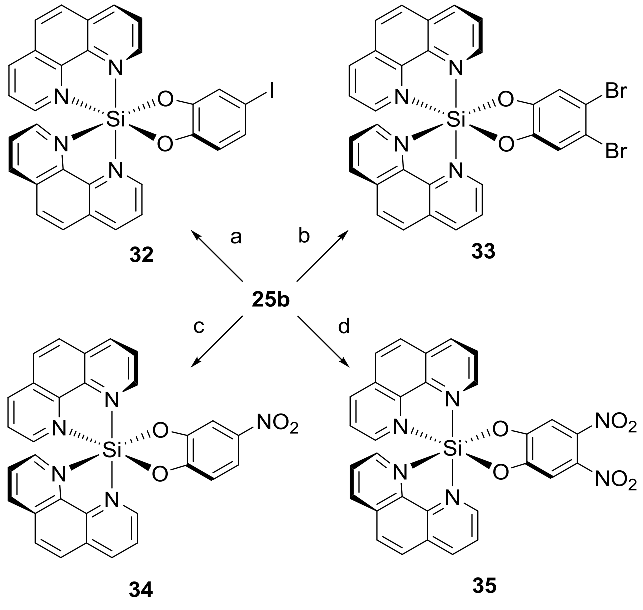

Meggers and coworkers have had considerable success in demonstrating biological activity of polypyridylsilicon(IV) complexes. In one study, they looked at the ability of a series of $[Si(phen)_2(arenediolates)]^{+2}$ to intercalate into DNA.[70] Complexes **25b**, **28b**, **29b**, and **31b** (8 μM, Tris–HCl 5mM (pH 7.4), NaCl 50 mM) were combined with a 15 mer duplex DNA (2 μM) and monitored at 260 nm while heating to obtain melting curves of the DNA. In the absence of any hexacoordinate silicon complexes, the DNA exhibited a melting temperature $T_m = 55.5 \pm 0.6$ ˚C. Very minor effects were observed with the catecholate complex, **25b** ($T_m = 56.5 \pm 1.0$ ˚C) and the 2,3–napthalenediolate complex, **28b** ($T_m = 56.2 \pm 0.9$ ˚C). A much greater melting point increase was observed with the larger arenediolate ligands 9,10–phenanthrenediolate, **29b** ($T_m = 66.4 \pm 0.6$ ˚C) and especially 4,5–pyrenediolate **31b** ($T_m = 74.8 \pm 0.1$ ˚C). Addition of **29b** and **31b** also resulted in significant changes to the CD spectrum of the DNA, reaching saturation at approximately a 1:5 DNA:complex ratio. Combination of DNA with **31b** also affected the $\pi \rightarrow \pi^*$ transition of **31b**, leading to a hypochromic and bathochromic shift. Titration experiments provided a binding constant of $(1.7 \pm 0.6) \times 10^6$ M^{-1}. Consequently, **31b** appears to intercalate into DNA with an affinity comparable to $[Ru(phen)_2(dppz)]^{+2}$ but without exhibiting the same photoactivity/phototoxicity.

In a subsequent study, Meggers and coworkers explored at the ability to detect DNA mismatches with bis–phenanthrolinesilicondiolate complexes.[71] In addition to the already proved DNA intercalator **31b**, they also looked at a methylated analog **31bMe**, and sandwich complexes with RuCp*, **31b-Ru** and **31bMe-Ru** (FIGURE 9). The sandwich complexes were synthesized by reacting **31b** or **31bMe** with

$[Cp^{*}Ru(MeCN)_3]PF_6$ to selectively afford the diastereomer which minimizes interaction between the Cp* and the phenanthroline ligands.

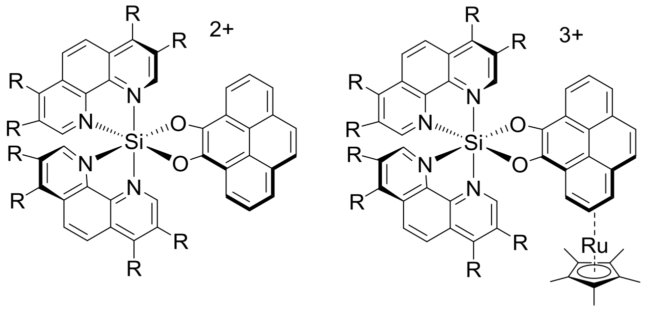

31b, R=H
31bMe, $R=CH_3$

31b-Ru, R=H
31bMe-Ru, $R=CH_3$

FIGURE 9: Complexes **31b, 31bMe**, **31b-Ru** and **31bMe-Ru** used in DNA binding experiments.[71]

Once again UV–melting curves (λ = 260 nm) were used to quantify interaction between the silicon complexes and the 19 mer DNA samples. When one equiv. of the silicon complex **31b** was combined with the correctly matched DNA duplex, a 3.0 ˚C increase in the melting point of the DNA was observed. Steric effects prevented significant intercalation of the other analogs, **31bMe** (ΔT_m = +1.1 ˚C), **31b-Ru** (ΔT_m = +0.1 ˚C), and **31bMe-Ru** (ΔT_m = ±0 ˚C). However, when a mismatched DNA duplex containing a cytosine–cytosine (CC) or cytosine–thymine (CT) mismatch was used with **31b-Ru** a large impact on the melting point was observed (ΔT_m = +7.2 ˚C for both DNA samples), much larger than the effect from **31b** (ΔT_m = +2.7 ˚C (CC) and +0.7 ˚C (CT)). Also, no significant effect was seen with either of the methylated species. The authors proposed a combined intercalation/insertion binding mode, in which the Ru–sandwich component inserts into the DNA at the site of the mismatch by ejecting the mismatched pairs and locally unwinding the DNA duplex.

The electrochemical properties of the bis–bipyridinesilicon(IV) hexafluorophosphate salts, **25a** and **36-39**, were measured using cyclic voltammetry by Maguylo *et al.* (FIGURE 10 and TABLE 5).[64] CV studies were conducted in MeCN/TBAPF$_6$ solution at a scan rate of 0.200 V/s using a platinum disk working electrode. All five complexes exhibit at least one chemically reversible reduction wave at approximately $E_{1/2}$ (+2/+1) = -1.1 V (V vs. Fc/Fc$^+$) nearly independent of the alkoxy or diolate substituent.

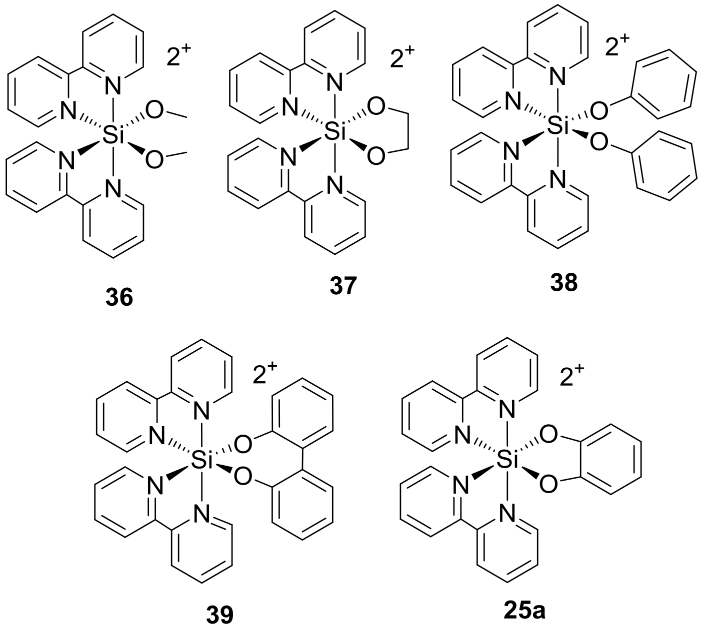

FIGURE 10: Bis–bipyridine silicon(IV) complexes **25a** and **36-39** with alkoxy– or diolate–type ligands.[64]

TABLE 5: $E_{1/2}^{o}$ and ΔE_p values for compounds **25a** and **36-39**. Electrochemistry studies conducted in MeCN/TBAPF$_6$ solution at scan rate = 0.200 V/s using a platinum disk working electrode.[64]

	$E_{1/2}^{o}$ (V vs. Fc/Fc$^+$)		
Complex	**+2/+1 (ΔE_p (mV))**	**+1/0 (ΔE_p (mV))**	**0/-1 (ΔE_p (mV))**
36	-1.147 (87) *reversible*	-1.382 (80) *limited chem. reversibility*	
37	-1.128 (86) *reversible*	-1.404 (102) *limited chem. reversibility*	
38	-1.074 (64) *reversible*	-1.359 (95) *limited chem. reversibility*	-1.911 (112) *limited chem. reversibility*
39	-1.080 (84) *reversible*	-1.366 (77) *reversible*	-1.914 (71) *limited chem. reversibility*
25a	-1.014 (75) *reversible*	-1.297 (73) *reversible*	-1.835 (93) *limited chem. reversibility*
$E_{1/2}^{o} = (E_{pc} + E_{pa})/2$; $\Delta E_p = E_{pc} - E_{pa}$			

DFT calculations also indicate that the LUMOs for all five complexes are localized on the bipyridine rings, and that the E_{LUMO} varies by less than 0.1 eV (B3LYP/6-31G*, Spartan 2010, FIGURE 11). A subsequent one–electron reduction to the neutral species was also observed for all of the species, but was chemically reversible on the CV time scale (0.200 V/s) only for the bidentate arenediolates (**39** and **25a**). In contrast to the easy reduction of the bipyridine ligand, the catechol ligand of complex **25a** was difficult to oxidize. While the catechol ligand is a well–known redox–active ligand capable of being oxidized to the semiquinone and quinone in many transition metal complexes, complex **25a** exhibited a poorly defined oxidation wave E_{pa} = +1.2 V (versus Fc/Fc$^+$) with no clear E_{pc}.

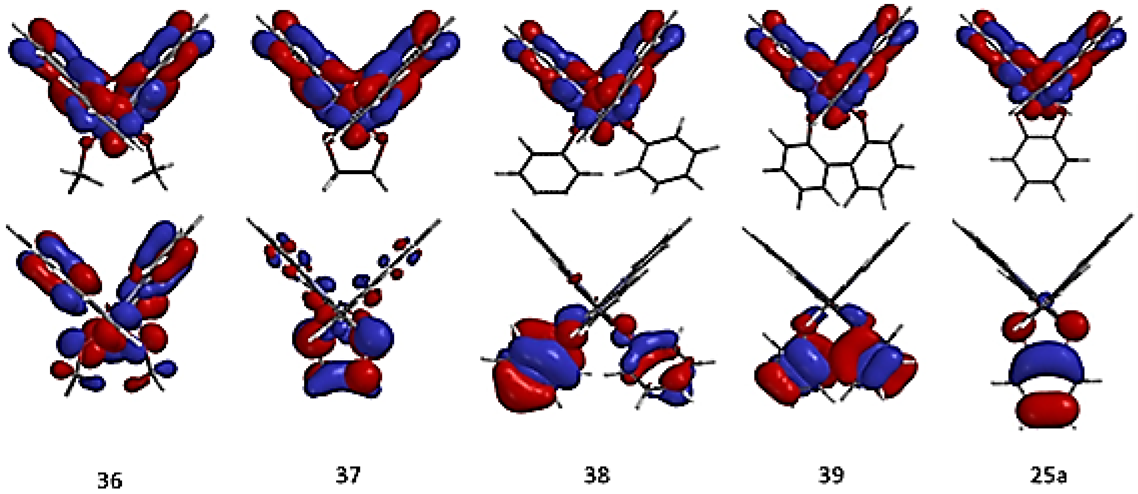

FIGURE 11: Calculated HOMO (bottom) and LUMO (top) levels of complexes **25a** and **36-39**. Calculations were performed using B3LYP/6-31G*, Spartan 2010.[64]

1.4.3. Complexes with Three Bipyridine or Phenanthroline Ligands

Tris(bipyridine)silicon(IV) was first synthesized by Herzog and Krebs in 1963.[77] Remarkably, it was first isolated as the very reactive neutral species. $Si(bpy)_3$ was synthesized by reacting two equiv. of Li_2bpy with $SiCl_4(bpy)$ in THF (SCHEME 12). Attempts to sublime $Si(bpy)_3$ under reduced pressure resulted in removal of one equiv. of bipyridine and deposition of crystals of $Si(bpy)_2$.[78] $Si(bpy)_3$ can be oxidized with halogens to generate the fully oxidized species, $[Si(bpy)_3]X_4$.

SCHEME 12: Synthesis of neutral tris(bipyridine)silicon(IV).[77]

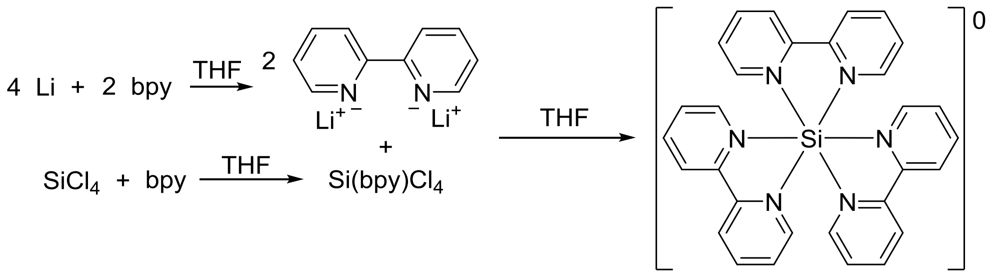

$[Si(bpy)_3]I_4$ and $[Si(phen)_3]I_4$ were also synthesized directly by combining SiI_4 with a large excess of the appropriate ligand and heating in a sealed heavy–wall glass pressure tube above the melting point of the ligand for 12 h (SCHEME 13).[79]

SCHEME 13: Synthesis of tris(bipyridine)silicon(IV) iodide by a melt reaction.[79]

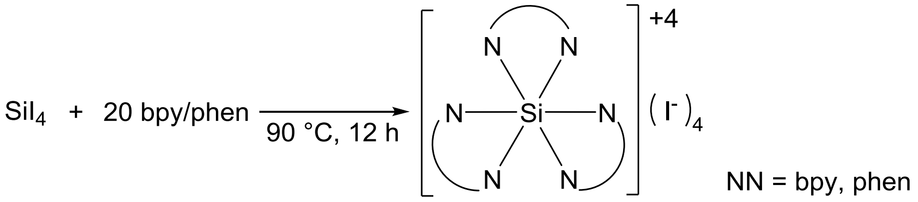

Alternatively, the reaction of SiI_4 and the appropriate ligand in pyridine or 2–methylpyridine (2–picoline) at 125 ˚C for 2 h provides the corresponding hexacoordinate species (SCHEME 14).[80]

SCHEME 14: Synthesis of tris(bipyridine)silicon(IV) iodide by a solvent–assisted reaction.[80]

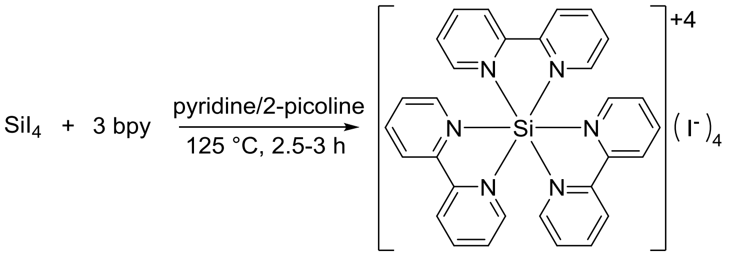

Terpyridine reacts under similar conditions with SiI_4 in pyridine to form $[Si(tpy)_2]I_4$. The polypyridylsilicon(IV) species are soluble in water as halide salts and precipitate out of solution as the hexafluorophosphate salts upon addition of $NH_4PF_6(aq)$. The hexafluorophosphate salts are soluble in acetonitrile and give ^{29}Si NMR peaks in the hexacoordinate region, ^{29}Si NMR (CD_3CN): $\delta = -155$ ppm for $[Si(bpy)_3](PF_6)_4$ and -153 ppm for $[Si(tpy)_2](PF_6)_4$. $[Si(bpy)_3]^{+4}$ and $[Si(phen)_3]^{+4}$ are inert enough to be resolved into their enantiomers with a Sephadex column and chiral tartrate mobile phases.[81-83] NMR evidence suggests that the antimonyltartrate ion approaches along the C_3 axis. Aqueous solutions of the resolved enantiomers did not undergo any change in their circular dichroism spectrum or their overall absorbance over a period of one month in solution. No structural data has been reported for any of these species.

Wieghardt has performed extensive calculations on the various charge states of polypyridyl complexes of group 14 elements.[84] In the case of silicon complexes, calculations indicate that the silicon center always remains tetravalent with ligand localized reductions. The series of redox states (+4 → -2) are best described as $[Si(bpy)_3]^{+4} \rightarrow [Si(bpy)_2(bpy^{\bullet})]^{+3} \rightarrow [Si(bpy)(bpy^{\bullet})_2]^{+2} \rightarrow [Si(bpy^{\bullet})_3]^{+1} \rightarrow [Si(bpy^{-2})(bpy^{\bullet})_2]^{0} \rightarrow [Si(bpy^{-2})_2(bpy^{\bullet})]^{-1} \rightarrow [Si(bpy^{-2})_3]^{-2}$. The most stable spin states for $[Si(bpy)_3]^{n}$ were also calculated where n = +1 ($S = ½$, $J_{calc} = -179\ cm^{-1}$), n = 0 ($S = 0$, $J_{calc} = -490\ cm^{-1}$), n = -1 ($S = ½$), and n = -2 ($S = 0$). The calculated coupling constant for singlet diradical state of $[Si(bpy)_3]^{0}$ is close to the experimentally reported value of $J_{exp} = -374\ cm^{-1}$.[85]

The redox activity of polypyridylsilicon(IV) complexes were explored using cyclic voltammetry.[80] $[Si(bpy)_3](PF_6)_4$ can be reduced electrochemically with up to 6 electrons (TABLE 6). The first three one–electron reduction waves were reversible on the electrochemical time scale. $[Si(tpy)_2](PF_6)_4$ exhibited five single–electron reduction waves. The difference between the reduction potentials is large enough to allow for the electrochemical preparation of nearly pure samples of each state. Discussion about the spectroelectrochemistry of $[Si(bpy)_3]^{+n}$ is presented in Chapter 2, and other novel hexacoordinate polypyridine silicon complexes are described in the proceeding chapters.

TABLE 6: Reduction potentials for $[Si(bpy)_3]^{+4}$ and $[Si(tpy)_2]^{+4}$ with a platinum disk working electrode in acetonitrile/0.100 M $TBAPF_6$ solution.[80]

		$E_{1/2}^{o}$ vs. Fc/Fc^+ (V)					
Compound	Solvent	+4/+3	+3/+2	+2/+1	+1/0	0/-1	-1/-2
$[Si(bpy)_3](PF_6)_4$	CH_3CN	-0.530	-0.758	-1.001	-1.453	-1.860	-2.240[a]
ΔE_p(mV)		66	66	76	72	70	74
$[Si(tpy)_2](PF_6)_4$	CH_3CN	-0.330	-0.560	-1.102	-1.419	-2.059	
ΔE_p(mV)		78	74	66	80	84	

[a]Scan rate = 0.200 V/s for all scans except $E_{1/2}^{o}([Si(bpy)_3]^{-1/-2})$ where scan rate = 0.600 V/s

$E_{1/2}^{o} = (E_{pc}+E_{pa})/2$ and $\Delta E_p = E_{pc} - E_{pa}$

1.5. Summary

Pyridine–containing ligands are one of the most important classes of ligands in coordination chemistry, and their impact on the field of hexacoordinate silicon chemistry is no exception. Fundamental studies have led to exquisite control over structure and bonding as exemplified with the oxyquinolate complexes of silacycloalkanes. The enhanced stability provided by the multidentate pyridine–containing ligands has provided new opportunities for application based research.

A wide variety of quinolate coordination complexes and polymers of Group 3 main group metals (B and Al) have been developed as efficient emitters in photoluminescent (PL) and electroluminescent (EL) applications. By comparison, very little has been reported about the fluorescence properties of the hexacoordinate silicon analogs. With its strong emission at 499 nm (DMSO, $\Phi_F = 0.98$), the 8–quinolinyl Schiff base complex, **17**, provides compelling evidence that Schiff base complexes are promising species and that further research in this area could provide a range of new PL/EL materials.

The stabilizing effect of the bipyridine ligand in $Si(bpy)(N_3)_4$, **20**, provides new opportunity for exploring high–energy material applications, especially as a potential replacement for the widely used but highly toxic primary explosive lead azide. Furthermore, variation of the diimine ligand could provide a tool for tuning the sensitivity, stability, hygroscopicity, and other properties of importance for explosive applications.

The development of silicon phthalocyanine (Pc 4) for photodynamic therapy has established a precedent for biological activity and pharmaceutical applications of hexacoordinate silicon complexes.[86-89] Polypyridylsilicon(IV) complexes appear to be promising new candidates for biological activity and applications, as structural analogs of transition metal complexes without the inherent phototoxicity. They are sufficiently stable with respect to hydrolysis and racemization, and the great versatility of the diimine ligand motif promises tremendous opportunity for tailoring the transport and binding properties of these complexes.

In transition metal coordination complexes, redox activity is often metal–centered with some degree of ligand noninnocence. In the case of the polypyridylsilicon(IV) complexes, such as $[Si(bpy)_3]^{+4}$, theoretical and experimental evidence both indicate that electrochemical reduction is almost entirely ligand–based. The silicon(IV) center makes the polypyridine ligand easy to reduce, with an anodic shift of 2 V relative to the first reduction potential of free bipyridine. The extensive redox chemistry along with the chemical stability of multiple oxidation states provides an opportunity to explore polypyridinesilicon(IV) complexes for electronic applications.

The ability of the pyridine–containing ligands to provide chemical stability, resistance to hydrolysis, and structural rigidity while at the same time providing a site for redox activity and/or photoluminescence capability, demonstrates their value as a ligand class for hexacoordinate silicon complexes. Pyridine–containing ligands are likely to feature prominently in the future development of the field of hexacoordinate silicon chemistry.

CHAPTER 2: ELECTROCHROMIC MATERIALS AND TRIS(BIPYRIDINE)SILICON(IV)

2.1. Introduction

Electrochromism is the characteristic of a material to change its absorbance in the visible part of the electromagnetic spectrum upon application of an electric field. Materials are classified as cathodic if they are positively–charged and thus interact and are reduced at the cathode or anodic if they are negatively–charged and thus interact and are oxidized at the anode. Electrochromic materials as a whole are rather popularly studied, boasting almost 7000 references in Chemical Abstracts at the time of this dissertation relating to the topic, including over one third of those referring to patents. Both anodic materials, such as with iron(II) hexacyanoruthenate(II) (ruthenium purple) or [β–(10–phenothiazyl)propoxyl]phosphonic acid,[90-91] and cathodic materials, are typically employed in tandem for electrochromic devices. A broader introduction to applications and devices will be presented in Chapter 4 while this chapter will focus further on the main types of materials being investigated for electrochromism and the author's contribution to the field.

2.1.1. Metal Oxides

The first use of tungsten(VI) oxide, WO_3, and the first discovery of the electrochromic effect, occurred in the work of Satyen Deb at the American Cyanamid Company in the late 1960s when he evaporated a 1 μm thick film of WO_3 onto glass with gold contacts in order to measure its electrical conductivity. He was able to observe a half hour change from a colorless bleached state to a blue reduced state and used it in conjunction with a photoconductive film to produce an image in his device (FIGURE 12).[92] He would also later expand this work by preparing films of different thicknesses as well as comparing amorphous versus annealed (crystalline) films and found an increase and red shift in the absorbance upon annealing of the films (FIGURE 13).[93]

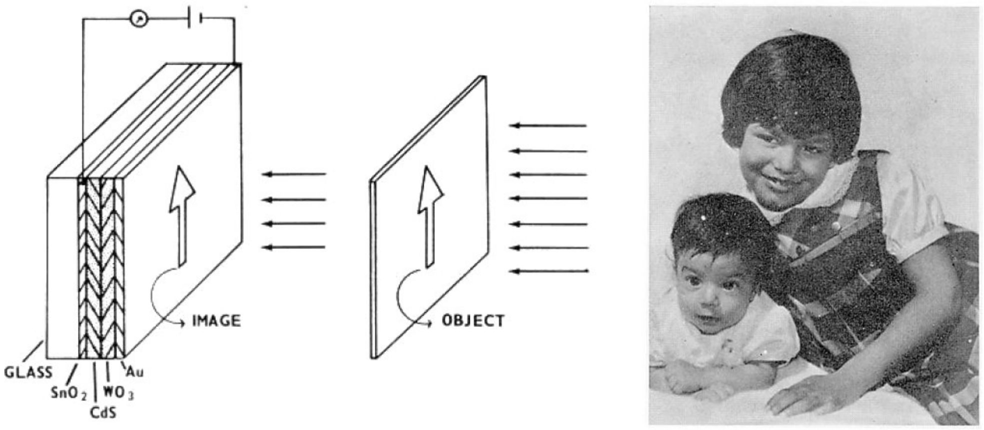

FIGURE 12: (left) Diagram of an electrophotographic arrangement using WO_3 as an electrochromic material. (right) Photograph of an image recorded on the electrophotographic structure.[92]

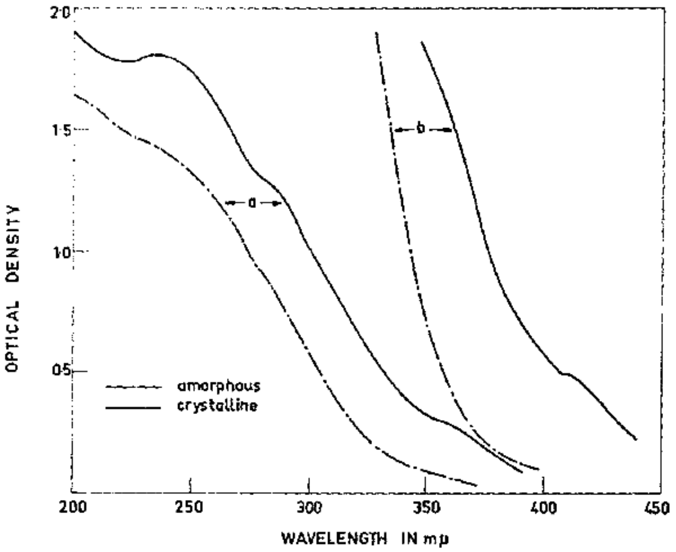

FIGURE 13: Absorption spectra of amorphous and crystalline films with thickness (a) 0.05 μm and (b) 1 μm of WO_3 at room temperature.[93]

40 years of work have now gone into improving the response of metal oxide materials, especially with tungsten(VI) oxide.[94-96] Cheng *et al.* produced two different films of WO_3, the first by dipping ITO–coated glass into a solution of tungsten(VI) chloride in absolute ethanol and letting the solvent evaporate while simultaneously oxidizing the tungsten in air at 40 ˚C. To a second solution, they added the tri–block copolymer Pluronic P_{123} purchased from BASF which segregated the tungsten upon drying and by extracting the copolymer and calcining the film at 300 or 400 ˚C for two h, were able to produce a mesoporous film of WO_3 with non–ordered pores between 4 and 5 nm in diameter. Upon testing the coloration of their films, the sol–gel–produced first film begins to decay rapidly upon cycling but the crystalline films show much greater stability.[97] Djaoued, Balaji, and Brüning focused on grain size of their films using organically modified silicates as a template material and annealed at 400, 500, and 600 ˚C to obtain 10, 19, and 25 nm grain sizes respectively (FIGURE 14). The electrochromism of the films calcined at the lower relative temperatures are rather similar bleached (yellow) and colored (blue) states in terms of % transmittance, but the 600 ˚C film does not reach 0% transmittance as the other films do and is instead green in color.[98]

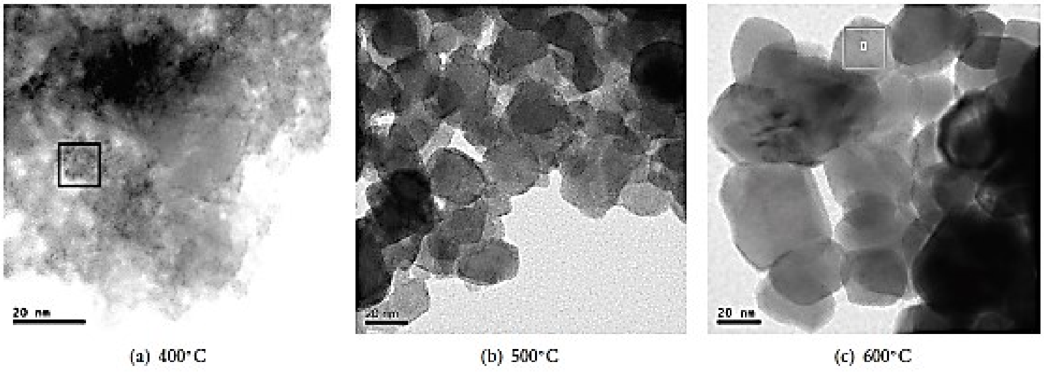

(a) 400°C (b) 500°C (c) 600°C

FIGURE 14: Transmission electron micrographs of tungsten oxide films prepared at 400 (grain size ~ 10 nm), 500 (grain size ~ 19 nm), and 600 ˚C (grain size ~ 25 nm).[98]

While tungsten oxide is a cathodically–coloring material, anodically–coloring metal oxides are known as well, such as commercially–used iridium oxide, which can be produced in a variety of iridium:oxygen:hydrogen ratios depending on the thin film preparation process. Ito and coworkers produced films of iridium oxide by reactive radio–frequency magnetron sputtering in either an oxygen or water atmosphere as different substrate temperatures (Ts).[99] The films that were produced at lower temperatures (-30 and 20 °C) were flat and smooth, while the films produced at higher temperatures (70 and 130 °C) were much rougher (SEM images, FIGURE 15). By applying voltages of -0.25 and +1.25 V vs. Ag/AgCl in 0.5 M aqueous sulfuric acid with 100 nm thick films, transition between bleached (-0.25 V) and colored (+1.25 V) states was achieved. The authors note that the films produced in the oxygen atmosphere are more likely to have pure iridium(IV) oxide (IrO_2) versus those formed in the water atmosphere, and that pure IrO_2 remains dark even upon application of a bleaching reduction potential (transmittance spectra, FIGURE 15).

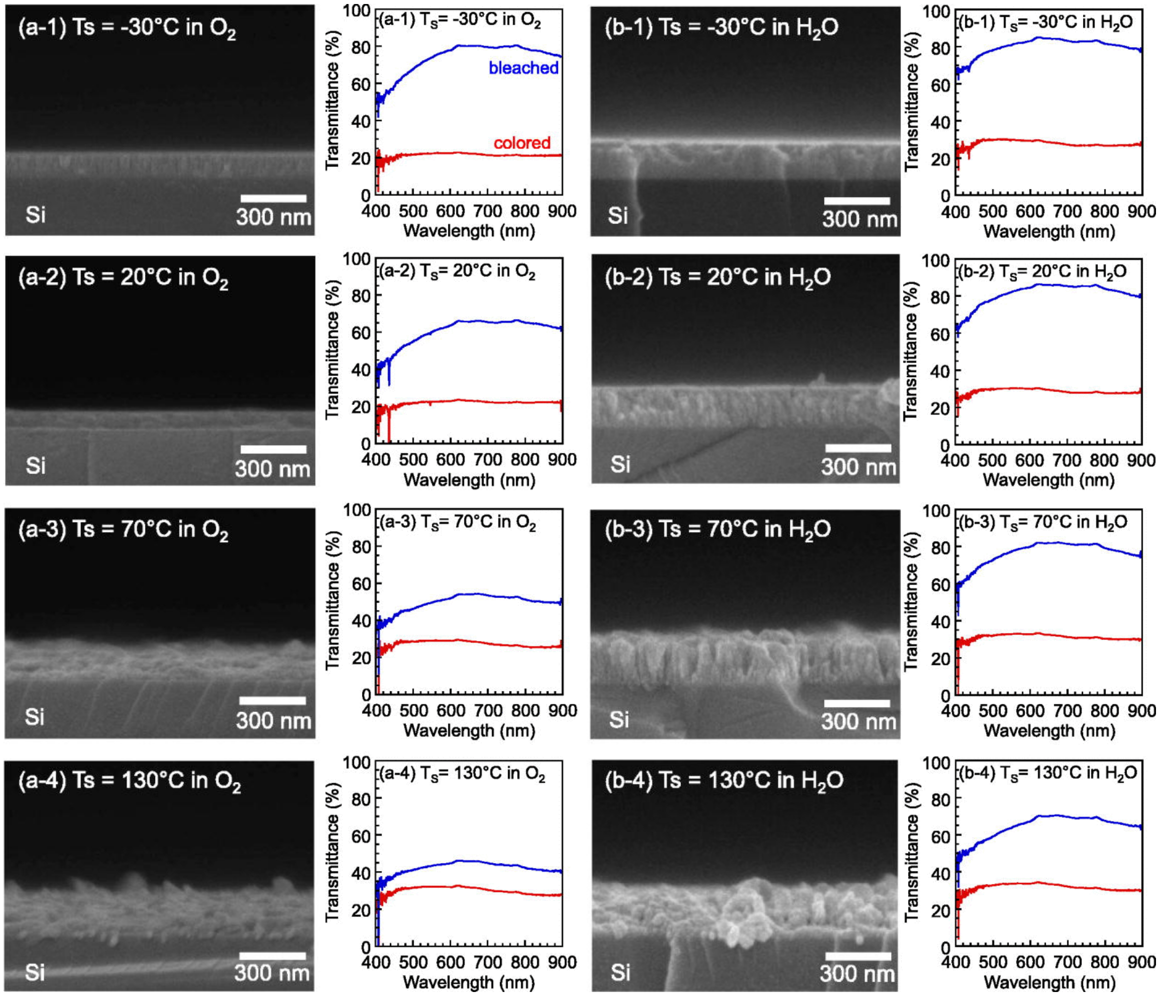

FIGURE 15: SEM images and transmittance spectra (blue = bleached, -0.25 V and red = colored, +1.25 V) of iridium oxide films prepared at different temperatures in (left) oxygen and (right) water atmospheres.[99]

2.1.2. Organic Electrochromic Materials

Two types of organic electrochromic materials are typically employed in electrochromic devices, *N*,*N*–dialkyl or *N*,*N*–diaryl–4,4'–bipyridinium salts, also called viologens (FIGURE 16), and conjugated organic polymers. Each will be presented in more depth herein.

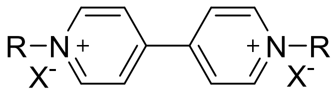

FIGURE 16: General structure of a viologen where R is any alkyl or aryl group and X^- is any halide or equivalent ion, such as tetrafluoroborate or triflate.

2.1.3. Viologens

Viologens are rather simple materials, consisting of two pyridine rings that can be alkylated or arylated to form a dicationic salt. They are called viologens because of the purple color produced upon the first reduction of the dication.[100] All of them being initially colorless, methyl viologen (MV) reduces to purple,[91] heptyl viologen (HV) reduces to purplish–red,[101] and vinyl benzyl viologen (VBV) reduces to dark blue,[102] and each diradical species is a light yellow color but with poor reversibility (FIGURE 17). The *N*,*N*'–substituent does slightly change the color produced by the singly–reduced species but the restriction to shades of blue and violet limit their potential uses.

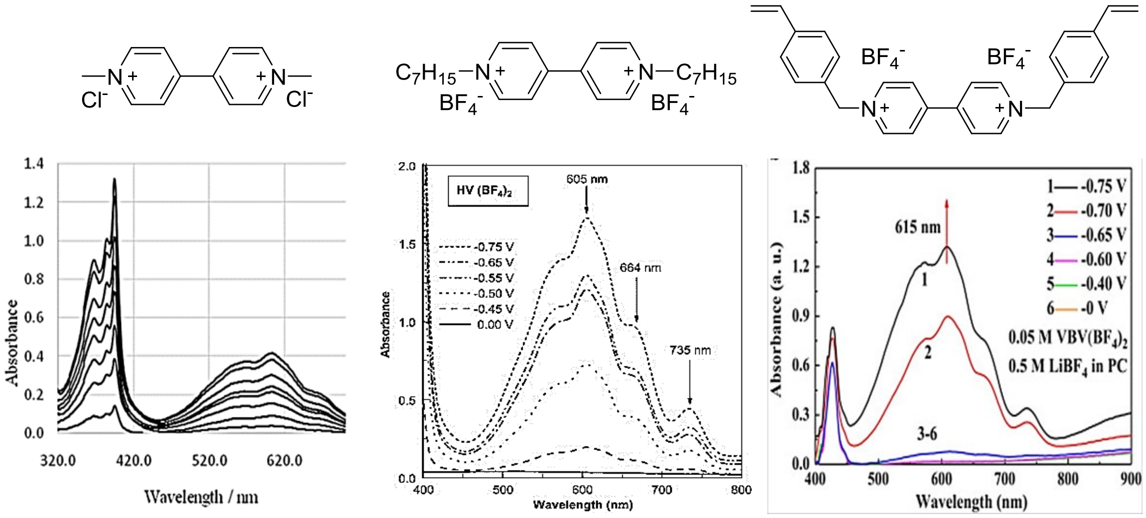

FIGURE 17: (left) Structure of methyl viologen and UV–Vis spectra measured at 20–second intervals with an applied potential of -0.9 V.[103] (middle) Structure of heptyl viologen and UV–Vis spectra measured at the indicated reduction potentials vs. Ag/Ag^+.[104] (right) Structure of vinyl benzyl viologen and UV–Vis spectra measured at the indictated reduction potentials vs. Ag/Ag^+.[102]

It must be mentioned that methyl viologen, also called paraquat, is frequently used as an herbicide because of many favorable properties such as not being absorbed through unbroken skin and allowing the roots to remain intact, preventing soil erosion. However, the Environmental Protection Agency (EPA) has labeled paraquat as Toxicity Category I by inhalation, Category II by ingestion, and Category III by skin contact, with Category I being the worst, as well as being associated with Parkinson's disease through its neurotoxicity, so diminished use of the compound in any application is to be desired.[105]

2.1.4. Conjugated Organic Polymers

Conjugated organic polymers have been a widely studied area for electrochromic applications and often possess a lot of variability in the backbone and as substituents off the main chain.[106-112] Conjugation is the necessary characteristic of these materials because it provides a tunable $\pi \rightarrow \pi^*$ transition in the material and changing the main chain and pendant components allows for adjustment of this transition.[113] The coloring of these polymers is dependent upon the formation of charge carriers such as polarons, bipolarons, and solitons, and on the injection of ions into the polymer upon reduction or oxidation.[114]

Polypyrrole (PPy) is an electropolymerized material that is known to give rigid straight–chain polymers with poor solubility and poor intercalation of ions because of this rigidity. Ak *et al.* were able to copolymerize pyrrole with a thiophene–containing octa(phenyl)silsesquioxane (OPS) to form an OPS–PPy polymer (FIGURE 18).[115] The relatively large silsesquioxane nanocages prevent the organization of the polymer into rigid chains and thus upon reduction, a larger change in the percent transmission was realizable from 17% in the pure PPy polymer to 30% in the OPS–PPy polymer (FIGURE 19).

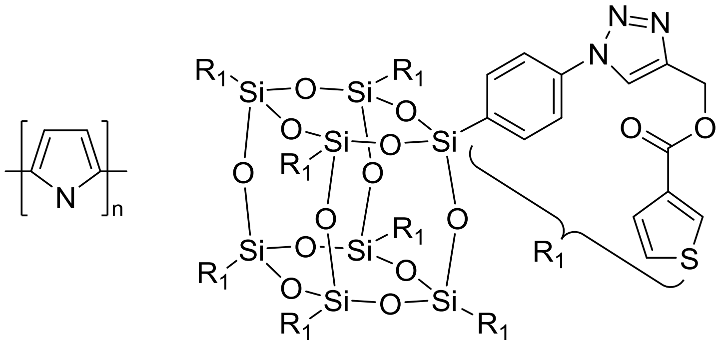

FIGURE 18: (left) Structure of polypyrrole (PPy) and (right) structure of a thiophene–containing octa(phenyl)silsesquioxane capable of being incorporated with Ppy by copolymerization at the thiophene ring.[115]

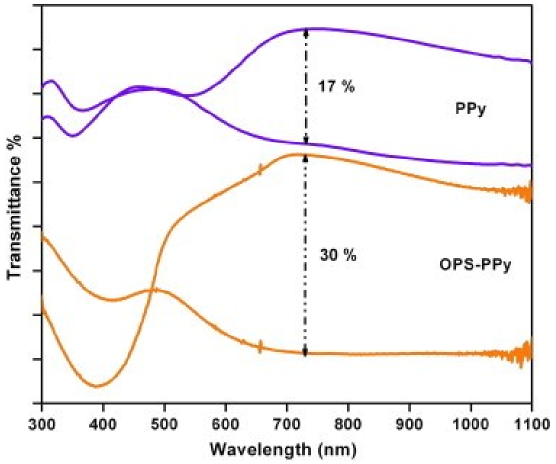

FIGURE 19: Transmittance spectra of PPy and OPS–PPy in two extreme (oxidized and neutral) states.[115]

Data and coworkers were able to synthesize a selenophene polymer with a position to change the alkyl chain off of each monomer unit.[116] They were able to produce one brown polymer film and three purple films with absorbance maxima at 511, 538, 546, and 556 nm. Upon reduction, these polymers lost their peak in the visible part of the spectrum and gained very wide–ranged absorption over their entire spectral range of 300-1700 nm with every wavelength absorbing greater than 0.10 absorbance units for their thin films (FIGURE 20). In order to obtain absorbance in such low–energy wavelengths, the authors surmise that diradical bipolarons must be forming within the polymer chain.

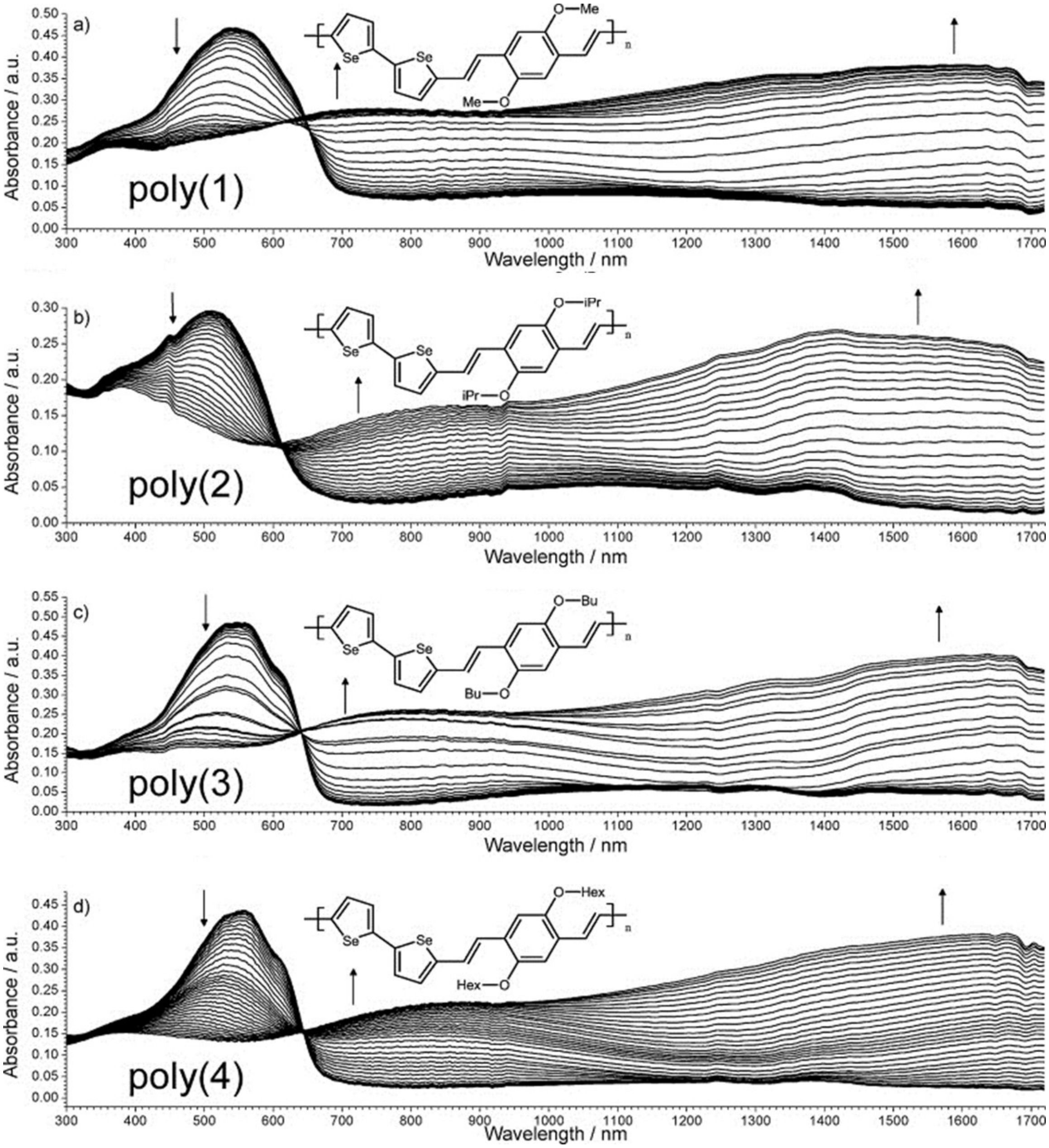

FIGURE 20: UV–Vis spectra of four different alkylated polyselenophenes upon electrochemical oxidation.[116]

There are a few examples that tie these two types of organic materials together.[117] DeLongchamp *et al.* were able to formulate a layer–by–layer process by using an anionic–based dispersion poly(3,4–ethylene dioxythiophene):poly(styrene sulfonate), which separately abbreviate as PEDOT and SPS, and a cationic viologen polymer, poly(hexyl viologen), abbreviated PXV (FIGURE 21).[118] They were able to produce films that could transition from an oxidized (0.5 V) colorless state to blue (-0.4 V) and purple (-0.9 V) reduced states.

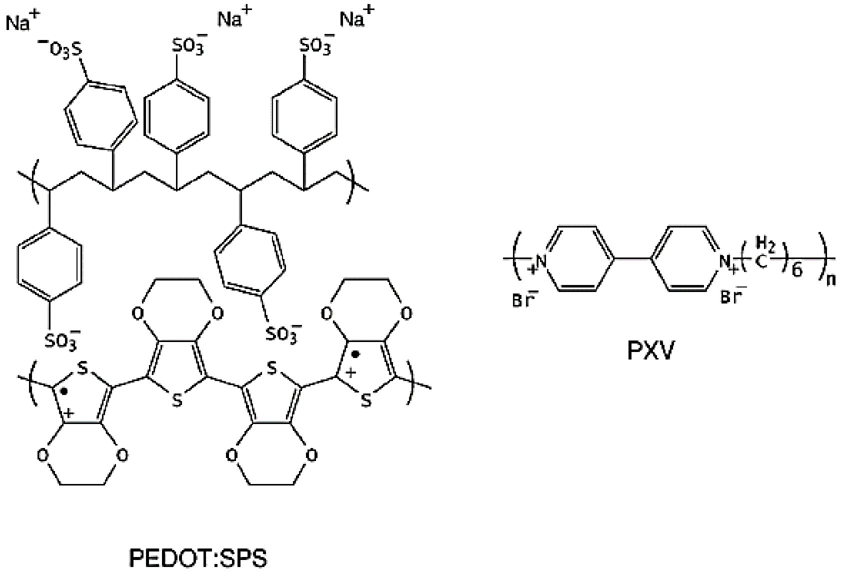

PEDOT:SPS

PXV

FIGURE 21: Anionic (PEDOT:SPS) and cationic (PXV) components used in a layer–by–layer dual electrochromic device.[118]

These layer well together because of electrostatic attraction, but Keshtov *et al.* indicate that trap states are likely because of interlayer joints and that reproducibility of this process is variable. With other neutral polymers, like pure PEDOT, phase separation with polyviologens is very apt to occur due to the polymer being neutral and the bipyridinium salts being positively charged. Keshtov was able to formulate an alternating copolymer between a pyridinium salt (4,4'–(1,4–phenylene)bis[2,6 –diphenyl]–pyridine) and several triaryl amines (FIGURE 22).[119] Each of these polymers was able to be reduced twice to form a violet diradical pyridinium species, similar to that of methyl viologen. However, the researchers' focus was on the two oxidations present in polymers using the **IVb** component from FIGURE 22, which went from the initial light yellow to having a peak at 850 nm (0-1.0 V vs. Ag/AgCl) and then disappearance of that peak with a new peak at 620 nm (1.0-1.2 V vs. Ag/AgCl).

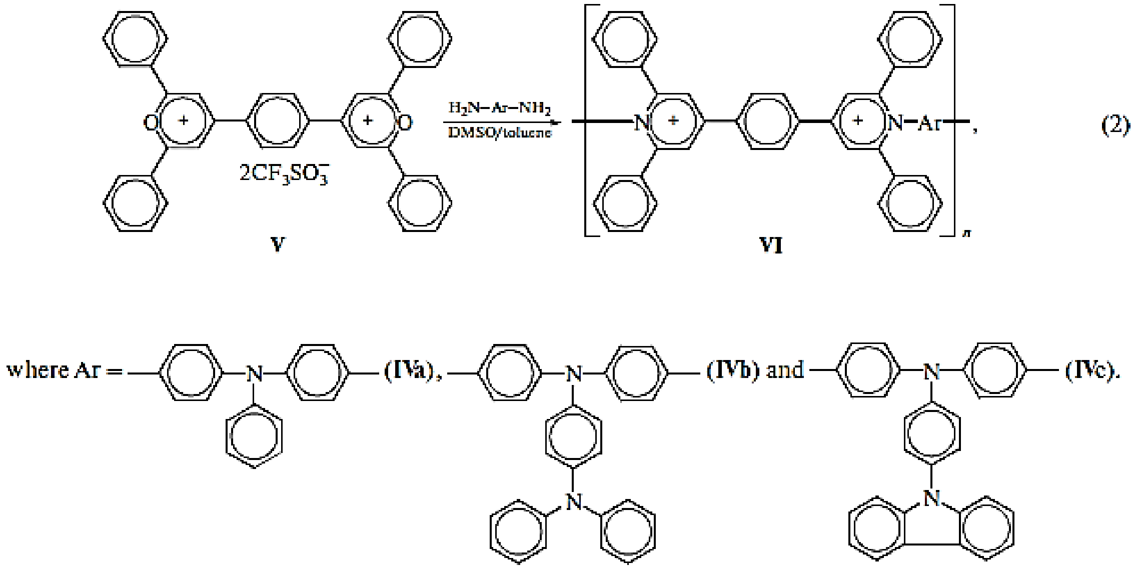

FIGURE 22: Electrochromic polymer consisting of pyridinium salts and triaryl amines.[119]

2.1.5. Transition Metal Complexes

The noninnocence of the 2,2'–bipyridine ligand has led to extensive experimental and theoretical research in recent years to assign oxidation states to reduced species of coordination complexes containing this ubiquitous ligand.[84, 120-128] UV–Vis/NIR spectroscopy has often been used to distinguish neutral bipyridine ligands from singly or doubly reduced ligands.[129-131] Polypyridyl transition metal complexes have been extensively explored for potential electrochromic applications and reviewed by Mortimer,[132] but electrochromism has most frequently been observed using ruthenium–based compounds.[133-137] Heath *et al.* reported the spectroelectrochemistry of $[Ru(bpy)_3]^{+2}$ and were able to attribute the observed transitions as either metal–to–ligand charge transfer, neutral bipyridine π → π* transitions, or π → π* transitions of the radical bipyridine anions generated upon reduction of the complex, as shown in FIGURE 23.[133] As expected, the π → π* transitions of the neutral ligand weaken and the π → π* of the radical anionic ligand strengthen as the complex is subsequently reduced three times. However, it is also notable that the MLCT band redshifts with these reductions as well, and since this absorption lies in the visible part of the spectrum, shifting of this peak corresponds to a change in color of the compound.

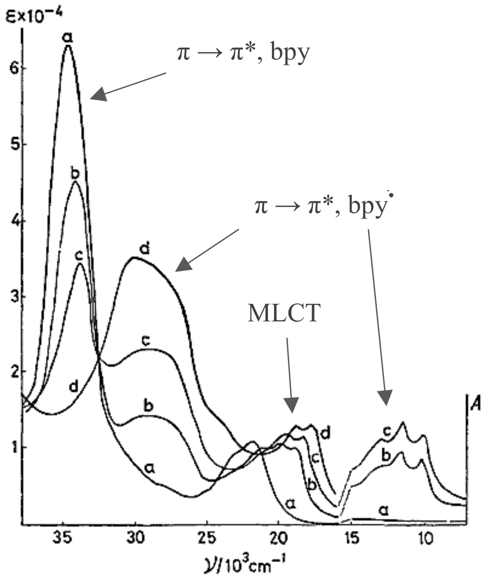

FIGURE 23: Absorption spectra of $[Ru(bpy)_3]^z$, where (a) z = +2, (b) z = +1, (c) z = 0, (d) z = -1, with corresponding transitions labeled.[133]

Elliott and Hershenhart took advantage of the ligand reduction's ability to affect the MLCT band of ruthenium complexes and prepared several complexes with ring–substituted bipyridines.[138] They were able to minimally achieve 3 reductions and one oxidation with each of the complexes (including $[Ru(bpy)_3]^n$) and the first reduction potential was roughly 1 V less negative compared to that of the free ligand. With the 4,4'–bis(ethoxycarbonyl)–2,2'–bipyridine and 5,5'–bis(ethoxycarbonyl)–2,2'–bipyridine, they were even able to achieve six reductions per complex. Pichot, Beck, and Elliott studied this further and explored double– and triple–bond substituents off the 5– and 5'–positions of the bipyridine ligand in ruthenium complexes (FIGURE 24).[134] The same correlation between ligand reduction potential and that of the complex was still present and they were able to get 4 or 6 reductions with each ligand, except for the imide complex for which they proposed decomposition due to the reactivity of noncyclic imides. Reduction of the complexes produced a variety of colors, shown in TABLE 7.

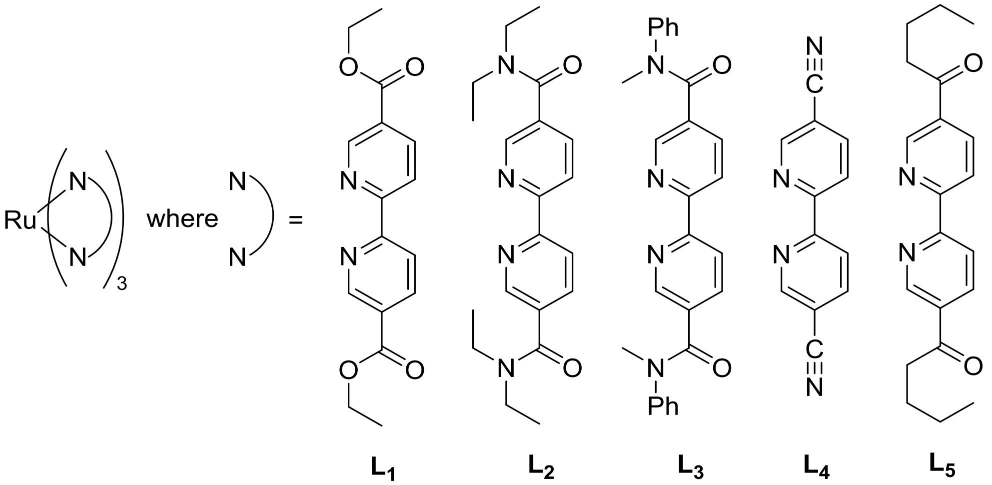

FIGURE 24: Homoleptic bipyridine ruthenium(II) complexes with double– and triple–bond substituents at the 5– and 5'– positions. L_1 = 5,5'–bis(ethoxycarbonyl)–2,2'–bipyridine, L_2 = 5,5'–bis(diethylamido)–2,2'–bipyridine, L_3 = 5,5'–di(*N*–methyl–*N*–phenylamido)–2,2'–bipyridine, L_4 = 5,5'–dicyano–2,2'–bipyridine, and L_5 = 5,5'–di(1–ketobutyl)–2,2'–bipyridine.[134]

TABLE 7: Observed colors for Ru(L)$_3$ complexes, where L_1 = 5,5'–bis(ethoxycarbonyl)–2,2'–bipyridine, L_2 = 5,5'–bis(diethylamido)–2,2'–bipyridine, L_3 = 5,5'–di(*N*–methyl–*N*–phenylamido)–2,2'–bipyridine, L_4 = 5,5'–dicyano–2,2'–bipyridine, and L_5 = 5,5'–di(1–ketobutyl)–2,2'–bipyridine.[134]

formal RuL_3 redox state	L_1	L_2	L_3	L_4	L_5
+2	orange	orange	orange	red–orange	red–orange
+1	purple	wine red	gray–blue	purple	red–brown
0	blue	purple	turquoise	blue	purple–brown
−1	green	blue	green	turquoise	gray–blue
−2	brown			aquamarine	green
−3	red			brown–green	purple

Polymerization schemes have been developed to deposit films of polypyridyl transition metals for electrochromic devices. Two of these schemes are an electroreductive precipitation adsorption process made by forming a bimetallic chain of ruthenium and iron using a 4',4''''–[(2,2'–bipyridine)–4,4'–diylbis(2,1–ethanediyl–4,1–phenylene)]bis(2,2':6',2''–terpyridine) bridging ligand (FIGURE 25)[136] and electropolymerization of vinyl–substituted polypyridine ruthenium complexes (FIGURE 26).[139-140] However, the presence of the MLCT transitions in transition metal complexes is generally undesirable for electrochromic applications requiring a colorless state.

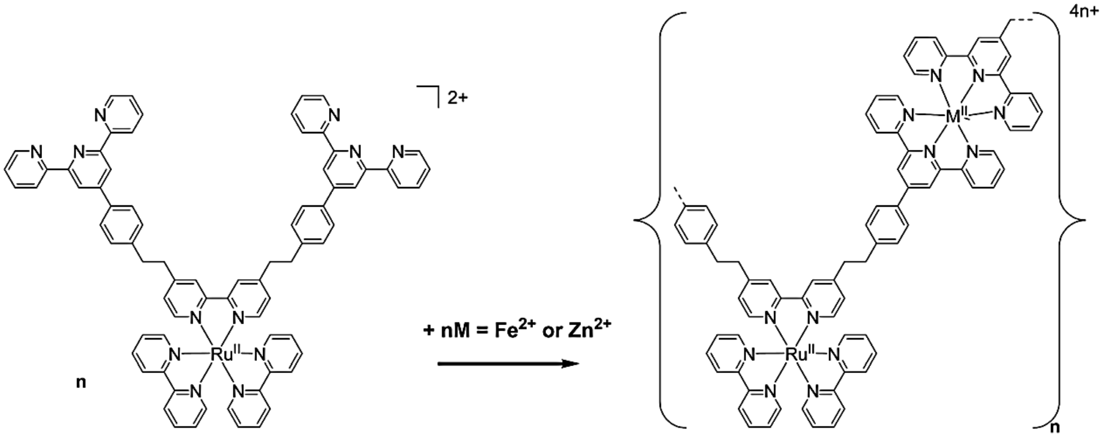

FIGURE 25: Chemical formulation of bimetallic polymers using a terpyridine–bipyridine–terpyridine bridging ligand.[136]

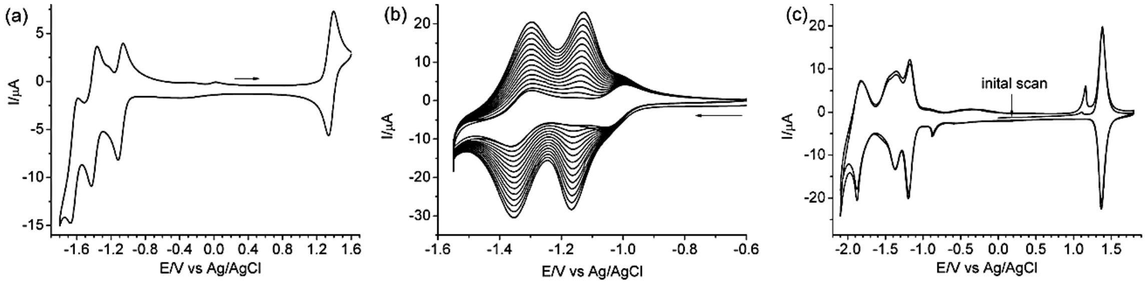

FIGURE 26: (a) CV of $[\mathrm{Ru(bpy)_2(5dvbpy)}](\mathrm{PF_6})_2$ in MeCN at a Pt electrode. (b) Reductive electropolymerization of $[\mathrm{Ru(bpy)_2(5dvbpy)}](\mathrm{PF_6})_2$ (0.5 mM in MeCN) on a Pt–disk electrode ($d = 2$ mm) by 15 repeated cyclic potential scans at 0.100 V/s between -0.60 and = 1.55 V vs. Ag/AgCl in 0.1 M $\mathrm{TBAClO_4}$/MeCN. (c) CV of the polymeric films obtained in (b) at a scan rate of 0.100 V/s in a clean supporting electrolyte solution.[140]

2.2. Results and Discussion[141]

Tris(bipyridine)silicon(IV), $[\mathrm{Si(bpy)_3}]^{+4}$, is analogous to the transition metal complexes, but in the case of bipyridine complexes of silicon, DFT calculations by Wieghardt and coworkers indicate a strong preference for the central atom to remain tetravalent with ligand–localized reductions.[84] Their calculations predict that $[\mathrm{Si(bpy)_3}]^{+1}$, for example, should contain three ligand–localized SOMOs ($\leq$ 3% Si character), and Mulliken spin density population analysis places one unpaired spin on each ligand and < 0.01 on the silicon atom. It therefore has the predicted electronic structure $[\mathrm{Si(bpy^{\bullet})_3}]^{+1}$.

As mentioned in Section 1.4.3, tris(bipyridine)silicon(IV) can be produced by several different synthetic routes. With the neutral reactive $[\mathrm{Si(bpy)_3}]^{0}$ complex being first isolated by Herzog and Krebs,[77] the +4 complex was not produced until contributions were made by Kummer *et al.* with two separate routes, one which involved oxidation of the $[\mathrm{Si(bpy)_3}]^{0}$ complex with elemental halogens, and the other which used silicon(IV) iodide ($\mathrm{SiI_4}$) and combined it with bipyridine in large excess (20 equiv.) as the solvent component.[79] This work was expanded by Suthar *et al.* by a solvent-assisted synthesis route using 2–picoline, SiI_4, and a more conservative ligand ratio (4 equiv.).[80] Although presented in the earlier chapter, the first and third synthetic routes are discussed further for the synthesis of novel polypyridine complexes in Chapter 3. Conversion to the hexafluorophosphate salt was reported as being done with addition of ammonium hexafluorophosphate (NH_4PF_6) after dissolution of the iodide salt in water and flash chromatography through silica, although working material was obtained through simple metathesis with NH_4PF_6 after dissolution in water. It must be noted that the material obtained through simple metathesis did not pass elemental analysis (EA), but did exhibit a clean ^1H NMR spectrum and CV before use in spectroelectrochemical characterization. Specific experimental parameters are presented in Section 2.4 and a brief discussion on attempted purification processes is given in Chapter 3.

Suthar explored the electrochemistry of $[Si(bpy)_3]^{+4}$ using cyclic voltammetry (FIGURE 27) and found that it exhibits three chemically reversible, one–electron reductions ($E_{1/2}^o$ (+4/+3) = -0.530 V, $E_{1/2}^o$ (+3/+2) = -0.758 V, and $E_{1/2}^o$ (+2/+1) = -1.001 V vs. Fc/Fc^+ at a platinum disk working electrode in acetonitrile/$TBAPF_6$ solution). These reduction potentials are much less negative than those of other bipyridine coordination complexes due to the tetravalent silicon center. Three additional reductions were observed, but they were only partially chemically reversible on the timescale of the CV.[80]

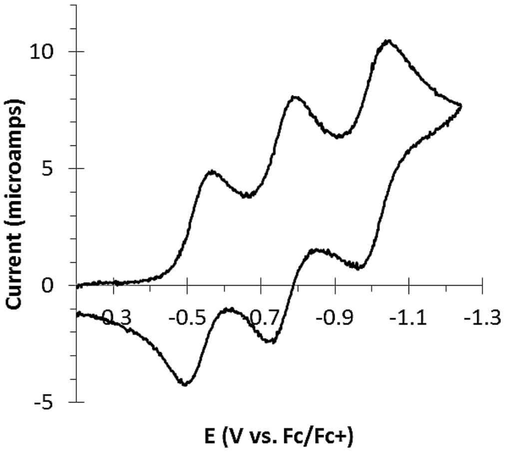

FIGURE 27: Cyclic voltammagram of $[Si(bpy)_3](PF_6)_4$ in acetonitrile/0.100 M $TBAPF_6$ vs. Fc/Fc^+ with a platinum disk working electrode. Scan rate = 0.200 V/s with iR compensation.[80]

The difference between the reduction potentials is large enough to allow for the electrochemical preparation of nearly pure samples of each state, as seen in the mole fraction distribution (FIGURE 28). The +3 and +2 species reach 98% mole fraction and the +4 and +1 can each exceed 99.9% at 25 ˚C. Consequently, an *in situ* spectroelectrochemical analysis of the first three reduced states $[Si(bpy)_3]^{+n}$ (n = 3, 2, 1) is possible.

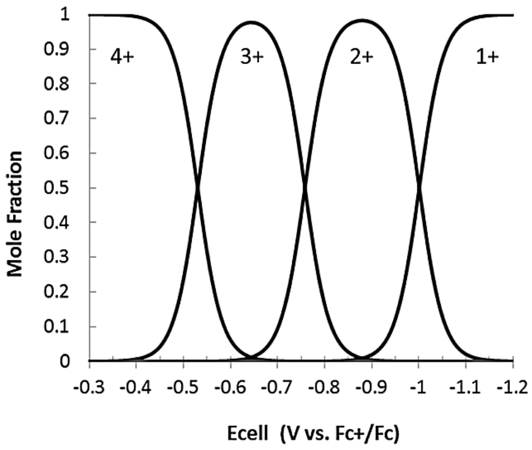

FIGURE 28: Mole fraction of $[Si(bpy)_3]^{4+}$ calculated from observed reduction potentials at 25 ˚C.

The UV–Vis spectrum of each state was obtained using an argon–flushed spectroelectrochemical cell with a 1.0 mm pathlength that consisted of a printed gold honeycomb working electrode, a gold counter electrode, and a Ag/AgCl reference electrode standardized to the ferrocene/ferrocenium couple. A schematic of the cell and electrodes is shown in FIGURE 29.[142] The working electrode operates at the honeycomb portion of the electrode card and thus oxidizes or reduces the solution specifically within the pores, allowing spectroscopic analysis on the solution inside the pores. The counter electrode is printed on the same card but primarily interacts with the solution in the upper part of the cell and does not affect the spectroscopic measurements. These are both connected to the potentiostat through a microUSB connection at the top of the card. The reference electrode is connected separately as a Ag/AgCl electrode with a saturated potassium chloride (KCl) solution. Bubbling with argon is done only in the upper portion of the cell but can be transferred throughout the entire cell by sliding the electrode card up and down.

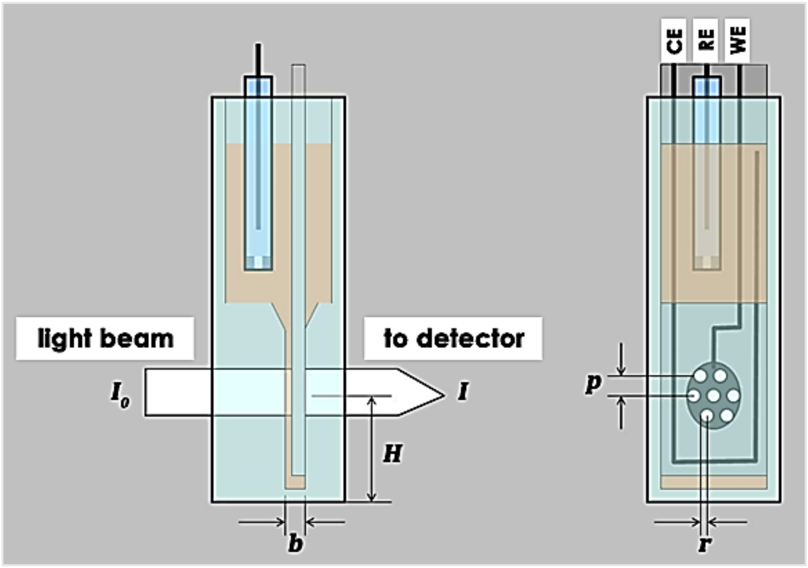

FIGURE 29: Spectroelectrochemical analysis with the honeycomb electrode.[142]

Samples of $[Si(bpy)_3](PF_6)_4$ were dissolved in an anhydrous acetonitrile solution that was 0.100 M in $TBAPF_6$. By using the potentials indicated by the CV and since the mole fraction distribution predicts smooth and full transitions of each species, the UV–Vis spectra corresponding to each reduced state can be obtained and confidently assigned (FIGURE 30). By measuring in smaller steps rather than larger ones to target each state, smooth transitions in the UV–Vis spectra of each species can be generated, such as with the +4 → +3 transition from -0.445 to -0.645 V vs. Fc/Fc^+ where clear isosbestic points can be noted at 216, 237, 314, and 352 nm (FIGURE 31). The fully oxidized +4 species can be recovered completely after each reduction.

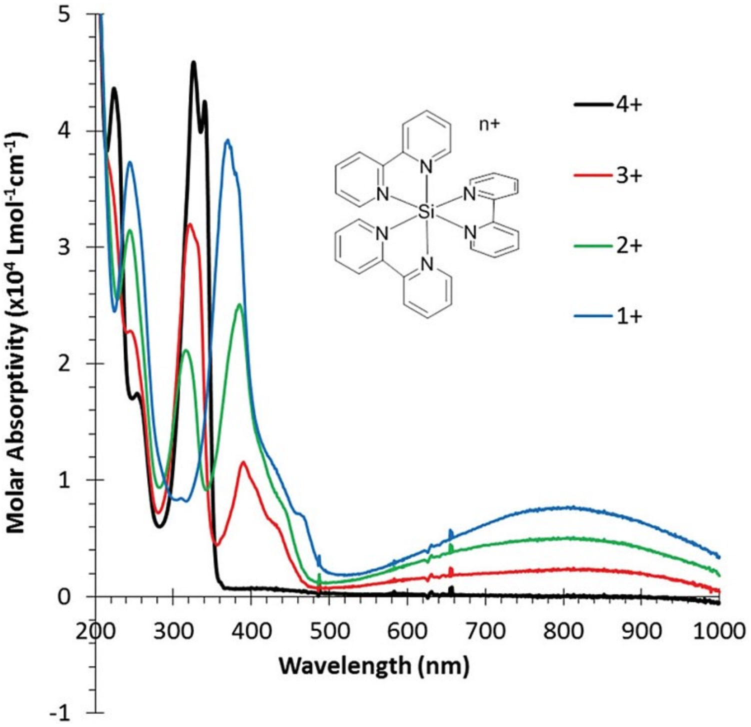

FIGURE 30: UV–Vis spectra of $[Si(bpy)_3]^{+n}$ states generated electrochemically at -0.445 V (black line, n = 4), -0.645 V (red line, n = 3), -0.895 V (green line, n = 2), and -1.095 V (blue line, n = 1) vs. Fc/Fc^+ with a gold working electrode.

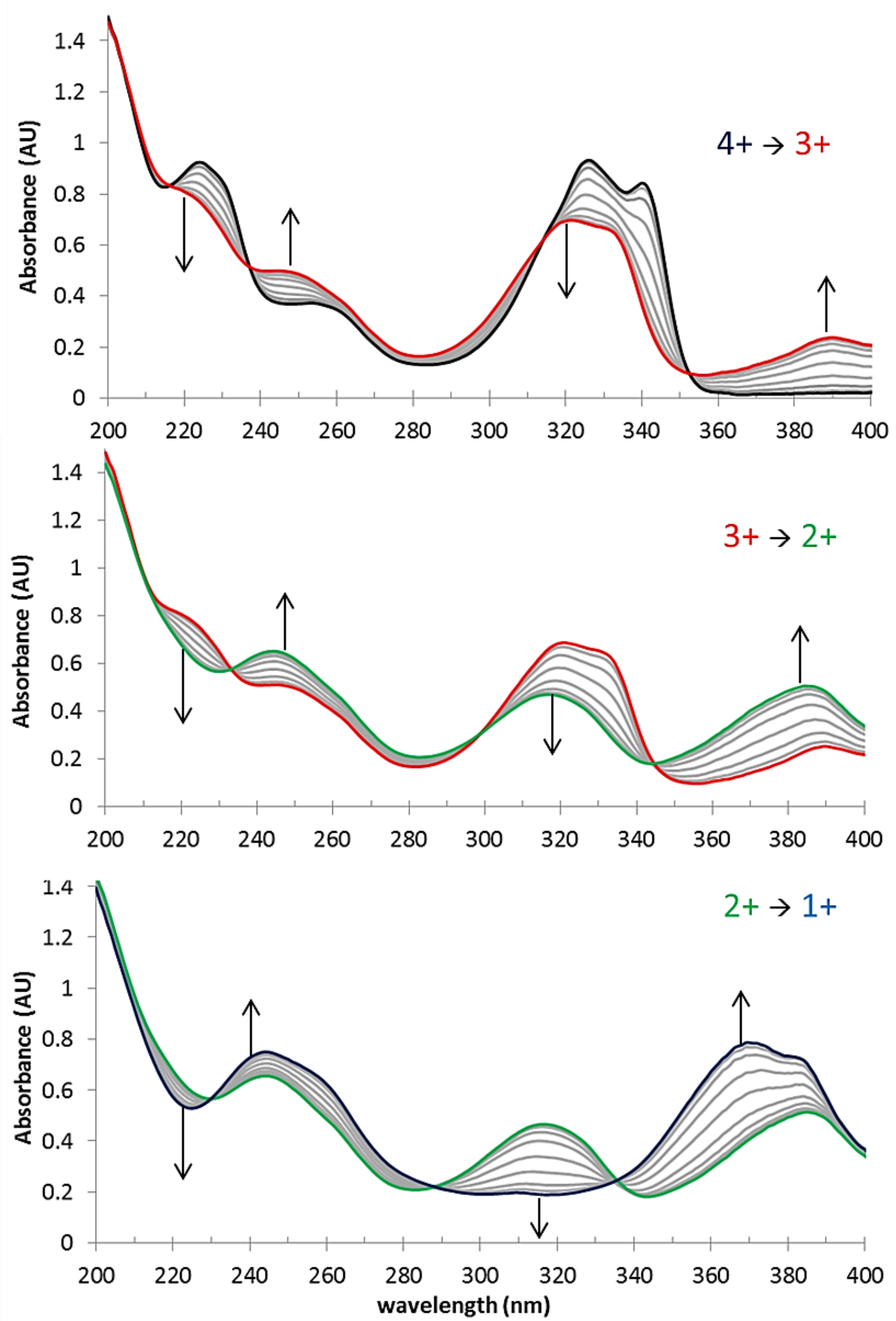

FIGURE 31: UV–Vis spectra of $[Si(bpy)_3](PF_6)_4$ in acetonitrile/0.100 M $TBAPF_6$ recorded at 25 mV intervals from -0.445 to -0.645 V (top), -0.670 to -0.870 V (middle), and -0.895 to -1.120 V (bottom) vs Fc/Fc^+ with a gold working electrode.

The +4 state (black line) possesses two overlapping peaks at 327 nm and 341 nm, which are consistent with π → π* transitions of bipyridine ligands in other coordination complexes. Upon reduction, the intensity of this peak decreases (and slightly blue shifts) as each of the bipyridine ligands becomes reduced. At the same time, a peak around 390 nm and a broad absorbance from 600-1000 nm consistent with π → π* transitions for a bipyridine radical anion emerge. Subsequent reductions result in further reduction of the neutral bipyridine intra-ligand transitions and an increase in transitions of the radical anion. Thus, the series of redox states (+4 → +1) are consistent with the calculations of Wieghardt and can be represented as the series, $[Si(bpy)_3]^{+4} \rightarrow [Si(bpy)_2(bpy^{\bullet})]^{+3} \rightarrow [Si(bpy)(bpy^{\bullet})_2]^{+2} \rightarrow [Si(bpy^{\bullet})_3]^{+1}$.[84] Attempts to reduce $[Si(bpy)_3](PF_6)_4$ further to the neutral species resulted in an irreversible, overall decrease in absorbance without isosbestic points, consistent with a plating out of $[Si(bpy)_3]^0$ on the electrode. This may not be a problem in an electrochemical device with the $[Si(bpy)_3]^{+n}$ dye already attached to the electrode, but it prevents accurate spectroscopic characterization with our current set–up. The bleached $[Si(bpy)_3]^{+4}$ is completely colorless, or nearly so, because of the lack of d–electrons on the silicon center and resulting absence of MLCT bands, while the reduced species appear green (FIGURE 32), which has traditionally been a more challenging color to obtain in electrochromic materials since it requires the presence of both red and blue absorption bands.[143] It is possible to obtain very large Δ%Ts for both bands: > 85% (362-387 nm) and > 40% (751-857 nm).

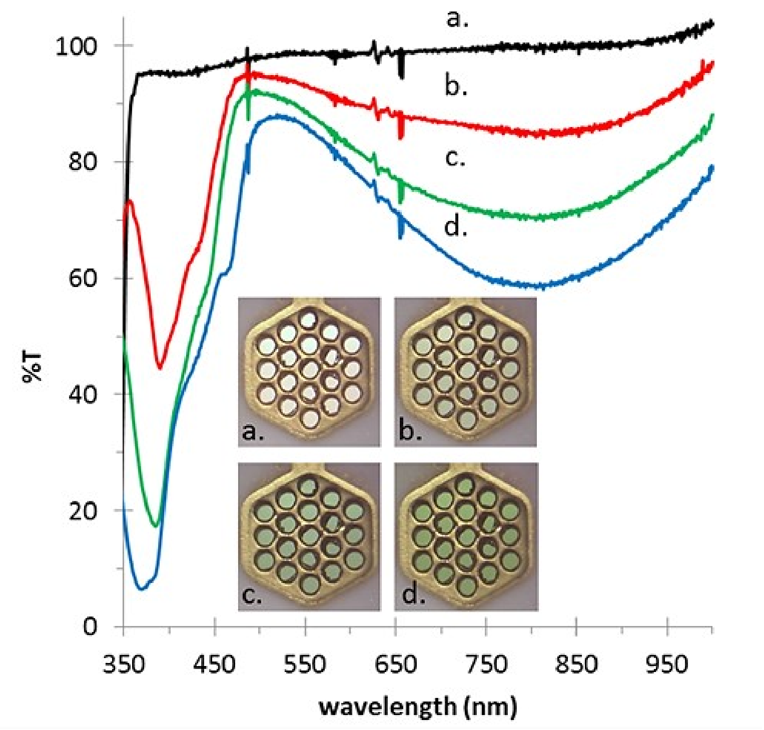

FIGURE 32: Transmittance and photos (inset) of (a) $[Si(bpy)_3]^{+4}$, (b) $[Si(bpy)_3]^{+3}$, (c) $[Si(bpy)_3]^{+2}$, and (d) $[Si(bpy)_3]^{+1}$.

2.3 Summary

This initial work with $[Si(bpy)_3]^{+4}$ demonstrates that polypyridylsilicon(IV) complexes present an excellent alternative to current electrochromic materials by providing several advantages: (1) they exhibit multiple stable oxidation states with well–behaved chemically reversible electrochemistry, (2) they are often colorless in the fully oxidized (+4) state, (3) they have very low reduction potentials attributed to the tetravalent silicon center, which could enable low–voltage devices and applications, (4) their reduced ligand–based transitions appear in the visible portion of the spectrum, and (5) they can be synthesized easily from earth–abundant elements. Other polypyridine silicon(IV) complexes are presented in Chapter 3.

2.4 Experimental Parameters

Tris(bipyridine)silicon(IV) hexafluorophosphate: $[Si(bpy)_3]^{+4}$ was synthesized according to the procedure published by Suthar *et al.* by combining 0.57 g of SiI_4 (1.06 mmol) with 0.66 g of 2,2'–bipyridine (4.23 mmol) in 3.50 g of 2–picoline in a heavy–wall GPT under nitrogen atmosphere.[80] The tube was then sealed and placed in a silicone oil bath at 125 ˚C for 3 h, producing a dark brown solid. At the end of the heating period, the tube was opened, and a small addition of methanol was added to quench incomplete reaction byproducts. Centrifugation and subsequent multiple rinses of the solid with methanol, chloroform, and ether yielded 0.6315 g (59.0%) of $[Si(bpy)_3]I_4$ as a brown solid that was dried under vacuum. Conversion to the hexafluorophosphate salt was done by dissolving $[Si(bpy)_3]I_4$ in water followed by precipitation of $[Si(bpy)_3](PF_6)_4$ after addition of saturated NH_4PF_6 in water. The solid was rinsed with methanol and ether before drying under vacuum. Dissolving the solid in deuterated acetonitrile (CD_3CN) provides the ^1H NMR spectrum (300 MHz, CD_3CN, FIGURE 33): δ 7.43 (d, $J = 5.5$ Hz, 6 H), 8.11-8.13 (m, 6 H), 8.91-8.94 (m, 6 H), 9.07 (d, $J = 7.7$ Hz, 6 H) with an impurity peak of water (at 2.13 ppm) that is often present in the CD_3CN ampoules.

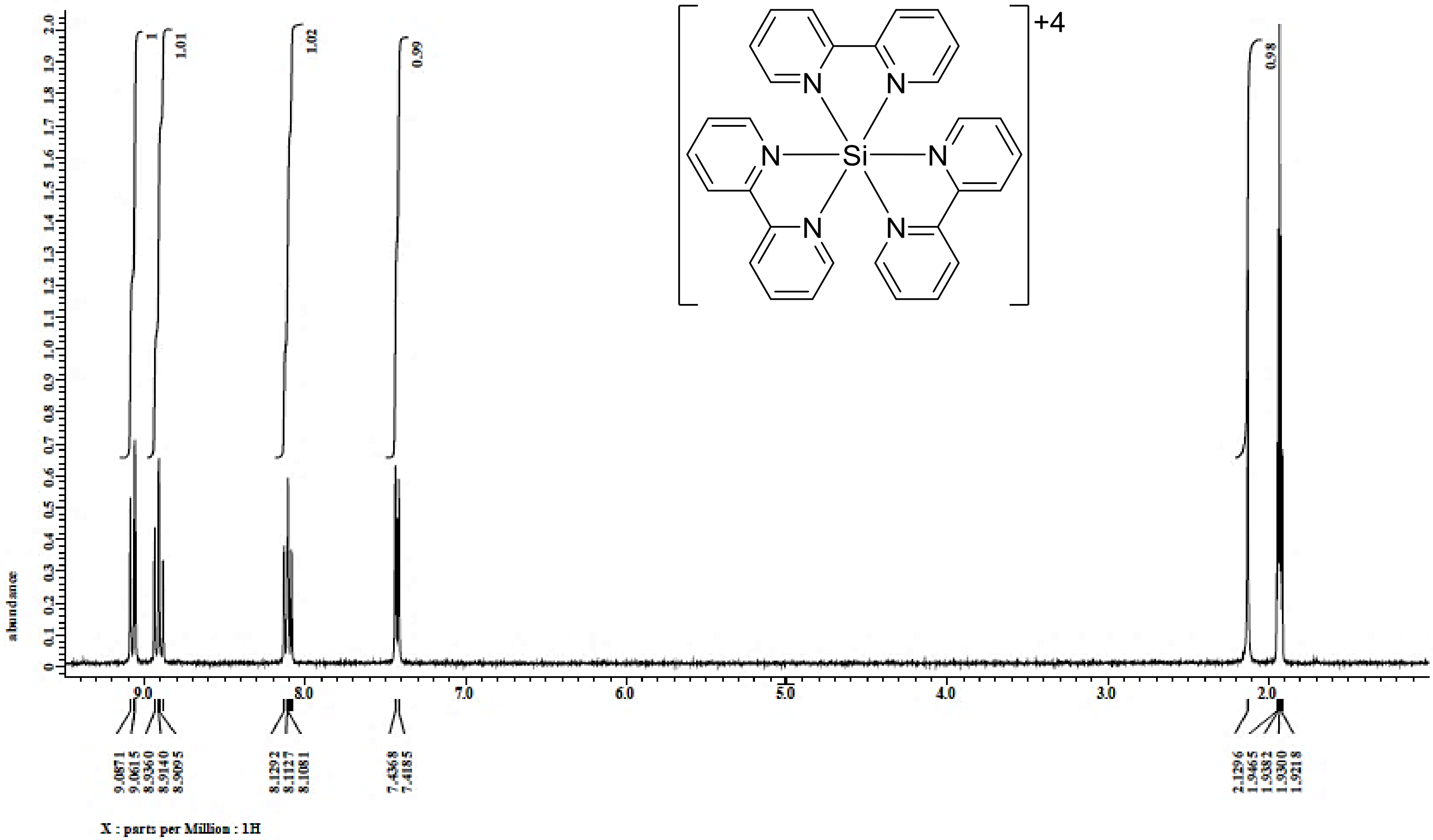

FIGURE 33: ^{1}H NMR spectrum of $[Si(bpy)_3](PF_6)_4$ in CD_3CN.

The spectroelectrochemical cell was purchased from Pine Research Instrumentation and consisted of a covered quartz cuvette with a 1.0 mm pathlength with a printed gold honeycomb working electrode, a gold counter electrode, and a Ag/AgCl reference electrode standardized to the ferrocene/ferrocenium couple. Samples of $[Si(bpy)_3](PF_6)_4$ (2.8×10^{-4} M) were prepared in anhydrous acetonitrile with 0.100 M $TBAPF_6$ and degassed with argon that had been bubbled through acetonitrile. Potentials were then applied to the solution with a Princeton Applied Research model 173 potentiostat/galvanostat and analyzed with an Agilent 8453 Diode Array Spectrometer in 25 mV increments with at least 45 s of equilibrium time before UV–Vis spectra were taken; two separate channels allowed for discrete steps between applied voltage values.

CHAPTER 3: EXPANDING THE COLOR PALETTE WITH POLYPYRIDINE SILICON(IV) COMPLEXES

3.1. Introduction

Color control and variety of color in electrochromic materials is very well–realized in conjugated organic polymers, especially through the research of John Reynolds.[144-147] In order to present polypyridine silicon(IV) complexes as effective alternatives, it is necessary to synthesize a library of the compounds. By using the work of Elliott[138] as inspiration, it was expected that changing the ligand for the silicon complexes would both affect the reduction potentials and the absorbance maxima of the reduction peaks. Several substituted bipyridine ligands and a few substituted 2,2':6',2"–terpyridine (tpy) ligands were easily and cheaply purchased (or synthesized, in the case of the 4'–*p*–tolyl–2,2':6',2"–terpyridine (ttpy)) and targeted by virtue of producing the largest number of complexes at the lowest cost (FIGURE 34). Two different routes, one starting from silicon(IV) iodide (SiI_4) and one from silicon(IV) chloride ($SiCl_4$), were adapted for synthesis of the complexes. Ruthenium(II) complexes containing all of these ligands have been published in the literature and the reduction potentials and spectroelectrochemistry of each will be compared to the silicon complexes.[148-153]

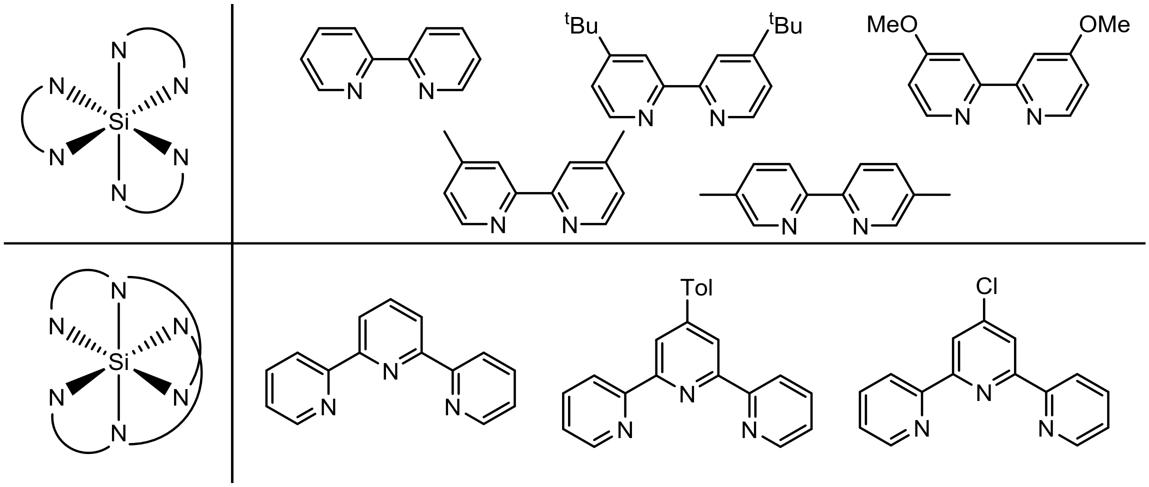

FIGURE 34: Substituted bipyridines (top row: 2,2’–bipyridine (bpy), 4,4’–di–*tert*–butyl–2,2’–bipyridine (4dtbbpy), 4,4’–dimethoxy–2,2’–bipyridine (4dmobpy); middle row: 4,4’–dimethyl–2,2’–bipyridine (4dmbpy), 5,5’–dimethyl–2,2’–bipyridine (5dmbpy)) and terpyridines (bottom row: 2,2’:6’,2”–terpyridine (tpy), 4’–*p*–tolyl–2,2’:6’,2”–terpyridine (ttpy), 4’–chloro–2,2’:6’,2”–terpyridine (Cltpy)) used in the synthesis of silicon(IV) complexes.

3.2. Results and Discussion

3.2.1. Synthesis

As initially mentioned in Section 1.4.3, the first synthesis route was performed by Suthar *et al.* by combining SiI_4 with the desired ligand in either pyridine or 2–picoline (SCHEME 15).

SCHEME 15: Representative reaction scheme of the SiI_4 route for the synthesis of bipyridine silicon complexes. For terpyridine complexes, only two equiv. of terpyridine ligand is required.[80]

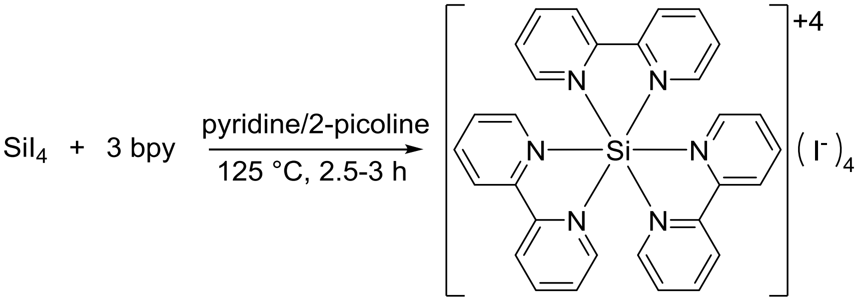

Because of the hydrolytic susceptibility of SiI_4, this compound is stored under nitrogen atmosphere in the glovebox and reactions are performed there as well. SiI_4 can also be used in a glovebag but it is much easier to accidentally poison the container and elemental iodine, a byproduct of SiI_4 decomposition, quickly stains the glovebag and makes it unusable. Inside the glovebox, SiI_4 was added to a heavy–wall glass pressure tube (GPT) along with either 4 equiv. of bipyridine or 2.5 equiv. of terpyridine and either pyridine or 2–picoline as a solvent. There is a slight excess of ligand added to promote the full tris–substitution in the case of the bipyridines or bis–substitution of the terpyridines. Once the tube is sealed, it can be removed from the glovebox without concern of air entering the vessel. It was then put into an oil bath at 125 ˚C and left stirring for 2.5 to 3 h. In all cases, this produced a colored solid that could be handled in open air. A small amount of methanol was added to the solution to quench byproducts before centrifuging and separating out the solid. It was then rinsed twice with chloroform and twice with ether before drying under vacuum. This route will heretofore be referred to as the SiI_4 route.

For the second synthesis route, Kummer isolated the halide salts of $[Si(bpy)_3]^{+4}$ by oxidizing the reactive $[Si(bpy)_3]^0$ complex of Herzog and Krebs with the elemental halogens (SCHEME 16).

SCHEME 16: Representative reaction scheme of the $SiCl_4$ route for the synthesis of bipyridine silicon complexes. For terpyridine complexes, no terpyridine ligand was combined with $SiCl_4$ prior to cannulation of the lithiated polypyridine.[77, 79]

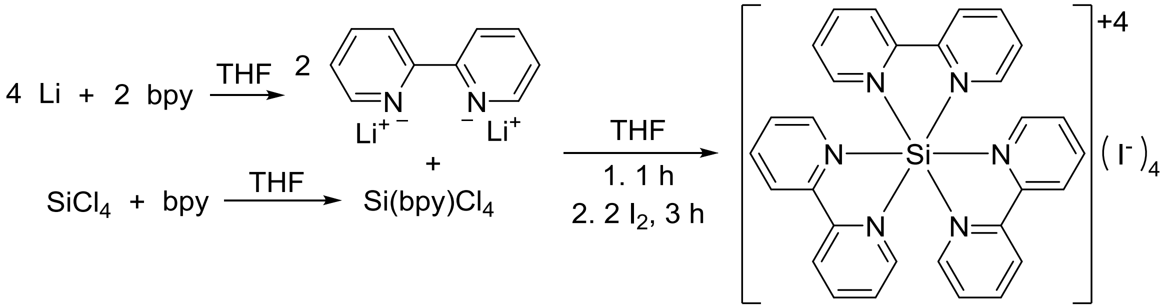

[Si(bpy)]^0 was prepared by first reacting two equiv. of bipyridine with elemental lithium, freshly cut, in anhydrous THF under argon atmosphere, since lithium metal is reactive with nitrogen gas. Only four equiv. of lithium are required to dilithiate the two equiv. of bipyridine but it is typically added in excess up to 12 equiv. to promote full dilithiation on a reasonable time scale, and cutting is necessary to expose fresh surfaces on the lithium wire to react. Progress of the reaction can be followed by the color of the solution, which is initially colorless, changing to wine red upon monolithiation and then to dark green/black upon dilithiation, within 3 to 4 h. In a second flask, one additional equiv. of bipyridine was dissolved in THF to which one equiv. of $SiCl_4$ was added to form a white precipitate. $SiCl_4$ was measured by mass using a tared syringe, although the volume amount is reported in the experimental as well. This white precipitate is indicative of forming the hexacoordinate Si(bpy)Cl_4 species. After the second color change had occurred, the dilithiated bipyridine solution was transferred via cannula into the second flask to get a black/dark brown solid. After 30-60 minutes, two equiv. of elemental iodine (I_2) versus $SiCl_4$ were added to the flask to produce a brown solid that could be filtered out and rinsed with fresh THF and ether before drying under vacuum.

This procedure was modified slightly for use of the terpyridine ligands. Two equiv. of terpyridine were dissolved into THF under argon atmosphere with an excess of lithium metal. Although terpyridine ligands have three nitrogen atoms capable of being lithiated, only two color changes were noticed, green upon monolithiation and black upon dilithiation, even for flasks that were left to react overnight with 12 equiv. of lithium. A second flask was prepared with only THF and one equiv. of $SiCl_4$ before cannulation of the dilithiated terpyridine solution to get a still dark–colored solution with black solid. After 30-60 minutes, two equiv. of I_2 versus $SiCl_4$ were added to the flask to get a more obvious solid and left to stir overnight. The resulting solid could then be filtered out and rinsed with THF and ether before drying under vacuum. This crude material is notably impure because side products such as lithium chloride are unlikely to have been separated out at this point. This route will heretofore be referred to as the $SiCl_4$ route.

Before it could be used as a ligand, tolylterpyridine was the only compound that could not be bought cheaply and had to be synthesized. This was done following the procedure of Liu *et al.*[154] Two equiv. of 2–acetylpyridine were reacted with one equiv. of *p*–tolualdehyde and two equiv. of sodium hydroxide (NaOH) in a mixed solution of ethanol and ammonia. The solution turned yellow as the NaOH slowly dissolved, then continued on until brown as the temperature was held at 34 ˚C and the solution stirred overnight. Upon cooling, the solution appeared orange with white precipitate. The precipitate was then filtered and recrystallized from ethanol to produce white powdery tolylterpyridine, which can be confirmed by GC–MS and ^1H NMR (FIGURE 35) with a water impurity peak present at 2.13 ppm. The chemical shifts and coupling constants are provided in Section 3.4.

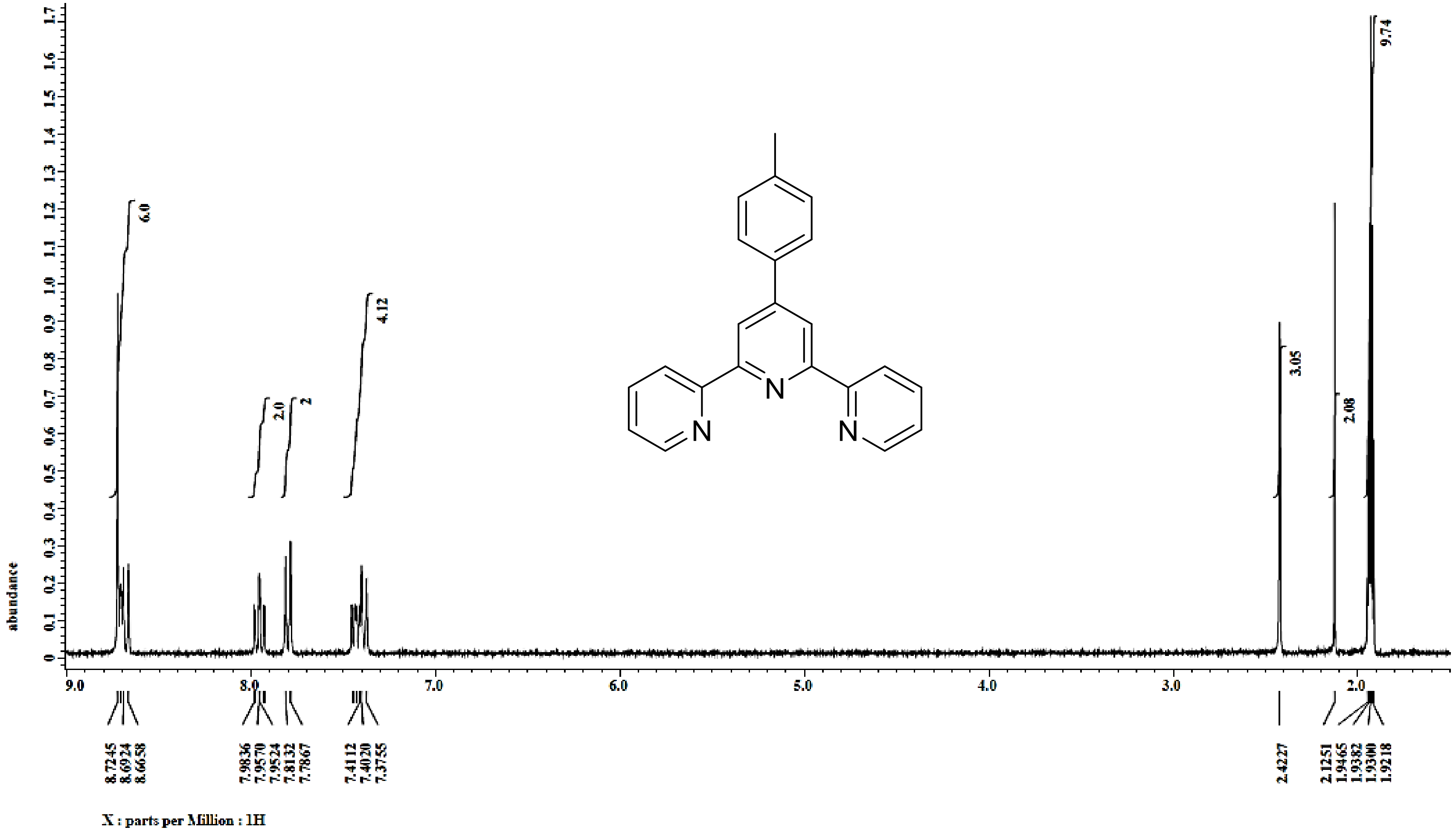

FIGURE 35: ^{1}H NMR spectrum of tolylterpyridine in CD_3CN.

Only two of the eight ligands, 4dmobpy and Cltpy, did not yield any solid products with the correct anticipated splitting pattern in their ^{1}H NMR spectra as the iodide salt. With 4dmobpy through the SiI_4 route, a yellow–tan solid in 31.4% crude yield was isolated when using pyridine as the solvent and a red/pink solid in 68.9% crude yield with 2–picoline as the solvent. The yellow–tan solid showed a splitting pattern indicative of bis –substitution rather than tris–substitution and the pink solid showed no aromatic peaks except for what could be comfortably assigned to 2–picoline. The $SiCl_4$ route was performed several times with 4dmobpy and a white precipitate was always formed upon mixing $SiCl_4$ and 4dmobpy suggesting formation of the hexacoordinate species. However, although a first red–purple color change was observed during the lithiation, no second color change ever was, suggesting that dilithiation was not taking place. It is suggested that perhaps sodium would be able to dimetallate the bipyridine and allow it to displace the chloride ligands.

Synthesis of the silicon complex containing the Cltpy ligand was only attempted through the SiI_4 route. The use of either pyridine or 2–picoline as solvents and changing of the reaction time and temperature were not even able to replicate the crude 36.8% yield reported in Section 3.4. The produced black solid did not provide the correct splitting pattern of a bis–subsitituted terpyridine complex and further synthetic attempts were not performed.

Two other ligands, 4dmbpy and tpy, yielded solids that displayed the expected splitting pattern but were unable to be converted to pure hexafluorophosphate salts for use in electro– and spectroelectrochemistry. By the SiI_4 route, 4dmbpy gave black solids with either solvent, but neither of these solids gave a splitting pattern indicative of tris–

substitution. By the $SiCl_4$ route, a dark tan solid in 41.5% yield did have the expected splitting pattern but upon dissolution in water and addition of NH_4PF_6, no precipitate was formed. This could be indicative that the solid is instead either a mono–substituted product or a bipyridinium salt which would all give the same splitting pattern as the tris–substituted product.

The solids isolated from the SiI_4 route with the tpy ligand were both black as well and the solid isolated from the $SiCl_4$ route was green. Any of these solids gave the expected splitting pattern in D_2O. However, the green solid produced no precipitate upon addition of NH_4PF_6, and the black solids produced precipitate that was dark blue in color but no longer gave the proper splitting pattern in ^1H NMR and also did not behave electrochemically.

The other four ligands, bpy (Section 2.2), 4dtbbpy, 5dmbpy, and ttpy, produced solids that gave the proper ^1H NMR splitting in D_2O and then were able to be converted to hexafluorophosphate salts with the proper splitting pattern as well. Bpy gave dark brown solids by either synthesis route and was the only ligand to yield confirmed product by the $SiCl_4$ route. The 4dtbbpy salts were shades of brown through any of the routes but the material isolated from the $SiCl_4$ route could not be converted. By the SiI_4 route, ttpy produced dark brown solids in good yield but by the $SiCl_4$ route, the black solid was insoluble in D_2O. This failure of the $SiCl_4$ route could be from reaction times that were too long or that the observed dilithiated ttpy was either not dilithiated (or dilithiated at positions other than the nitrogen atoms) or that the dilithiated ligand is unable to produce the desired hexacoordinate silicon species upon reaction with $SiCl_4$. 5dmbpy gave black solids through the SiI_4 (2–picoline) and $SiCl_4$ routes that were not soluble in D_2O, but the dark red solid from the SiI_4 (pyridine) route was soluble and gave the expected splitting pattern.

3.2.2. Purification

Conversion to the hexafluorophosphate salt was reported by Suthar *et al.* as being done by dissolving the iodide salt in water then using flash chromatography with silica.[80] This was unable to be realzed with either $[Si(bpy)_3]I_4$ or $[Si(tpy)_2]I_4$ (the two solids reported by Suthar) because no movement of any colored bands occurred, even with the use of 1.0 M NaCl or 0.01 M HCl. Because Sephadex has been used in the literature to separate chiral enantiomers of silicon(IV) complexes with tartrate salts, this was also investigated, but the column quickly became fouled, presumably by excess iodine or reactive byproducts.[83] Other processes such as using silver nitrate, lead(II) hexafluorophosphate, and recrystallization or vapor diffusion with different solvents were all attempted to no avail. However, simple dissolution of the iodide salt in water followed by addition of saturated NH_4PF_6 in water (in large excess to promote conversion of the iodide to the hexafluorophosphate counterion) produced solids that could be isolated and rinsed once with water to remove NH_4PF_6, twice with isopropanol, and twice with ether before drying under vacuum. Although none of these salts passed EA, they all appeared to be spectroscopically clean in NMR, CV, and UV–Vis and therefore were then used for spectroelectrochemical characterization.

$[Si(bpy)_3]I_4$ converted from a brown solid to light gray $[Si(bpy)_3](PF_6)_4$. $[Si(5dmbpy)_3]I_4$ converted from a dark red solid to light gray $[Si(5dmbpy)_3](PF_6)_4$. $[Si(4dtbbpy)_3]I_4$ converted from a brown solid to light yellow $[Si(4dtbbpy)_3](PF_6)_4$ with the assistance of chloroform by an unknown mechanism. This was attempted because of the hypothesis that the PF_6^- salt might be soluble in the chloroform due to the greater organic character afforded by the *tert*–butyl groups, but it was not. $[Si(ttpy)_2]I_4$ converted from a dark brown solid to dark yellow $[Si(ttpy)_2](PF_6)_4$.

3.2.3. Electrochemical and Spectroelectrochemical Characterization

Cyclic voltammetry was first used to determine the electrochemical reversibility and reduction potentials for the complexes using the PF_6^- salt at 1.0 mM concentration with acetonitrile/0.100 M $TBAPF_6$ as the supporting electrolyte, in collaboration with Dr. Jon Merkert and Dr. Bernadette Donovan–Merkert. Spectroelectrochemistry was performed using a spectroelectrochemical cell from Pine Research Instrumentation with a covered quartz cuvette with a 1.0 mm pathlength, a printed gold or platinum electrode, consisting of both a honeycomb working electrode and counter electrode, and a Ag/AgCl reference electrode standardized to the ferrocene/ferrocenium couple. Samples were prepared at approximately 2×10^{-4} M concentrations and degassed with argon that was bubbled through acetonitrile, to prevent evaporation of the solution in the cell. Potentials were applied in 25 mV increments using 2 separate channels in discrete steps and analyzed with at least 45 s of equilibrium time before UV–Vis spectra were taken.

$[Si(4dtbbpy)_3](PF_6)_4$ displays three chemically reversible reductions in acetonitrile/0.100 M $TBAPF_6$ (FIGURE 36: $E_{1/2}$ = -0.705, -0.915, and -1.140 V vs. Fc/Fc^+).

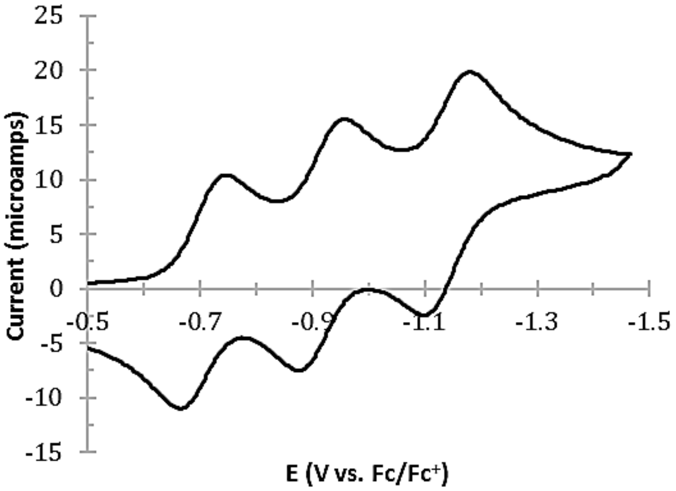

FIGURE 36: Cyclic voltammagram of 1.0 mM $[Si(4dtbbpy)_3](PF_6)_4$ in acetonitrile/0.100 M $TBAPF_6$ vs. Fc/Fc^+ with a platinum disk working electrode. Scan rate = 0.200 V/s with iR compensation.

To measure the spectroelectrochemistry, 0.17 mg of $[Si(4dtbbpy)_3](PF_6)_4$ was dissolved in 5 mL of acetonitrile/0.100 M $TBAPF_6$. A UV–Vis spectrum was measured to show two overlapping peaks at 321 and 334 nm with no absorbance in the visible. Upon the first reduction, these peaks begin to disappear with a new peak emerging at 391 nm and a very broad peak around 807 nm. Two further reductions see the initial neutral bipyridine $\pi \rightarrow \pi^*$ peak blue shift while continuing to disappear, the emerging radical bipyridine $\pi \rightarrow \pi^*$ peak also blue shifting to have a final absorbance maximum at 377 nm, and a strengthening with no shifting of the broad 807 nm peak. FIGURE 37 displays each separate transition with very well–defined isosbestic points and FIGURE 38 displays the spectra corresponding to each electrochemical state.

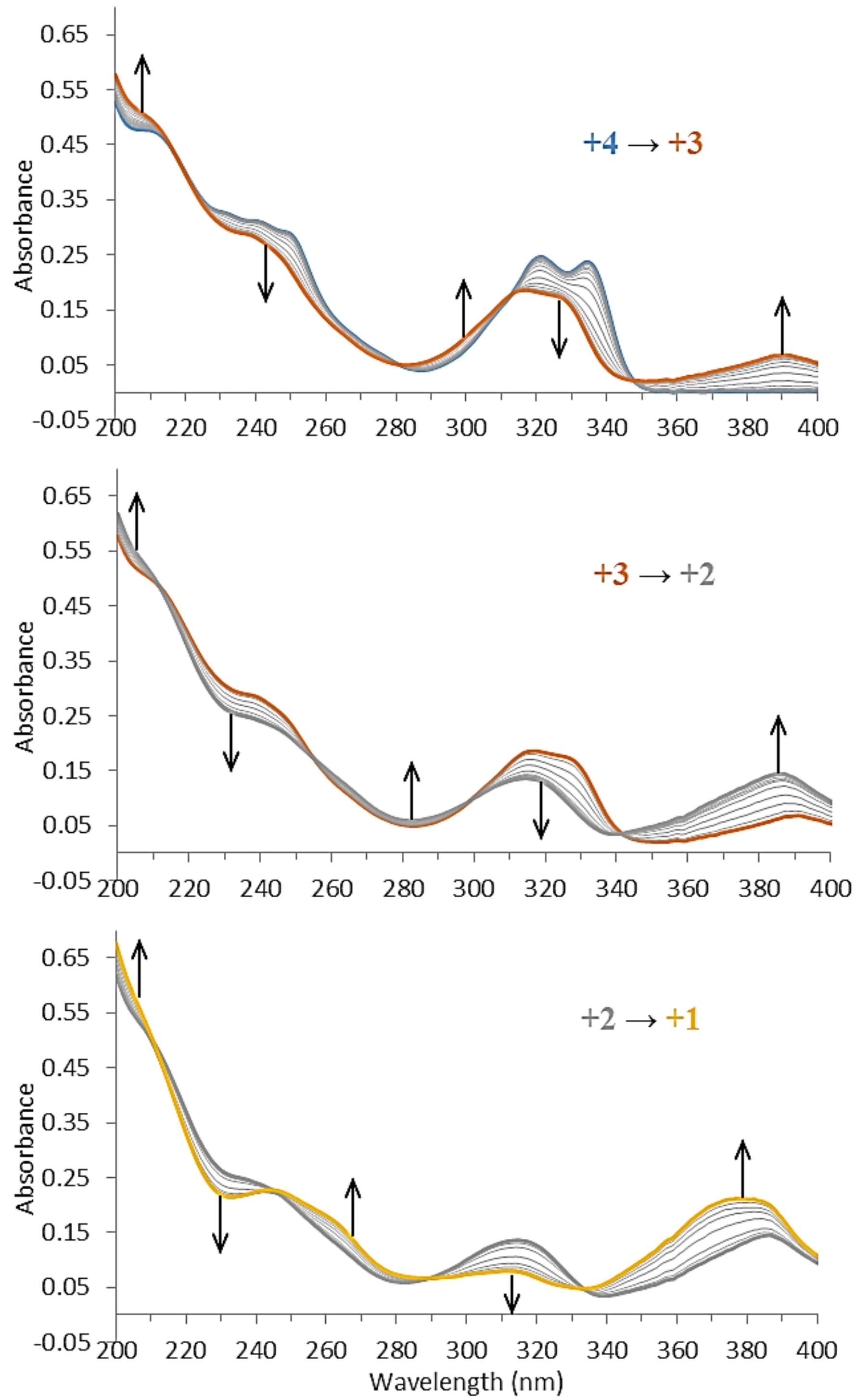

FIGURE 37: UV–Vis spectra of $[Si(4dtbbpy)_3](PF_6)_4$ in acetonitrile/0.100 M $TBAPF_6$ recorded at 25 mV intervals from -0.445 to -0.845 V (top), -0.845 to -1.070 V (middle), and -1.070 to -1.270 V (bottom) vs Fc/Fc^+ with a platinum working electrode.

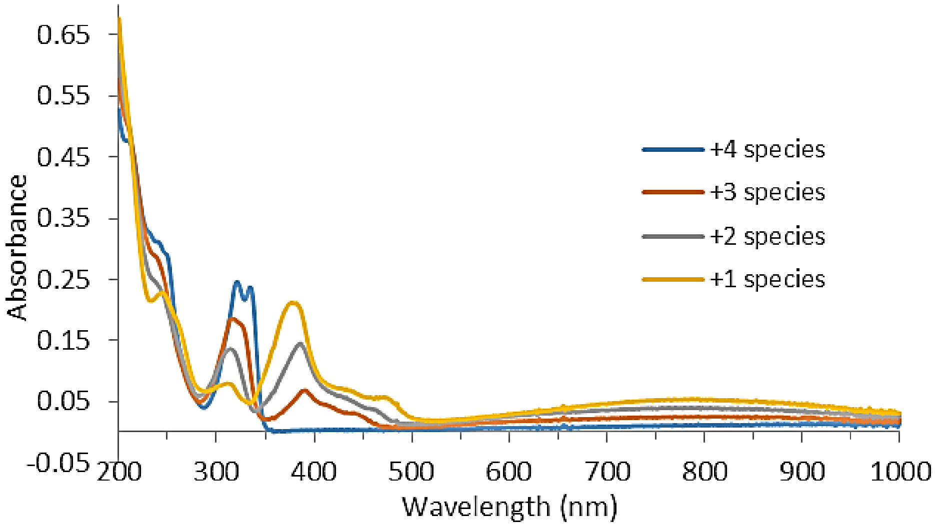

FIGURE 38: UV–Vis spectra of $[Si(4dtbbpy)_3]^{+n}$ states generated electrochemically at -0.445 V (blue line, n = 4), -0.845 V (red line, n = 3), -1.070 V (gray line, n = 2), and -1.270 V (yellow line, n = 1) vs Fc/Fc$^+$ with a platinum working electrode.

$[Si(5dmbpy)_3](PF_6)_4$ displays three chemically reversible reductions in acetonitrile/0.100 M $TBAPF_6$ (FIGURE 39: $E_{1/2}$ = -0.650, -0.875, and -1.140 V vs. Fc/Fc$^+$). A possible adsorption to the electrode past -1.200 V is seen more obviously when the complex is further reduced to the neutral complex (Appendix A), but still displays chemical reversibility. Possible plating out of the neutral complex on the electrode can be supported by the loss of spectral signature pertaining to the +1 species in solution and loss of reversibility when applying a potential greater than -1.200 V in the spectroelectrochemical characterization (Appendix B).

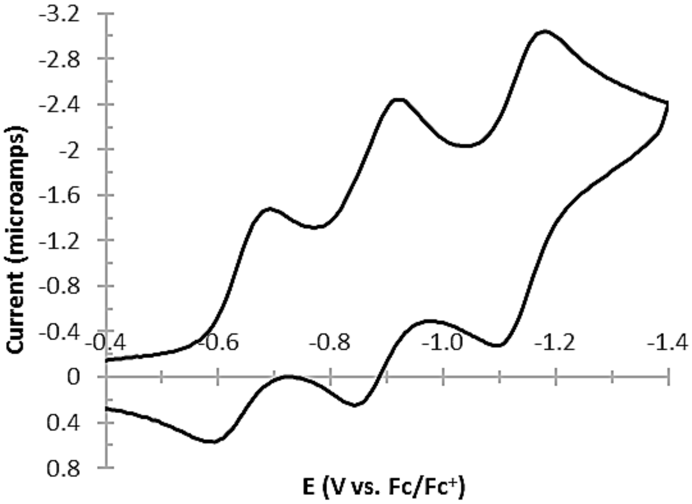

FIGURE 39: Cyclic voltammagram of $[Si(5dmbpy)_3](PF_6)_4$ in acetonitrile/0.100 M $TBAPF_6$ vs. Fc/Fc^+ with a platinum disk working electrode. Scan rate = 0.200 V/s with iR compensation.

0.23 mg of $[Si(5dmbpy)_3](PF_6)_4$ was dissolved in 5 mL of acetonitrile/0.100 M $TBAPF_6$. A UV–Vis spectrum was measured to show two overlapping peaks at 340 and 356 nm with no absorbance in the visible. Upon the first reduction, these peaks begin to disappear with a broad new peak emerging centered at 413 nm and no other higher wavelength peak, just a slight raising in the red and near–IR part of the spectrum. Two further reductions produce a similar occurrence to the other bipyridine complexes, with a blue shift and disappearance of the initial neutral bipyridine $\pi \rightarrow \pi^*$ peak, a blue shift in the emerging radical bipyridine $\pi \rightarrow \pi^*$ peak to have a final flat–topped peak with two absorbance maxima at 384 and 397 nm, and appearance and strengthening of a broad 830 nm peak. FIGURE 40 displays each separate transition with very well–defined isosbestic points while FIGURE 41 displays the spectra corresponding to each electrochemical state. It must be noted that the final spectrum is likely a mix of +2 and +1 species considering it was measured at -1.195 V vs. Fc/Fc^+ while the $E_{1/2}$ value is -1.140 V.

However, this spectrum is being reported here because, as partially supported by the cyclic voltammagram going out to four reductions shown in Appendix A, an irreversible reaction was observed immediately afterwards in the UV–Vis spectrum (Appendix B).

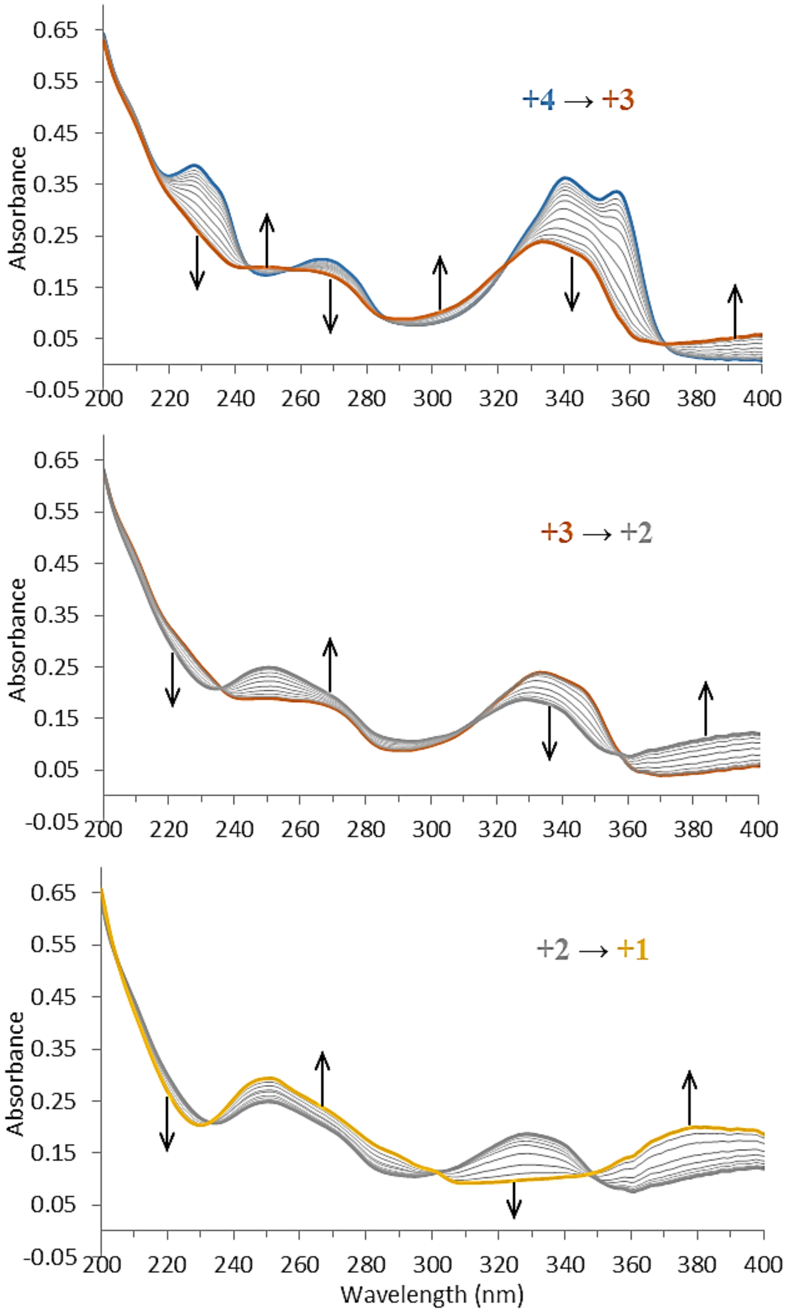

FIGURE 40: UV–Vis spectra of $[Si(5dmbpy)_3](PF_6)_4$ in acetonitrile/0.100 M $TBAPF_6$ recorded at 25 mV intervals from -0.445 to -0.770 V (top), -0.770 to -0.995 V (middle), and -0.995 to -1.195 V (bottom) vs Fc/Fc^+ with a platinum working electrode.

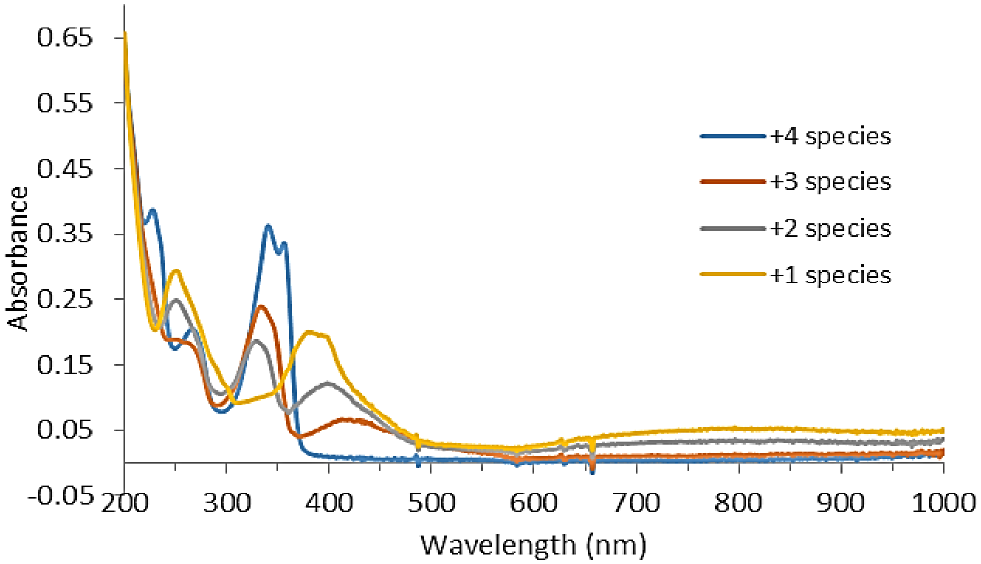

FIGURE 41: UV–Vis spectra of $[Si(5dmbpy)_3]^{+n}$ states generated electrochemically at -0.445 V (blue line, n = 4), -0.770 V (red line, n = 3), -0.995 V (gray line, n = 2), and -1.195 V (yellow line, n = 1) vs Fc/Fc^+ with a platinum working electrode.

$[Si(ttpy)_2](PF_6)_4$ displays four chemically reversible reductions in acetonitrile/0.100 M $TBAPF_6$ (FIGURE 42: $E_{1/2}$ = -0.420, -0.620, -1.120, and -1.400 V vs. Fc/Fc^+).

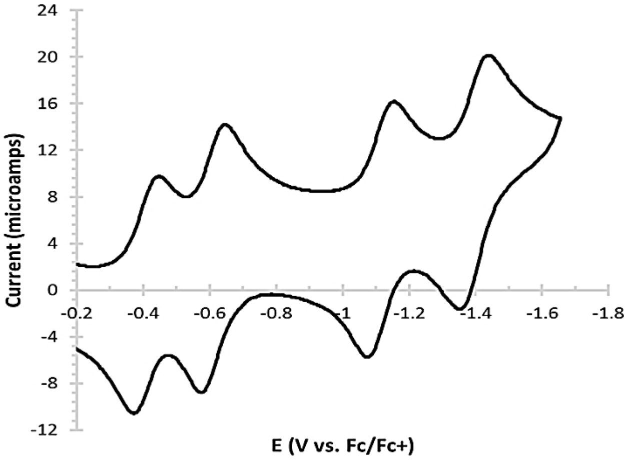

FIGURE 42: Cyclic voltammagram of 1.0 mM $[Si(ttpy)_2](PF_6)_4$ in acetonitrile/0.100 M $TBAPF_6$ vs. Fc/Fc^+ with a platinum disk working electrode. Scan rate = 0.200 V/s with iR compensation.

1.21 mg of $[Si(ttpy)_2](PF_6)_4$ was dissolved in 5 mL of acetonitrile/0.100 M $TBAPF_6$. A UV–Vis spectrum was measured to show a sharp peak at 301 nm and two rather broad overlapping peaks at 378 and 407 nm with no other peaks at higher wavelengths. Upon the first and second reductions, these peaks begin to disappear but the lower–wavelength absorbance peaks get complicated. A broad new peak emerges at 653 nm corresponding to the singly–reduced ttpy π → π* transition. Upon the third and fourth reductions, a new visible peak first at 495 then at 514 nm with a long tail out to 1000 nm appears corresponding to the doubly–reduced ttpy π → π* transition. FIGURE 43 displays the spectra corresponding to each electrochemical state and FIGURE 44 displays each separate transition with very well–defined isosbestic points.

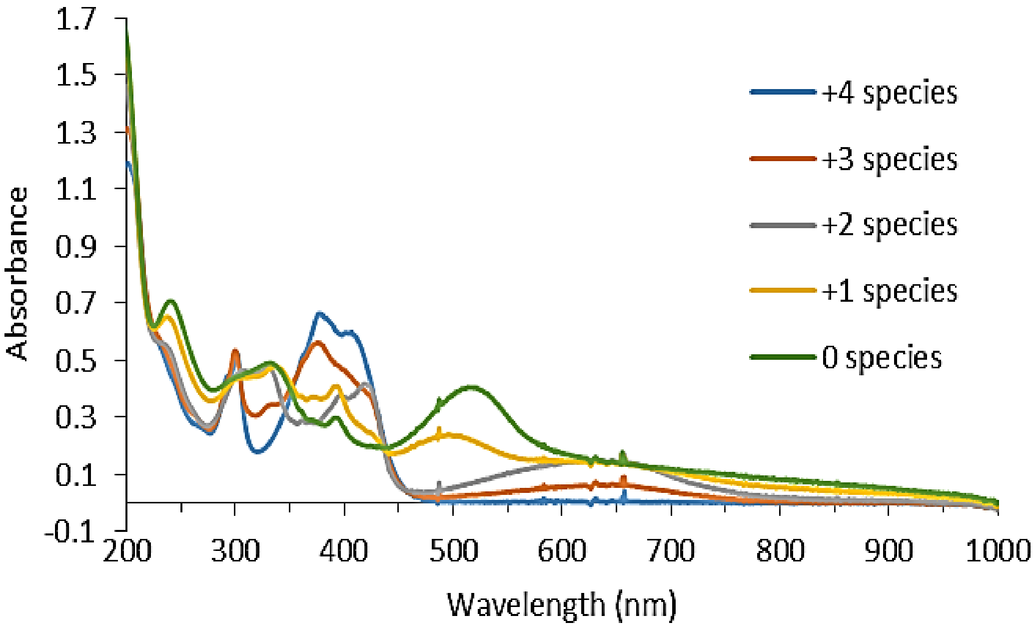

FIGURE 43: UV–Vis spectra of $[Si(ttpy)_2]^{+n}$ states generated electrochemically at -0.245 V (blue line, n = 4), -0.520 V (red line, n = 3), -0.945 V (gray line, n = 2), -1.370 V (yellow line, n = 1), and -1.695 V (green line, n = 0) vs Fc/Fc^+ with a gold working electrode.

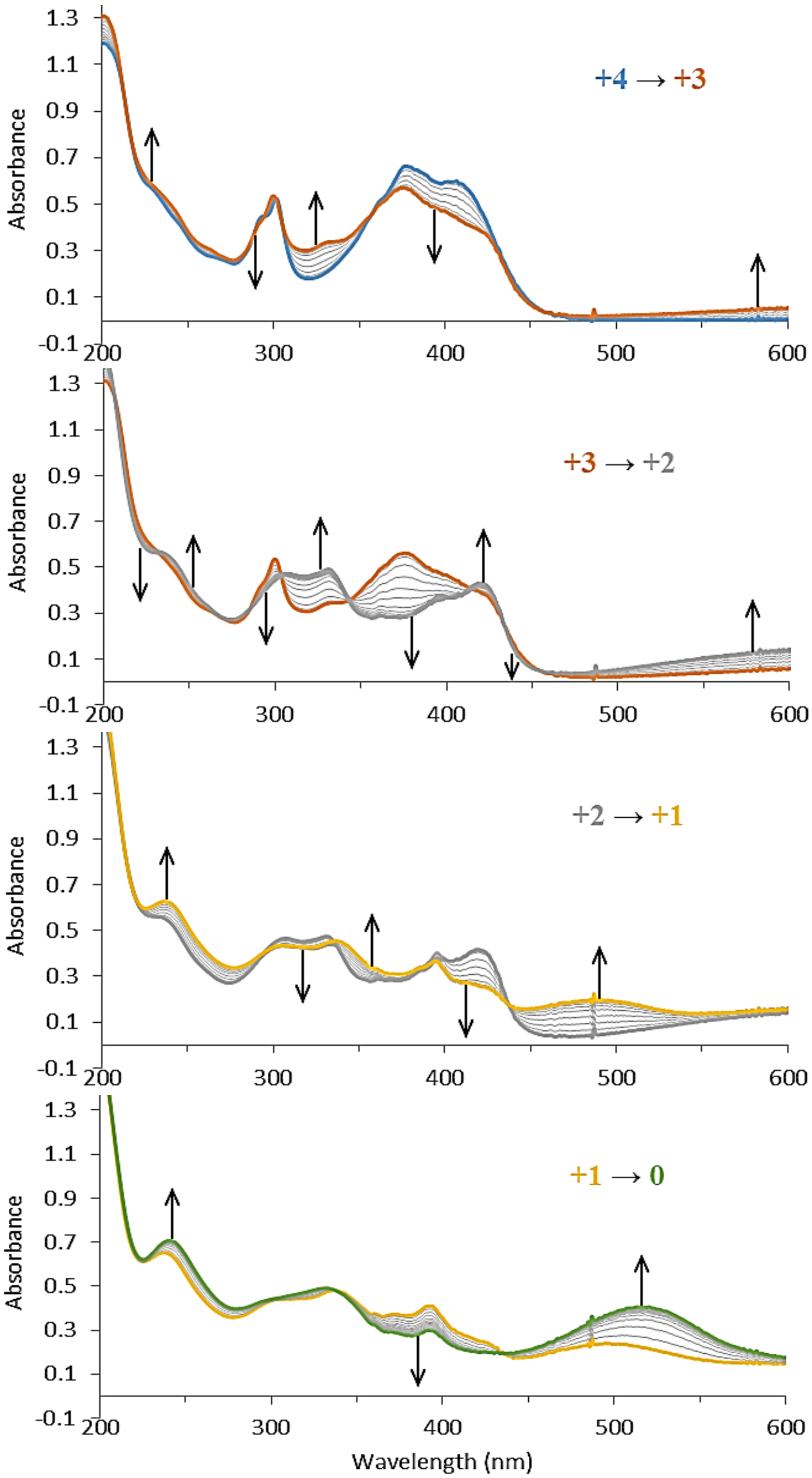

FIGURE 44: UV–Vis spectra of $[Si(ttpy)_2](PF_6)_4$ in acetonitrile/0.100 M $TBAPF_6$ recorded at 25 mV intervals from -0.245 to -0.520 V (top), -0.520 to -0.945 V (top middle), -0.945 to -1.370 V (bottom middle), and -1.370 to -1.695 V (bottom) vs Fc/Fc^+ with a gold working electrode.

By using UV–Vis spectroscopy to measure the absorbance of the unreduced species with specific concentrations, the molar absorptivity (ε) of the complex can be determined using Beer's Law (FIGURE 45). Thus, using an average ε_{378} of 4.38×10^4 $M^{-1} \cdot cm^{-1}$, it can be calculated that the spectra shown in FIGURE 43 and FIGURE 44 were measured at a concentration of 1.5×10^{-4} M, remembering to take into account the decreased pathlength.

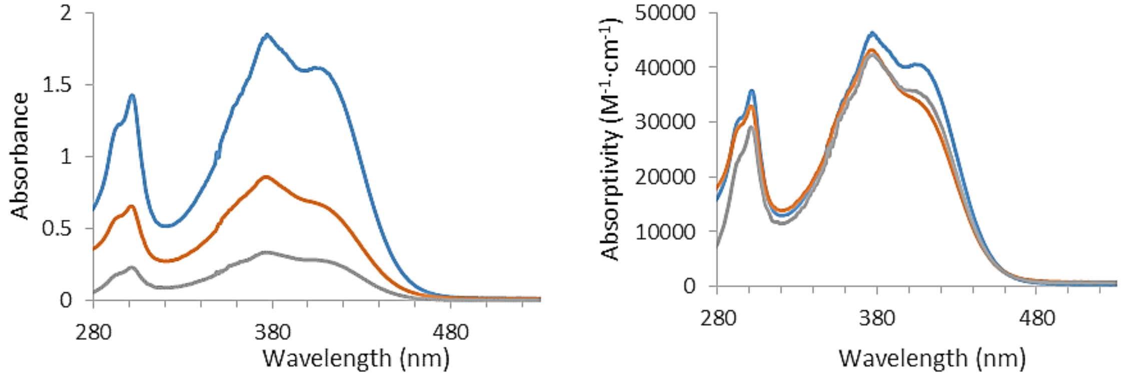

FIGURE 45: UV–Vis spectra of $[Si(ttpy)_2](PF_6)_4$ measured as (left) absorbance vs. wavelength and (right) absorptivity vs. wavelength. The blue line is measured at a concentration of 4.0×10^{-5} M, the red line is 2.0×10^{-5} M and the gray line is 8.0×10^{-6} M.

There are several connections that can be made between the data from $[Si(bpy)_3](PF_6)_4$ in Section 2.2 and the data from the three complexes presented in this chapter. Out of the four ligands, all four of the ruthenium analogs ($[Ru(bpy)_3]^{+2}$, $[Ru(4dtbbpy)_3]^{+2}$, $[Ru(5dmbpy)_2]^{+2}$, and $[Ru(ttpy)_2]^{+2}$) have been characterized electrochemically. Only $[Ru(bpy)_3]^{+2}$ has been characterized spectroelectrochemically, although the absorbance maxima of the MLCT of the +2 species of each complex in acetonitrile as the PF_6^- salt have been reported.[148, 151-152]

In all cases, the half–wave potentials (and subsequently the reduction potentials) of the silicon complexes are more than 1 V less negative than the ruthenium complexes, due to the higher positive charge on the silicon center versus that on ruthenium (TABLE 8). This property could be beneficial in devices because it would require lower applied potentials to enact reduction of the species. When compared to the free ligands themselves, the first reduction potentials of the complexes are about 2.0 V less negative than that of the free ligands, which are -2.57 V for bpy and -2.86 V for 5dmbpy (artificially approximated vs. Fc/Fc^+).[138] The values for ttpy and 4dtbbpy were not found in the literature, but several series of transition metal complexes using these ligands support the same correlation that it is easiest to reduce complexes incorporating ttpy and hardest to reduce complexes containing 4dtbbpy.[155-157]

TABLE 8: Half–wave potentials of the discussed silicon(IV) complexes and of the analogous ruthenium(II) complexes.

Half–Wave Potentials (V) of Silicon(IV) Complexes[a]				**Half–Wave Potentials(V) of Ruthenium(II) Complexes[b]**			
Ligand	**+4 → +3**	**+3 → +2**	**+2 → +1**	**Ligand**	**+2 → +1**	**+1 → 0**	**0 → -1**
bpy	-0.530	-0.758	-1.001	**bpy[148]**	-1.72	-1.90	-2.13
4dtbbpy	-0.705	-0.915	-1.140	**4dtbbpy[148]**	-1.81	-2.02	-2.19
5dmbpy	-0.650	-0.875	-1.140	**5dmbpy[149]**	-1.94	-2.13	-2.39
ttpy	-0.420	-0.620	-1.120	**ttpy[152]**	-1.63	-1.87	NA

[a] Potentials for the silicon complexes were measured vs. Fc/Fc^+

[b] Potentials for the ruthenium complexes are artificially approximated vs. Fc/Fc^+

The strong MLCT transitions reported for each of the ruthenium complexes are, as expected and supported by DFT calculations in literature, completely absent in the silicon complexes, each of which is colorless in the bleached state, or only slightly colored in the case of $[Si(ttpy)_2]^{+4}$ (FIGURE 46).

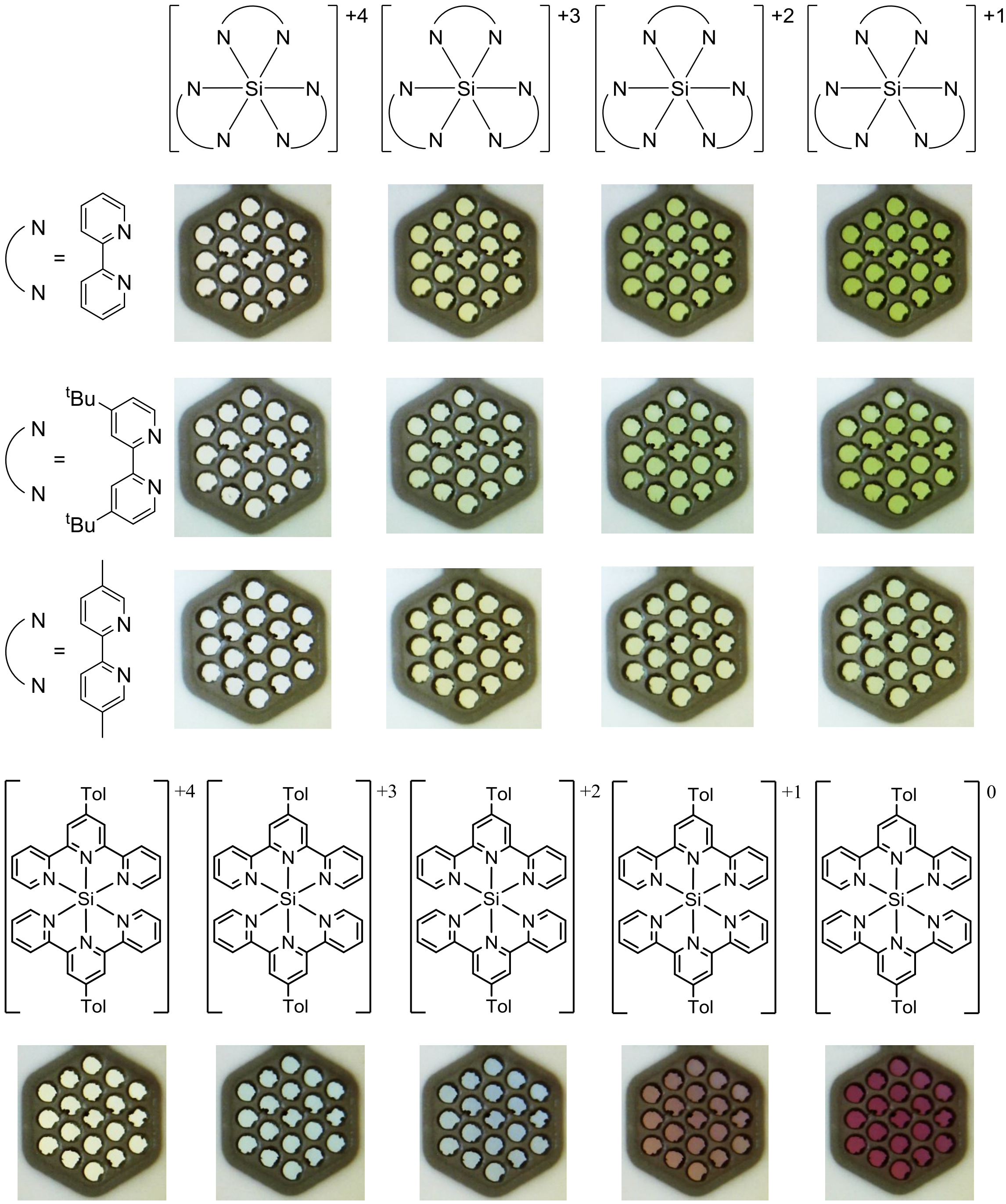

FIGURE 46: Structures and photos of the initial and reduced states for the discussed silicon complexes using a honeycomb platinum electrode.

Although $[Ru(bpy)_3]^{+2}$ is the only complex with spectroelectrochemistry reported from these ligands, it can be seen that radical bipyridine π → π* transitions occur in the

UV and in mid–300 and high–800 nm ranges, but with the tris–bipyridine silicon complex, these same transitions are shifted to high–300 and low–800 nm ranges (TABLE 9), leading to what would be different colors even if ruthenium had no MLCT bands.[138, 151] In comparing the bipyridine complexes, very little difference (< 30 nm) was present in the peak maxima of each corresponding peak, but this slight difference does contribute to subtle differences in the color of the complexes (FIGURE 46). Because of the intrinsic difference in the transitions of the $[Si(ttpy)_2]^n$ complex, it had drastically different colors than the bipyridine complexes.

TABLE 9: Absorbance maxima of the discussed silicon(IV) complexes.

	Absorbance Maxima (nm) of Silicon(IV) complexes				
Ligand	**+4 species**	**+3 species**	**+2 species**	**+1 species**	**0 species**
bpy	327 341	322 390 802 (br)	318 385 802 (br)	370 802 (br)	NA
4dtbbpy	321 334	317 391 807 (br)	314 386 807 (br)	312 377 807 (br)	NA
5dmbpy	340 356	333 413	328 398 830 (br)	384 397 830 (br)	NA
ttpy	301 378 407	300 376 653 (br)	303 333 420 653 (br)	393 495 (long tail)	391 514 (long tail)

Also, understanding that the initial peak is affected by π → π* transitions of three neutral ligands and the second near–UV peak is affected by π → π* transitions of three reduced ligands, the peak heights in the $[Ru(bpy)_3]^{+2}$ and $[Ru(bpy)_3]^{-1}$ are the same, and this is similarly seen in the triply–reduced species for the bpy and 4dtbbpy complexes. However, this was not observed with the 5dmbpy complex likely because of not reaching the fully reduced +1 species due to the possible adsorption of the neutral species.

For the 4dtbbpy and 5dmbpy complexes, attempts to reduce them from the +1 to the neutral species resulted in an immediate, irreversible decrease in absorbance, which would be consistent with plating out of the neutral complex on the electrode (Appendix B). And for all complexes, reduction in the presence of oxygen, when the spectroelectrochemical cell had not been properly mixed and degassed, led to an irreversible chemical reaction and the appearance of an unidentified species that absorbs in the 400-500 nm range and not at higher wavelengths (Appendix C). Although the species are unknown, their difference in absorbance in comparison to the degassed samples would allow for a visual indication of the presence of oxygen in a compromised system or device.

3.3. Summary

Four polypyridine silicon(IV) complexes, $[Si(bpy)_3](PF_6)_4$, $[Si(4dtbbpy)_3](PF_6)_4$, $[Si(5dmbpy)_3](PF_6)_4$, and $[Si(ttpy)_2](PF_6)_4$, were synthesized and isolated. All of them displayed chemically reversible reductions and electrochromism upon spectroelectrochemical characterization. Several other ligands were used to produce complexes as well, but although most of them displayed ^{1}H NMR evidence that the proper complex was formed, the hexafluorophosphate salts could not be isolated.. The SiI_4 route seems to be much less viable in providing a general procedure for synthesizing complexes with any polypyridine ligand, while the $SiCl_4$ appears to be limited by the extent to which the polypyridine can be dimetallated. More work is required to enhance the usability of these reaction routes. Expanding the color palette could be done more significantly with ligands that have electronically active substituents or by the formation of heteroleptic complexes that could mix the electronics of different ligands. Chapter 4 will discuss progress made towards synthesizing a polymerizable silicon complex that could be immobilized on a substrate for device application.

3.4. Experimental Parameters

All reagents were used as received without further purification. SiI_4, pyridine, and 2–picoline were all stored and used under a nitrogen atmosphere in the glovebox. THF was always taken freshly from a solvent purification system (SPS–400, Innovative Technologies) and acetonitrile was HPLC–grade solvent from Sigma Aldrich. $TBAPF_6$ was synthesized by mixing 95%/5% TBACl/TBABr with NH_4PF_6 in acetone, followed by removal of the byproduct solid, evaporation to dryness, recrystallization twice from ethanol and once from ethyl acetate, then drying under vacuum.

NMR spectra were acquired using a JEOL 300 MHz NMR spectrometer. A 60° pulse width with a relaxation delay of 10 s, due to the addition of tris(acetylacetonato)chromium(III) ($Cr(acac)_3$), was used for the ^{29}Si spectra. No pre–transform blip routine was performed, so the broad peak corresponds to the signal obtained from the silica of the glass NMR tube. Although referenced by figure numbers in this section, all NMR spectra are provided in Appendix D.

Cyclic voltammetry was performed using a Princeton Applied Research model 273A potentiostat/galvanostat employing a conventional three–electrode setup consisting of a platinum disk working electrode, a Ag/AgCl reference electrode, and a platinum wire auxiliary electrode. Acetonitrile with 0.100 M $TBAPF_6$ was used as the solvent and supporting electrolyte and ferrocene was used as an internal standard.

The spectroelectrochemical cell was purchased from Pine Research Instrumentation and consisted of a covered quartz cuvette with a 1.0 mm pathlength with a printed gold or platinum honeycomb working electrode, a matching (gold or platinum) counter electrode, and a Ag/AgCl reference electrode standardized to the ferrocene/ferrocenium couple. Only samples with hexafluorophosphate counterions were prepared in acetonitrile with 0.100 M $TBAPF_6$ and degassed with argon that had been bubbled through acetonitrile. Potentials were then applied to the solution with a Princeton Applied Research model 173 potentiostat/galvanostat and analyzed with an Agilent 8453 Diode Array Spectrometer. UV–Vis spectra were taken using two separate channels in 25 mV increments with at least 45 s of equilibrium time between applied voltage values.

4'–*p*–tolyl–2,2':6'2"–terpyridine: 100 mL of ethanol was stirred in a 250 mL RBF equipped with a reflux condenser. 4.8276 g (39.9 mmol) of 2–acetylpyridine, 2.4312 g (20.2 mmol) of *p*–tolualdehyde, 1.6318 g (40.8 mmol) of solid NaOH, and 65 mL concentrated aqueous ammonia were then added and stirred for 24 h at 34 °C. The resulting precipitate upon cooling was filtered and recrystallized three times from ethanol before drying under vacuum. This afforded 2.3851 g of white tolylterpyridine in 36.4% yield. GC–MS: 323.4 m/z. ^{1}H NMR (300 MHz, CD_3CN, FIGURE 35): δ 2.42 (s, 3 H), 7.38-7.46 (m, 4 H), 7.80 (d, J = 8.0 Hz, 2 H), 7.92-7.98 (m, 2 H), 8.67-8.72 (m, 6 H).

The SiI_4 (pyridine/2–picoline) route was initiated in the glovebox under nitrogen atmosphere. Four equiv. of bipyridine or 2.5 equiv. of terpyridine was combined with one equiv. of SiI_4 and 2.50 mL of solvent in a heavy–wall GPT. The GPT was then removed from the glovebox and typically stirred at 125 °C for 2.5-3 h. Upon completion of the heating period, the tube was opened in air and less than 1 mL of methanol was added to quench byproducts. The contents were then transferred to a centrifuge tube with the use of minimal additional solvent. The solid was isolated then rinsed twice with chloroform and twice with ether before drying under vacuum.

The $SiCl_4$ route was performed using a Schlenck line under an argon atmosphere. Four equiv. of bipyridine or terpyridine was dissolved in THF in a two–necked pear–shaped flask (PSF) before addition of at least 12 equiv. of freshly cut lithium metal. This flask was stirred for several hours, sometimes overnight, until two color changes had occurred. Additional lithium was often added after 3 to 4 h if no second color change had occurred. In a three–necked round bottom flask (RBF), one equiv. of bipyridine or no additional terpyridine was dissolved in THF and then one equiv. $SiCl_4$ was added by syringe. After stirring for a maximum of one h, two equiv. of iodine were added to the flask and stirred for several hours up to two weeks since this product was assumed to be stable.

Conversion to the hexafluorophosphate salt was done by dissolution of the iodide salt in water followed by addition of saturated NH_4PF_6 in water. The resulting precipitate was isolated by centrifugation before being rinsed twice by isopropanol and twice with ether then dried under vacuum at 40 °C.

$[Si(4dtbbpy)_3]I_4$: SiI_4 route (pyridine)– 0.5010 g (1.87 mmol) of 4dtbbpy, 0.25 g (0.47 mmol) of SiI_4, 2.50 mL of pyridine, 125 ˚C, 2.5 h. The supernatant was orange–brown and the precipitate was dark reddish–brown. This produced 0.2961 g of solid for a crude yield of 47.3%. $SiCl_4$ route– In the PSF, 0.4969 g (1.85 mmol) of 4dtbbpy, 30 mL of THF, 0.0877 g (12.6 mmol) of cut Li. An initial wine red color was observed then left overnight before turning yellowish–brown. In the RBF, 0.2555 g (0.95 mmol) of 4dtbbpy, 20 mL of THF. Mistakenly, the lithiation flask (PSF) was cannulated into the second flask (RBF) to make a purple solution before 0.1596 g (0.108 mL, 0.94 mmol) of $SiCl_4$ was added by syringe to form a brown and yellow suspension. This was not reperformed. After 2 h, 0.2414 g (0.95 mmol) of I_2 was added and left to stir overnight. A dark brown solid was filtered out from a dark brown solution. This produced 0.3675 g of solid for a crude yield of 28.8%. ^{1}H NMR (300 MHz, D_2O, FIGURE 58): δ 1.32 (s, 54 H), 7.81-7.83 (m, 6 H), 8.23 (s, 6 H), 8.59 (d, *J* = 5.9 Hz, 6 H).

$[Si(4dtbbpy)_3](PF_6)_4$: 0.0102 g (7.61 μmol) of $[Si(4dtbbpy)_3]I_4$ was added to a centrifuge tube along with 5 mL of chloroform and 5 mL (large excess) of saturated NH_4PF_6. After sonication, a light yellow salt persisted between the layers which could be carefully isolated and rinsed. ^{1}H NMR (300 MHz, CD_3CN, FIGURE 59): δ 1.49 (s, 54 H), 7.25 (d, *J* = 6.6 Hz, 6 H), 7.98 (dd, *J* = 2.0, 6.6 Hz, 6 H), 8.96 (d, *J* = 1.7 Hz, 6 H).

$[Si(4dmbpy)_3]I_4$: SiI_4 route (pyridine)– 0.4040 g (2.19 mmol) of 4dmbpy, 0.25 g (0.47 mmol) of SiI_4, 2.50 mL of pyridine, 125 ˚C, 2.5 h. The supernatant was black and the precipitate was black. This produced 0.1892 g of solid for a crude yield of 37.2%. SiI_4 route (2–picoline)– 0.35 g (1.9 mmol) of 4dmbpy, 0.25 g (0.47 mmol) of SiI_4, 3.00 mL of 2–picoline, 125 ˚C, 2.5 h. The supernatant was orange and the precipitate was black. This produced 0.3533 g of solid for a crude yield of 69.6%. $SiCl_4$ route– In the PSF, 0.4925 g (2.67 mmol) of 4dmbpy, 10 mL of THF, 0.0539 g (7.77 mmol) of cut Li. An initial wine red color was observed then left overnight before turning yellowish–brown. In the RBF, 0.2741 g (1.49 mmol) of 4dmbpy, 18 mL of THF, 0.2374 g (0.160 mL, 1.40 mmol) of $SiCl_4$. Cannulation of the lithiation flask caused immediate precipitation of tan solid. After 2 h, 0.3497 g (1.38 mmol) of I_2 was added to get a darkening of the suspension and left to stir overnight. A dark tan solid was filtered out from a dark brown solution. This produced 0.6382 g of solid for a crude yield of 41.5%. ^{1}H NMR (300 MHz, D_2O, FIGURE 60): δ 2.50 (s, 18 H), 7.59 (d, *J* = 5.7 Hz, 6 H), 8.11 (s, 6 H), 8.52 (d, *J* = 5.5 Hz, 6 H).

$[Si(5dmbpy)_3]I_4$: SiI_4 route (pyridine)– 0.3440 g (1.87 mmol) of 5dmbpy, 0.25 g (0.47 mmol) of SiI_4, 2.50 mL of pyridine, 125 ˚C, 2.5 h. The supernatant was dark brown and the precipitate was dark red. This produced 0.3868 g of solid for a crude yield of 76.1%. SiI_4 route (2–picoline)– 0.3480 g (1.89 mmol) of 5dmbpy, 0.25 g (0.47 mmol) of SiI_4, 3.00 mL of 2–picoline, 125 ˚C, 2.5 h. The supernatant was orange–yellow and the precipitate was black. This produced 0.0819 g of solid for a crude yield of 16.1%. $SiCl_4$ route– In the PSF, 0.5120 g (0.278 mmol) of 5dmbpy, 17 mL of THF, 0.2286 g (32.9 mmol) of cut Li. An initial wine red color was observed before turning green in only 1 h. In the RBF, 0.2585 g (1.40 mmol) of 5dmbpy, 20 mL of THF, 0.2379 g (0.161 mL, 1.40 mmol) of $SiCl_4$. Cannulation of the lithiation flask caused immediate precipitation of yellowish–brown solid. After 1 h, 0.6888 g (2.71 mmol) of I_2 was added to get a darker red suspension and left to stir over two weeks. A black solid was filtered out from a dark brown solution. This produced 0.0519 g of solid for a crude yield of 3.4%. ^{1}H NMR (300 MHz, D_2O, FIGURE 61): δ 2.31 (s, 18 H), 7.18 (s, 6 H), 8.70 (d, *J* = 8.5 Hz, 6 H), 8.98 (d, *J* = 8.5 Hz, 6 H).

$[Si(5dmbpy)_3](PF_6)_4$: 0.0500 g (0.046 mmol) was dissolved in 200 mL of water in a beaker. After several hours, 5 mL (large excess) of saturated NH_4PF_6 was added to get immediate precipitation of a light–colored salt. This salt was filtered then rinsed. ^{1}H NMR (300 MHz, CD_3CN, FIGURE 62): δ 2.40 (s, 18 H), 6.94 (s, 6 H), 8.68 (d, *J* = 8.2 Hz, 6 H), 8.88 (d, *J* = 8.3 Hz, 6 H).

[Si(4dmobpy)$_3$]I$_4$: SiI$_4$ route (pyridine)– 0.4040 g (1.87 mmol) of 4dmobpy, 0.25 g (0.47 mmol) of SiI$_4$, 2.50 mL of pyridine, 125 ˚C, 2.5 h. The supernatant was brown and the precipitate was yellowish-tan. This produced 0.1735 g of solid for a crude yield of 31.4%. SiI$_4$ route (2–picoline)– 0.4287 g (1.98 mmol) of 4dmobpy, 0.25 g (0.47 mmol) of SiI$_4$, 3.20 mL of 2–picoline, 125 ˚C, 2.5 h. The supernatant was yellow and the precipitate was red/pink. This produced 0.3808 g of solid for a crude yield of 68.9%. SiCl$_4$ route– In the PSF, 0.4999 g (2.31 mmol) of 4dmobpy, 25 mL of THF, 0.2045 g (29.5 mmol) of cut Li. An initial red–purple color was observed quickly, but no second color change after 3 h of reaction. Another 0.0526 g (7.58 mmol) of Li was cut in and left to stir overnight with still no second color change. In the RBF, 0.2600 g (1.20 mmol) of 4dmobpy, 15 mL of THF, 0.1872 g (0.126 mL, 1.10 mmol) of SiCl$_4$. Cannulation of the lithiation flask seemed to form a dark gray solid. After 1 h, 0.5731 g (2.26 mmol) of I$_2$ was added to get a yellowish–brown suspension and left to stir over two weeks. A black solid was filtered out from a dark brown solution. This produced 0.0623 g of solid for a crude yield of 4.7%.

[Si(tpy)$_2$]I$_4$: SiI$_4$ route (pyridine)– 0.1994 g (0.62 mmol) of tpy, 0.22 g (0.41 mmol) of SiI$_4$, 2.52 mL of pyridine, 125 ˚C, 3 h. The supernatant was yellowish–brown and the precipitate was black. This produced 0.2842 g of solid for a crude yield of 69.0%. SiI$_4$ route (2–picoline)– 0.2210 g (0.68 mmol) of tpy, 0.25 g (0.47 mmol) of SiI$_4$, 3.00 mL of 2–picoline, 125 ˚C, 3 h. The supernatant was brown and the precipitate was black. This produced 0.3072 g of solid for a crude yield of 65.7%. SiCl$_4$ route– In the PSF, 0.5009 g (1.55 mmol) of tpy, 15 mL of THF, 0.1798 g (25.9 mmol) of cut Li. An initial blue–green color was observed with a black color change 5 h later. In the RBF, 22 mL of THF, 0.1623 g (0.110 mL, 0.96 mmol) of $SiCl_4$. Cannulation of the lithiation flask provided no obvious signs of reaction or precipitation. After 1 h, 0.4880 g (1.92 mmol) of I_2 turned the solution dark yellowish–brown and was left to stir overnight. A green solid was filtered out from a dark brown solution. This produced 0.6309 g of solid for a crude yield of 65.1%. ^{1}H NMR (300 MHz, D_2O, FIGURE 63): δ 8.05-8.09 (m, 4 H), 8.30-8.36 (m, 2 H), 8.48-8.50 (m, 4 H), 8.65-8.73 (m, 8 H), 8.87-8.89 (m, 4 H).

$[Si(ttpy)_2]I_4$: SiI_4 route– 0.2444 g (0.76 mmol) of ttpy, 0.16 g (0.30 mmol) of SiI_4, 3.00 mL of pyridine, 125 ˚C, 3 h. The supernatant was brown and the precipitate was dark brown. This produced 0.3021 g of solid for a crude yield of 85.5%. SiI_4 route (2–picoline)– 0.3010 g (0.93 mmol) of ttpy, 0.25 g (0.47 mmol) of SiI_4, 3.00 mL of 2–picoline, 125 ˚C, 3 h. The supernatant was greenish–yellow and the precipitate was dark brown. This produced 0.3418 g of solid for a crude yield of 61.9%. $SiCl_4$ route– In the PSF, 0.5134 g (1.59 mmol) of ttpy, 15 mL of THF, 0.1493 g (21.5 mmol) of cut Li. An initial dark green color was observed with no second color change in 3 h. Another 0.0360 g (5.19 mmol) of Li was added to the flask then left to stir, turning a black color overnight. In the RBF, 20 mL of THF, 0.1452 g (0.098 mL, 0.86 mmol) of $SiCl_4$. Cannulation of the lithiation flask produced a dark brown/black solution that became dark green after 1 h. 0.4043 g (1.59 mmol) of I_2 turned the solution dark yellowish–brown and left to stir over two weeks. A black solid was filtered out from a dark brown solution. This produced 0.2176 g of solid for a crude yield of 21.3%. ^{1}H NMR (300 MHz, D_2O, FIGURE 64): δ 2.44 (s, 6 H), 7.58 (d, J = 7.7 Hz, 4 H), 7.80-7.88 (m, 8 H), 8.24 (d, J = 8.0 Hz, 4 H), 8.62 (t, J = 7.8 Hz, 4 H), 9.13 (d, J = 8.3 Hz, 4 H), 9.67 (s, 4 H).

$[Si(ttpy)_2](PF_6)_4$: 0.0500 g (0.042 mmol) of $[Si(ttpy)_2]I4_4$ was dissolved in 40 mL of water in a centrifuge tube. Addition of 5 mL (large excess) of saturated NH_4PF_6 in water caused immediate precipitation of a yellow–colored salt which could be isolated and rinsed. ^{1}H NMR (300 MHz, CD_3CN, FIGURE 65): δ 2.62 (s, 6 H), 7.72-7.86 (m, 8 H), 7.86 (t, *J* = 7.8 Hz, 4 H), 8.40 (d, *J* = 8.0 Hz, 4 H), 8.68 (t, 7.8 Hz, 4 H), 9.09 (d, *J* = 7.7 Hz, 4 H), 9.54 (s, 4 H). $^{13}C\{^1H\}$ NMR (75 MHz, CD_3CN, FIGURE 66): δ 21.21, 124.63, 127.77, 130.11, 131.00, 131.35, 141.15, 143.90, 145.72, 147.69, 148.86. ^{29}Si NMR (59.6 MHz, CD_3CN, FIGURE 67): δ -154.

$[Si(Cltpy)_2]I_4$: SiI_4 route (pyridine)– 0.1008 g (0.38 mmol) of Cltpy, 0.08 g (0.15 mmol) of SiI_4, 2.50 mL of pyridine, 125 ˚C, 18 h. The supernatant was dark brown and the precipitate was black. This produced 0.0589 g of solid for a crude yield of 36.8%.

CHAPTER 4: APPLICATIONS AND DEVICES FOR ELECTROCHROMIC MATERIALS– TOWARDS POLYMERIZABLE SILICON COMPLEXES

4.1. Introduction

There are several applications for which electrochromic materials are being commercially used. These include dual–use materials for batteries and capacitors,[158-159] such as the color indication of lithium ion intercalation and storage with TiO_2 nanorods,[160] and multichromic materials for flexible displays,[161] such as the mixing of heptyl viologen and a polymer electrolyte that induced dimerization and an additional maroon coloring of the viologen (FIGURE 47).[162]

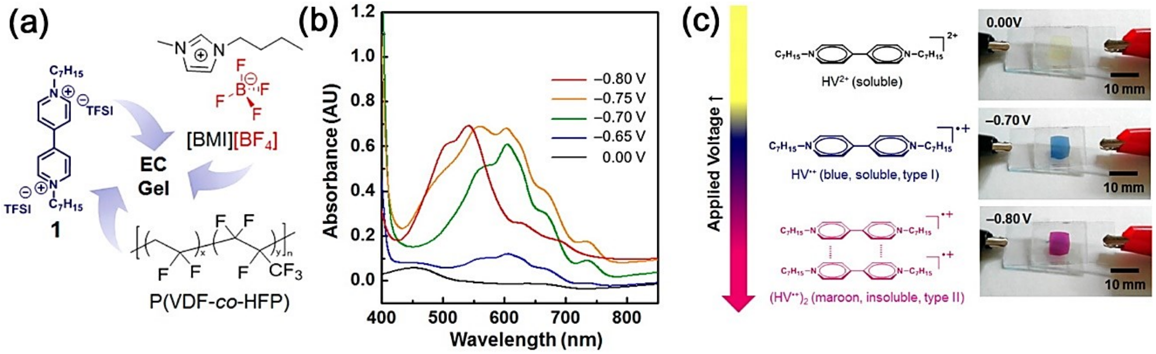

FIGURE 47: (a) Key components of the electrochromic (EC) gel. (b) Effect of applied potential on the UV–Vis spectra of the EC gel. (c) Photographs of the states at 0.00, -0.70, and -0.80 V along with color–contributing species.[162]

By far, however, the greatest use of electrochromic materials to date is in smart windows and similar applications, where the materials' changing absorbance spectrum can provide either different colors or different opacities to the windows in which they are being used. Besides the applications in aircraft windows and rear–view mirrors, smart windows are of great importance to the windows of buildings, where they could provide desirable colors or tinting for the inhabitants, improve energy efficiency, and adjust heat retention or shielding.[163] In order to test many of the properties and present viable materials for electrochromic applications, incorporation into devices is the necessary end goal.

Smart windows in their simplest form must consist of two electrodes (a substrate with a transparent electrical conductor) sandwiching an electrochromic layer and an electrolyte layer. As mentioned in Section 2.1, often two separate electrochromic materials are used, one at each electrode, as shown in FIGURE 48, either for an increase in the intensity of the coloring or for greater variability in the available colors. The electrolyte most frequently employed is a solid–state electrolyte like ionic gels and polymer electrolytes, a few of which are reviewed by Thakur *et al.*[164] In order to maximize switching speeds and avoid reconversion of a material to its bleached state, the electrochromic material is typically designed to be kept in contact with its appropriate electrode. This can be done by growth and annealing of a metal oxide onto another conducting oxide,[165] ink–jet printing of a polymer onto conducting plastic,[166] self–assembly of transition metal complexes into monolayers[167] or layered molecular assemblies,[168] or electropolymerization of the electrochromic layer directly to the electrode.[169]

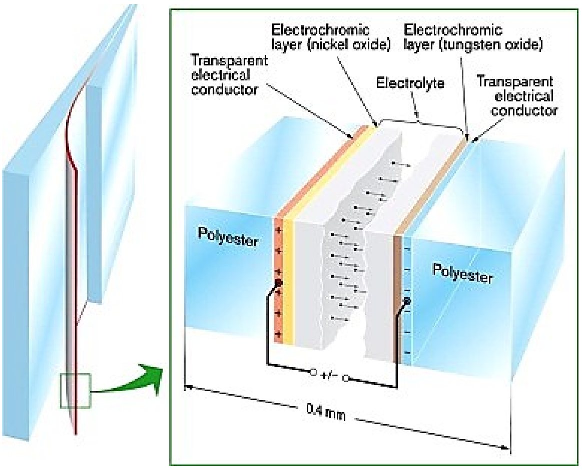

FIGURE 48: Schematic of an electrochromic device using metal oxides and polyester backing for flexibility. Other devices can use different electrochromic layers and hard glass as backing.[170]

The work of Nie *et al.* presents the best opportunity of synthesizing initial silicon analogs for complexes that could be electropolymerized onto an electrode. The visible absorption spectra of several ruthenium complexes containing 5,5'–divinyl–2,2'–bipyridine (5dvbpy) ligands are shown in FIGURE 49 and incorporating more 5dvbpy ligands decreases and broadens the MLCT peak (Compounds 1, 3, and 4 in FIGURE 49) while a greater effect is seen by adding phenyl groups at either the 4,4'– or the 5,5'–positions, the second of which are more likely to be influencing the geometry of the polymer.[140] The following sections summarize the work conducted towards synthesizing silicon complexes with a single 5dvbpy ligand.

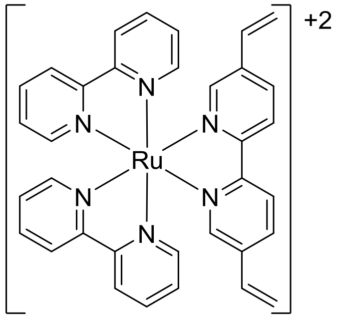

1

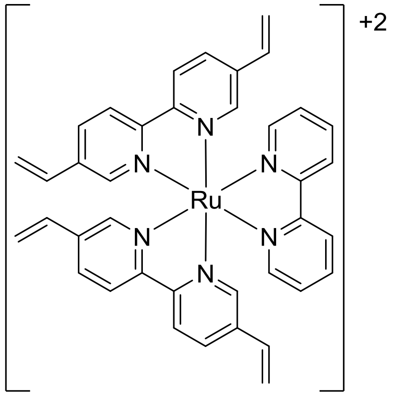

3

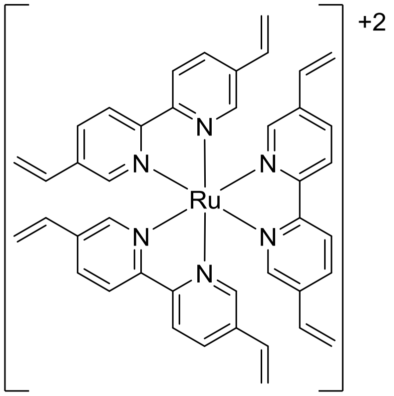

4

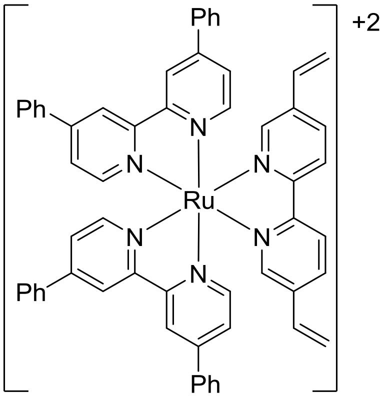

5

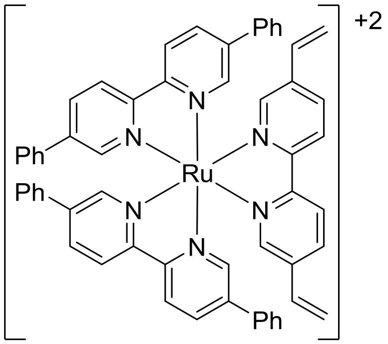

6

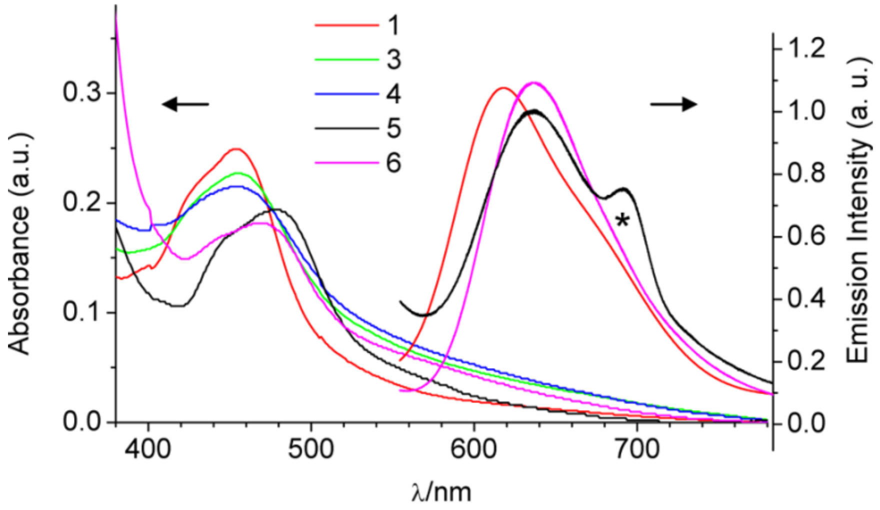

FIGURE 49: (top) Structures of (1) $[Ru(5dvbpy)(bpy)_2]^{+2}$, (3) $[Ru(5dvbpy)_2(bpy)]^{+2}$, (4) $[Ru(5dvbpy)_3]^{+2}$, (5) $[Ru(5dvbpy)(4dpbpy)_2]^{+2}$, (6) $[Ru(5dvbpy)(5dpbpy)_2]^{+2}$. (bottom) Representative absorption and emission spectra of polymeric films of each of the above complexes on optically transparent ITO glass electrodes immersed in MeCN. (The asterisk denotes noise from imperfect background correction.)[140]

4.2. Results and Discussion

4.2.1. 5,5'–dibromo–2,2'–bipyridine (Br_2bpy)

In order to synthesize the 5dvbpy ligand, 5,5'–dibromo–2,2'–bipyridine (Br_2bpy) is needed as a precursor material. Three processes for synthesizing the Br_2bpy were used. The first process involves a Stille–type coupling which couples organotin compounds with organohalide compounds using palladium as a catalyst (SCHEME 17).[171]

SCHEME 17: Coupling reaction scheme for the synthesis of 5,5'–dibromo–2,2'–bipyridine.[171]

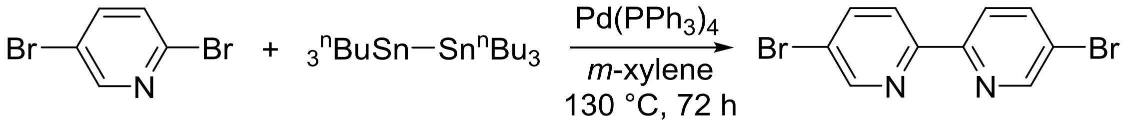

2,5–dibromopyridine (Br_2py) was mixed with hexa–*n*–butylditin to form a tinillated pyridine species *in situ* and was coupled by tetrakis(triphenylphosphine)palladium(0) ($Pd(PPh_3)_4$). This reaction was performed in a glovebag due to the reactivity of the Pd(0) catalyst with oxygen. Although Br_2py possesses two bromine atoms theoretically capable of reacting, it couples nearly exclusively at the 2–position, leaving bromine atoms at the 5– and 5'–positions for further activity. Success with this process yielded very little material (< 200 mg, < 15.1%) and an alternative preparation was found to synthesize much more product.

Large–scale synthesis of Br_2bpy was first done using a neat approach with a reaction bomb and liquid bromine (SCHEME 18).[172]

SCHEME 18: Reaction scheme for the synthesis of 5,5'–dibromo–2,2'–bipyridine using 2,2'–bipyridine dihydrobromide and bromine.[172]

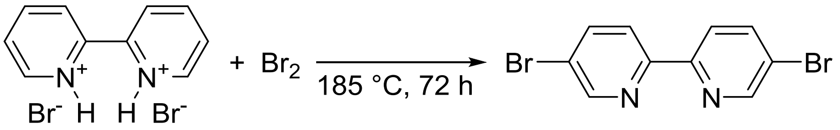

This procedure used a precursor of 2,2'–bipyridine dihydrobromide (bpydhb) which could be made very efficiently by combining bipyridine with either hydrobromic acid or acetyl bromide in methanol.[172] In a fume hood, this bpydhb was then carefully ground together in a mortar with a slight excess of liquid bromine to prepare an orange solid, being careful to minimize the evaporation of bromine. By compressing this solid into a glass vial, the vial could be loaded into a pressure–sealed metal bomb and heated to 185 ˚C for 72 h. This produced a hard orange–brown cake that proved to be a mixture of bpy, 5–bromo–2,2'–bipyridine (Brbpy), and Br_2bpy. It was found that using boiling acetone would dissolve the bpy and Brbpy with very little dissolution of the Br_2bpy. Thus, several washes with hot acetone produced pure off–white Br_2bpy. This process worked well until the yield decreased to the point of no longer producing the Br_2bpy, and it is thought that the bomb was being corroded and losing its efficacy.

Since the bomb was no longer a viable option, this large–scale synthesis was then adapted to use with a heavy–wall GPT. Because of the rubber o–rings that are used to seal GPTs, failure occurred if too much bromine was used due to too high of pressure being reached. Thus, a smaller scale than that with the bomb had to be used because of the volume of the GPTs available. Br_2bpy was isolated in much better yield through this and regardless of the route, can be easily identified by ^{1}H NMR or GC–MS.

4.2.2. 5,5'–divinyl–2,2'–bipyridine (5dvbpy)

The bromine substituents in Br_2bpy can be replaced by vinyl groups by using a Suzuki–Miyaura coupling, which couples organoborate compounds with organohalides using palladium as a catalyst (SCHEME 19).

SCHEME 19: Coupling reaction scheme for the synthesis of 5,5'–divinyl–2,2'–bipyridine.[173]

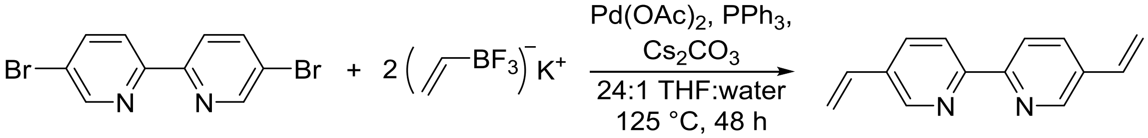

Although $Pd(PPh_3)_4$ could be used, it can also be formed *in situ* by using palladium(II) acetate and triphenylphosphine, and this reaction is necessarily done in a glovebag as well. This palladium catalyst couples Br_2bpy and potassium(vinyltrifluoroborate) in a mixed solvent of THF and water, using Cs_2CO_3 to assist in the capture of byproducts. Upon reacting, the solution would become yellow and often have a gray or black solid, presumably palladium catalyst that had gotten used up. After completion, 5,5'–divinyl–2,2'–bipyridine (5dvbpy) can be extracted into chloroform and evaporated to a dark yellow solid. Purification was modified slightly from the conditions of the paper, which called for 35:50:1 petroleum ether/dichloromethane/ammonia, because the mixture was extremely volatile and the ammonia kept separating out. Thus, 85:15 petroleum ether/ethyl acetate provided a light yellow solid that could be identified as 5dvbpy using ^{1}H NMR or GC–MS. However, in both forms of characterization, impurities were noticed that had low molecular weight and low chemical shifts, but these were unable to be separated out using recrystallization techniques or different chromatography mobile phases and ultimately prevented further progress with this project.

4.2.3. Dibromobipyridine and Divinylbipyridine Silicon Complexes

Once both ligands were obtained and purified, they could be combined with a silicon complex that had two open sites available to bind the bipyridine. Using SiI_4 as the starting silicon source with a slight excess of two equiv. of bipyridine and chloroform as the solvent, the bis–substituted product can be synthesized, rather than coordinating all the way to the tris–bipyridine complex (SCHEME 20).[75]

SCHEME 20: Representative reaction scheme for the synthesis of bis–bipyridine silicon(IV) Complexes.

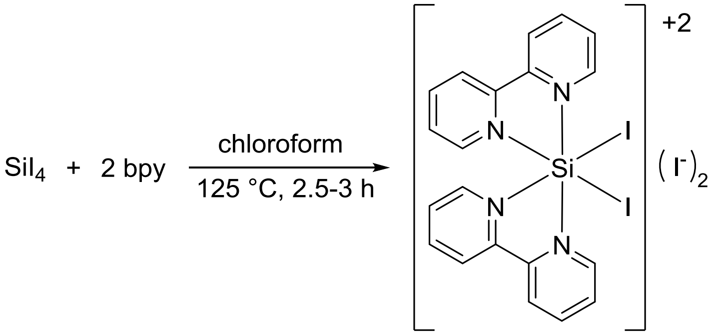

As long as this product is isolated in the glovebox, two iodide ligands are available to be replaced by other ligands. A similar procedure was performed for 4dmbpy and 4dtbbpy to obtain the bis–substituted silicon complexes of these ligands as well. Because of their reactivity, ^1H NMR spectroscopy of these complexes cannot be directly assessed, but by reacting them in deuterated methanol to displace the iodides, one can assess the splitting pattern of the aromatic region to determine whether bis–substitution has occurred, which is unique in its symmetry. All three complexes show this splitting pattern and the ^{1}H NMR spectra of each complex after reaction in CD_3OD is given in Appendix E.

Specifically, the bis–bipyridine complex was then combined with both Br_2bpy and 5dvbpy in pyridine in a similar fashion to the SiI_4 route discussed in the previous chapters. These silicon complexes could then hopefully be polymerized by either reductive polymerization (for the 5dvbpy complex) or coupling with bis(1,5–cyclooctadiene)nickel(0) (Ni(COD)$_2$, for the Br_2bpy complex), as shown in SCHEME 21.

SCHEME 21: Available polymerization routes for the discussed silicon complexes.

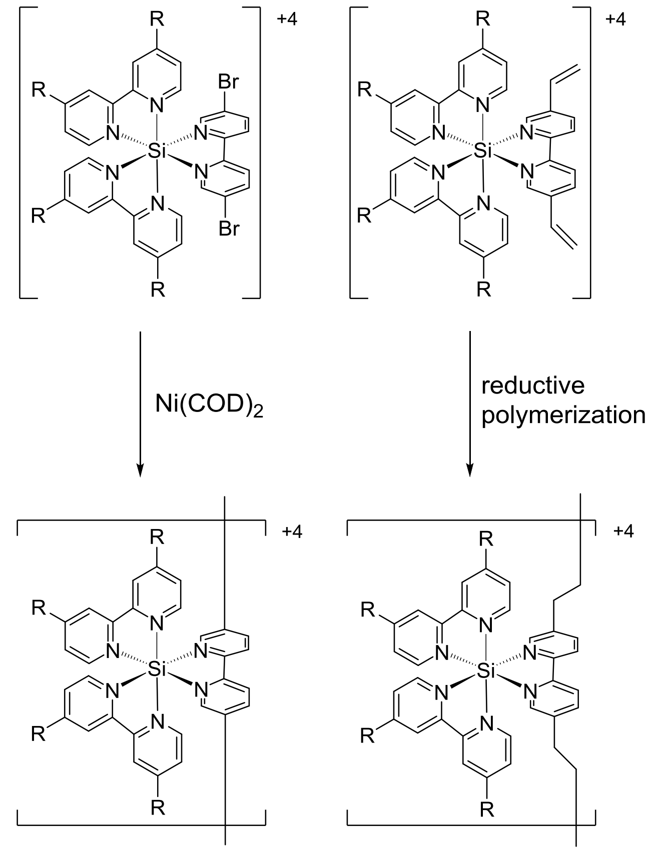

Conjugated polyelectrolyte Redox-active polymers

But although solid product was isolated, the obtained ^{1}H NMR spectra did not contain any new aromatic peaks corresponding to the newly–added ligand and the peaks that were present were similar to those in the ^{1}H NMR spectrum of the $[Si(bpy)_2I_2]I_2$ complex. The crude ^{1}H NMR spectra obtained after these attempted syntheses are also given in Appendix E. Further optimization for synthesizing these complexes could still be done, such as changing reaction time and temperature or the amount of monomer ligand added in greater excess. These options were not performed because of minimal amounts of purified ligand to use in these syntheses. The 5dvbpy complex could also be targeted through the $SiCl_4$ route using bipyridine in the dilithiation flask but adding 5dvbpy to $SiCl_4$ in the second flask to form the white precipitate. This is more likely to create side products using the Br_2bpy because of the reactivity of the bromine substituents.

4.3. Summary

Progress towards polymerizable silicon complexes that could be immobilized onto an electrode for use in an electrochromic device was demonstrated. 5,5’–dibromo–2,2’–bipyridine can be synthesized by several different procedures and used in turn to synthesize 5,5’–divinyl–2,2’–bipyridine. Although initial investigations into using the SiI_4 route to form heteroleptic complexes with the Br_2bpy or 5dvbpy ligands did not succeed, opportunity is still available in tailoring the reaction conditions or through use of the $SiCl_4$ route. This also provides a look into the viability of forming heteroleptic complexes with other bipyridine ligands, showing that a general procedure is unlikely to work with every available ligand, as seen with the homoleptic complexes in Chapter 3.

4.4. Experimental Parameters

All reagents were used as received without further purification. Most reagents were handled under nitrogen atmosphere in either the glovebox or a glovebag. NMR spectroscopy was performed using a JEOL 300 MHz spectrometer.

2,2'–bipyridine dihydrobromide (bpydhb): Option A– 10.0 g (0.064 mol) of bpy combined with 21.5 mL (~ 0.204 mol) of 48% (wt/wt) aqueous HBr in 50 mL of methanol at 0 °C. After addition, stirred at R.T. for 30 min then evaporated to dryness using a rotary evaporator and vacuum pump before storing in a closed lab drawer. Option B– 10.0 g (0.064 mol) of bpy combined with 12.0 mL (~ 0.162 mol) of acetyl bromide in 75 mL of methanol at 0 °C. After addition, stirred at R.T. for 30 min then evaporated to dryness using a rotary evaporator and vacuum pump before storing in a closed lab drawer.

5,5'–dibromo–2,2'–bipyridine (Br_2bpy): Stille–type coupling– 0.9875 g (3.15 mmol) of 2,5–dibromopyridine was mixed with 1.3353 g (2.30 mmol) of hexa–*n*–butylditin, 0.200 g (0.17 mmol) of tetrakis(triphenylphosphine)palladium(0), and 35 mL of *m*–xylene in a heavy–wall GPT in a glovebag under nitrogen atmosphere. Heating the reaction to 130 ˚C for 72 h gave a yellow solution with tan solid. This crude suspension was combined with 25 mL of 1 M aqueous EDTA and extracted with $CHCl_3$. The organic layer was evaporated to dryness. Silica chromatography for the first fluorescent fraction using 1:4 hexanes/ethyl acetate yielded < 0.200 g (< 15.1%). Bomb reaction– 7.81 g (24.8 mmol) of bpydhb was ground together in a mortar with 4.5 mL (87.2 mmol) of liquid bromine. This solid was compressed into a large (20 dram) glass vial then loaded into a pressure–sealed metal bomb and heated to 185 ˚C for 72 h. Liberation of the hard cake was done by breaking the vial. Several washes with hot acetone produced pure off–white Br_2bpy (1.1427 g, 14.6%). GPT reaction– 3.00 g (9.51 mmol) of bpydhb was ground together in a morter with 1.3 mL (25.2 mmol) of liquid bromine. This solid was then compressed into a GPT and heated to 185 ˚C for 72 h. Several washes with hot acetone produced 1.20 g of Br_2bpy in 40.3% yield. GC–MS: 313.9 m/z. ^1H NMR (300 MHz, $CDCl_3$): 7.94 (dd, *J* = 2.5, 8.5 Hz, 2 H), 8.29 (d, *J* = 8.5 Hz, 2 H), 8.71 (d, *J* = 2.5 Hz, 2 H).

5,5'–divinyl–2,2'–bipyridine (5dvbpy): 0.70g (2.23 mmol) Br_2bpy, 1.15 g (8.58 mmol) potassium(vinyltrifluoroborate), 2.33 g Cs_2CO_3 (7.15 mmol), 0.01 g (0.04 mmol) palladium(II) acetate, 0.05 g (0.19 mmol) triphenylphosphine and 35 mL of 24:1 THF:water were added together in a heavy–wall GPT in a glovebag under nitrogen atmosphere. The tube was then removed from the glovebag and heated at 85 ˚C for 48 h. The solution was yellow and with gray/black solid. After completion, the tube was opened to air and diluted with 35 mL of water and extracted three times with 100 mL of chloroform. The organic layer was then rinsed with saturated aqueous sodium chloride before being evaporated to a dark yellow solid. This solid was chromatographed through silica using 85:15 petroleum ether/ethyl acetate to provide 0.3639 g of light yellow solid in 78.5% yield. GC–MS: 208.3 m/z. ^1H NMR (300 MHz, $CDCl_3$, FIGURE 50): 5.42 (d, *J* = 11.0 Hz, 2 H), 5.90 (d, *J* = 17.9 Hz, 2 H), 6.77 (dd, *J* = 8.0, 17.6 Hz, 2 H), 7.87 (dd, *J* = 2.2, 8.5 Hz, 2 H), 8.37 (d, *J* = 8.3 Hz, 2H), 8.67 (d, *J* = 2.2 Hz, 2 H).

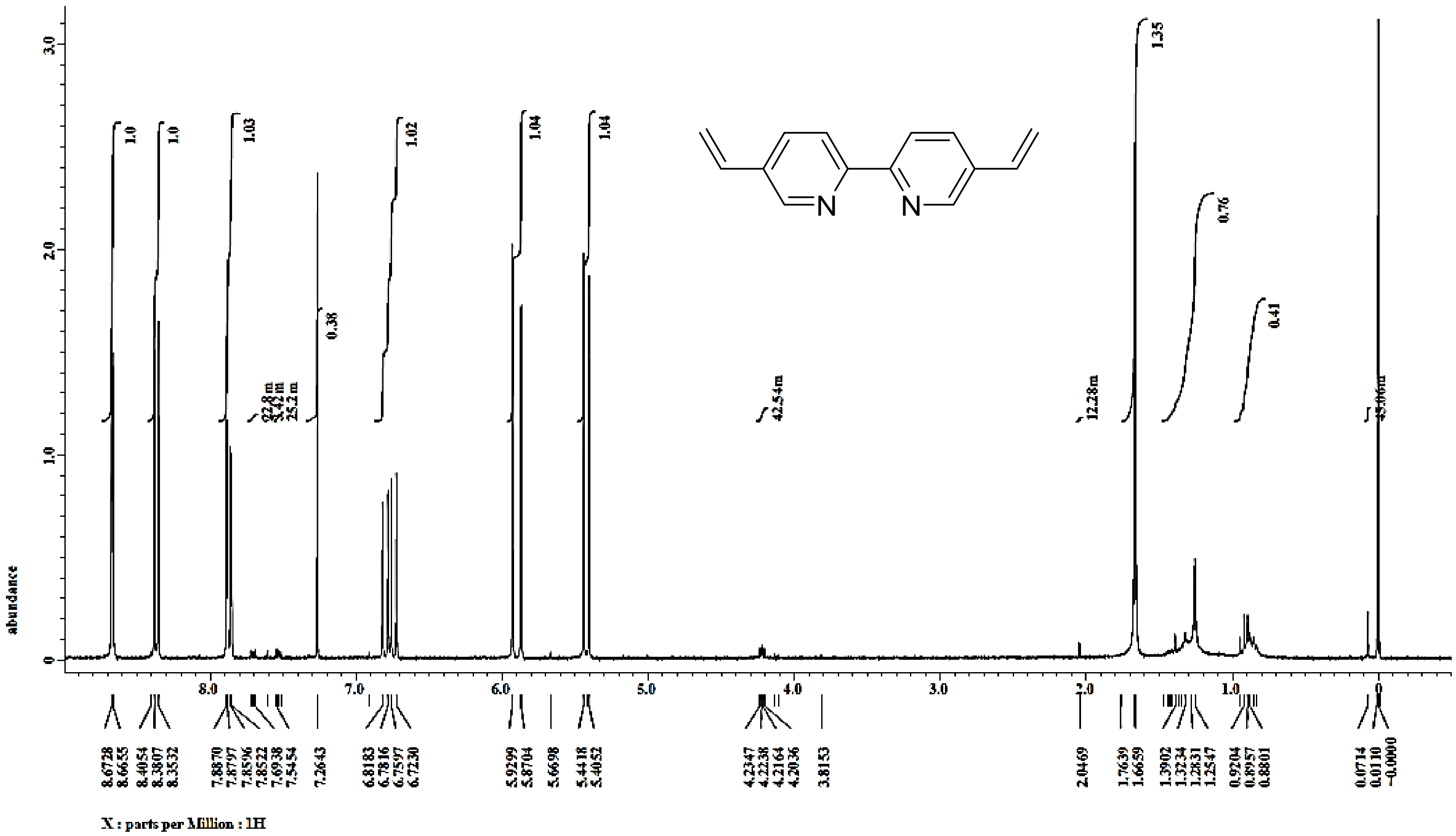

FIGURE 50: ^{1}H NMR spectrum of 5,5’–divinyl–2,2’–bipyridine in $CDCl_3$ with some impurities.

General Method for Bis–Bipyridine Silicon Complexes: In the glovebox, 2.5-3 equiv. of bipyridine were measured into a heavy–wall glass pressure tube (GPT) with 1 equiv. of SiI_4 and 6 mL of chloroform. The tube was then sealed and removed from the glovebox and put into an oil bath at 85 °C for 24 h. After completion, the tube was brought back into the glovebox and vacuum filtered. The solid was rinsed twice with chloroform and briefly dried on the filter paper before being transferred to a vial. The vial was then dried in the vacuum port overnight. A CD_3OD ampoule and NMR tube were brought into the glovebox in order to prepare a sample for NMR spectroscopy. Although labeled with figure numbers here, the ^1H NMR spectrum of each complex is given in Appendix E.

$[Si(bpy)_2I_2]I_2$: General method– 0.12 g (0.77 mmol) of bpy, 0.25 g (0.47 mmol) of SiI_4, 6 mL of chloroform, 85 °C, 24 h. Solid turned dark red during reaction and filtered and dried to the same color. This produced 0.30 g of solid for a 75.8% yield. ^1H NMR (300 MHz, CD_3OD, FIGURE 68): 7.47 (d, J = 5.8 Hz, 2 H), 7.75 (t, J = 6.3 Hz, 2 H), 8.39-8.51 (m, 4 H), 8.90-8.96 (m, 4 H), 9.16 (d, J = 8.0 Hz, 2 H), 9.62 (d, J = 5.8 Hz, 2 H).

$[Si(4dmbpy)_2I_2]I_2$: General method– 0.27 g (1.47 mmol) of 4dmbpy, 0.31 g (0.58 mmol) of SiI_4, 6 mL of chloroform, 85 °C, 24 h. Solid turned yellow during reaction but filtered and dried to red–orange. This produced 0.30 g of solid for a 57.3% yield. ^1H NMR (300 MHz, CD_3OD, FIGURE 69): 2.57 (s, 6 H), 2.88 (s, 6 H), 7.21 (d, J = 5.8 Hz, 2 H), 7.51 (d, J = 6.0 Hz, 2 H), 8.17 (d, J = 6.1 Hz, 2 H), 8.76 (s, 2 H), 8.98 (s, 2 H), 9.38 (d, J = 6.0 Hz, 2 H).

[Si(4dtbbpy)$_2$I$_2$]I$_2$: General method– 0.3086 g (1.15 mmol) of 4dtbbpy, 0.25 g (0.47 mmol) of SiI$_4$, 6 mL of chloroform, 85 °C, 24 h. Solid turned orange–yellow during reaction but filtered and dried to peach colored. This produced 0.29 g of solid for a 57.9% yield. ^{1}H NMR (300 MHz, CD$_3$OD, FIGURE 70): 1.40 (s, 18 H), 1.64 (s, 18 H), 7.28 (d, J = 6.3 Hz, 2 H), 7.73 (d, J = 6.1 Hz, 2 H), 8.36 (d, J = 6.3 Hz, 2 H), 8.98 (s, 2 H), 9.18 (s, 2 H), 9.44 (d, J = 6.3 Hz, 2 H).

[Si(bpy)$_2$(Br$_2$bpy)]I$_4$: 0.27 g (0.32 mmol) of [Si(bpy)$_2$I$_2$]I$_2$, 0.10 g (0.32 mmol) of Br$_2$bpy, and 1.9 mL of pyridine were added to a heavy–wall GPT in the glovebox. The tube was then removed from the glovebox and put in an oil bath at 125 °C for 3 h. The supernatant was dark red and the solid brown. The suspension was transferred to a centrifuge tube and the solid isolated. The solid was rinsed twice with chloroform and twice with ether before drying under vacuum. No yield was measured. The crude ^{1}H NMR is given at the end of this chapter in FIGURE 71.

[Si(bpy)$_2$(5dvbpy)]I$_4$: 0.25 g (0.30 mmol) of [Si(bpy)$_2$I$_2$]I$_2$, 0.0786 g (0.38 mmol) of 5dvbpy, and 2.9 mL of pyridine were added to a heavy–wall GPT in the glovebox. The tube was then removed from the glovebox and put in an oil bath at 125 °C for 3 h. The supernatant was dark red and the solid red–orange. The suspension was transferred to a centrifuge tube and the solid isolated. The solid was rinsed twice with chloroform and twice with ether before drying under vacuum. No yield was measured. The crude ^{1}H NMR is given in Appendix E in FIGURE 72.

CHAPTER 5: CONCLUSIONS AND FUTURE DIRECTIONS

Pyridine–containing ligands are an important class of ligands that have been well studied in transition metal chemistry but not yet incorporated enough into silicon chemistry. Opportunities for biological study and as high–energy, photoluminescent, electroluminescent, or electronic materials are unexplored areas of research and ones that are impacted by the unique properties of these ligands.

Specifically, this dissertation sought to assess the viability of using polypyridine silicon(IV) complexes as electrochromic materials. By using silicon as the center atom, the lack of d–electrons and MLCT bands was expected to provide an initial colorless state, which could be desirable in certain coloring applications. The synthetic variability of the polypyridine ligand would then be able to provide opportunity to fine tune the spectral and spectroelectrochemical properties of the complexes. This was shown successfully with four different complexes, $[Si(bpy)_3]^n$, $[Si(4dtbbpy)_3]^n$, $[Si(5dmbpy)_3]^n$, and $[Si(ttpy)_2]^n$, with colorless, yellow, green, blue, and red–violet options being accessible. However, several more complexes were assessed as well and greater work towards the synthesis and purification of those complexes is still required.

Once this base set of compounds is completed, several other avenues of research are also available by the vast amount of work done with analogous transition metal complexes. More complex and electronically–involved ligands such as the amide– and ester–substituted bipyridines used by Pichot, Beck, and Elliott,[134] or bipyridine–containing hexadentate ligands like the one synthesized by Beeston, Larson, and

Fitzgerald,[149] could be incorporated. Other multidentate ligands such as terpyridines or tripodal tripyridine compounds offer different geometries in the complexes and are nearly completely unresearched. And further work into the heteroleptic complexes could be done as well, either to mix the $\pi \rightarrow \pi^*$ absorptions of different bipyridine ligands or to add functionality to the complexes, such as polymerizability investigated in Chapter 4 or the DNA intercalation ability of Meggers' silicon–ruthenium complexes.[71]

A surprisingly untapped field of research lies available for work in polypyridine silicon chemistry and hopefully this dissertation serves to direct others to further explore these materials.

REFERENCES

1. The information contained in this chapter is adapted from Peloquin, D. M.; Schmedake, T. A. Recent advances in hexacoordinate silicon with pyridine–containing ligands: Chemistry and emerging applications. *Coord. Chem. Rev.* **2016**. doi:10.1016/j.ccr.2016.02.005.

2. Chuit, C.; Corriu, R. J. P.; Reye, C.; Young, J. C., Reactivity of penta– and hexacoordinate silicon compounds and their role as reaction intermediates. *Chem. Rev.* **1993,** *93*, 1371-1448.

3. Holmes, R. R., Comparison of phosphorus and silicon: Hypervalency, stereochemistry, and reactivity. *Chem. Rev.* **1996,** *96*, 927-950.

4. Tandura, S. N.; Voronkov, M. G.; Alekseev, N. V., Molecular and electronic structure of penta– and hexacoordinate silicon compounds. In *Structural Chemistry of Boron and Silicon*, Springer Berlin Heidelberg: Berlin, Heidelberg, 1986; pp 99-189.

5. Chuit, C.; Corriu, R. J. P.; Reye, C., Structure and reactivity of hypercoordinate silicon species. In *Chemistry of Hypervalent Compounds*, Akiba, K. y., Ed. Wiley-VCH: New York, 1999; pp 81-146.

6. Corriu, R. J. P., Hypervalent species of silicon: Structure and reactivity. *J. Organomet. Chem.* **1990,** *400*, 81-106.

7. Kost, D.; Kalikhman, I., Hydrazide–based hypercoordinate silicon compounds. *Adv. Organomet. Chem.* **2004,** *50*, 1-106.

8. Kost, D.; Kalikhman, I., Hypercoordinate silicon complexes based on hydrazide ligands. A remarkably flexible molecular system. *Acc. Chem. Res.* **2009,** *42*, 303-314.

9. Gel'mbol'dt, V. O.; Eunan, A. A., Stereochemistry and electronic structure of hexacoordination silicon fluoro complexes. *Zh. Neorg. Khim.* **1994,** *39*, 424-34.

10. Voronkov, M. G.; Gubanova, L. I., Penta– and hexacoordinate silicon compounds containing silicon–fluorine bonds. *Main Group Met. Chem.* **1987,** *10*, 210-86.

11. Wagler, J.; Boehme, U.; Kroke, E., Higher–coordinated molecular silicon compounds. *Struct. Bond.* **2014,** *155*, 29-105.

12. Bain, V. A.; Killean, R. C. G.; Webster, M., Crystal and molecular structure of tetrafluorobis(pyridine)silicon(IV). *Acta Crystallogr., Sect. B: Struct. Crystallogr. Cryst. Chem.* **1969,** *25*, 156-159.

13. Kohl, J.; Wiedemann, D.; Troyanov, S. I.; Palamidis, E.; Lerch, M., Ternary transition–metal fluoride precursors for the fluorolytic sol–gel route: New insights into speciation and decomposition. *Dalton Trans.* **2015,** *44*, 13272-13281.

14. Lipke, M. C.; Tilley, T. D., High electrophilicity at silicon in η^3–silane σ–complexes: Lewis base adducts of a silane ligand, featuring octahedral silicon and three Ru–H–Si interactions. *J. Am. Chem. Soc.* **2011,** *133*, 16374-16377.

15. Fleischer, H.; Hensen, K.; Stumpf, T., The first SiH_2^{2+} complex, dihydridotetrakis(3–picoline)silicon dichloride–tetrakis(chloroform), $[H_2Si(3pic)_4]Cl_2 \cdot 4\ CHCl_3$: Formation, chemical equilibria, and structural investigation by NMR spectroscopy and single–crystal X-ray diffraction. *Chem. Ber.* **1996,** *129*, 765-771.

16. Bolte, M.; Faber, A., Dihydridotetrakis(4–picoline–N)silicon dibromide chloroform hexasolvate. *Acta Crystallogr., Sect. E: Struct. Rep. Online* **2001,** *57*, o207-o208.

17. Stumpf, T.; Bolte, M., Dihydridotetrakis(4–picoline–N)silicon dichloride chloroform hexasolvate. *Acta Crystallogr., Sect. E: Struct. Rep. Online* **2001,** *57*, o209-o211.

18. Bolte, M.; Faber, A., Dihydridotetrakis(3–picoline)silicon dibromide chloroform tetrasolvate. *Acta Crystallogr., Sect. E: Struct. Rep. Online* **2001,** *57*, o276-o278.

19. Bechstein, O.; Ziemer, B.; Hass, D.; Troyanov, S. I.; Rybakov, V. B.; Maso, G. N., Halogen exchange on silicon halides. XIII. Structure and reactivity of silicon halide–pyridine compounds. *Z. Anorg. Allg. Chem.* **1990,** *582*, 211-16.

20. Hensen, K.; Mayr–Stein, R.; Spangenberg, B.; Bolte, M., Complexes of mixed silicon halides with 4–picoline. *Acta Crystallogr., Sect. C: Cryst. Struct. Commun.* **2000,** *56*, 610-613.

21. Hensen, K.; Mayr–Stein, R.; Ruhl, S.; Bolte, M., trans-Dichlorotetrakis(4–methylpyridine)silicon bis(triiodide) chloroform solvate. *Acta Crystallogr., Sect. C: Cryst. Struct. Commun.* **2000,** *56*, 614-615.

22. Wagler, J., *Private Communication to the Cambridge Structural Database* **2012**, CCDC 916502.

23. Fester, G. W.; Wagler, J.; Brendler, E.; Boehme, U.; Roewer, G.; Kroke, E., Octahedral adducts of dichlorosilane with substituted pyridines: Synthesis, reactivity and a comparison of their structures and Si–29 NMR chemical shifts. *Chem. – Eur. J.* **2008,** *14*, 3164-3176.

24. Bolte, M.; Faber, A., *Private Communication to the Cambridge Structural Database* **2001**, CCDC 157517.

25. Bolte, M.; Hensen, K.; Spangenberg, B., Complexes of silicon tetrabromide with pyridine and 3,5–dimethylpyridine. *J. Chem. Crystallogr.* **2000,** *30*, 245-249.

26. Hensen, K.; Stumpf, T.; Bolte, M.; Nather, C.; Fleischer, H., Experimental investigations and ab initio studies on hexacoordinated complexes of dichlorosilane. *J. Am. Chem. Soc.* **1998,** *120*, 10402-10408.

27. Fester, G. W.; Wagler, J.; Brendler, E.; Bohme, U.; Gerlach, D.; Kroke, E., Octahedral $HSiCl_3$ and $HSiCl_2Me$ adducts with pyridines. *J. Am. Chem. Soc.* **2009,** *131*, 6855-6864.

28. Fester, G. W.; Wagler, J.; Brendler, E.; Kroke, E., Stable trichlorosilane–pyridine adducts. *Eur. J. Inorg. Chem.* **2008**, 5020-5023.

29. Cheng, H. J.; Lippe, K.; Kroke, E.; Wagler, J.; Fester, G. W.; Li, Y. L.; Schwarz, M. R.; Saplinova, T.; Herkenhoff, S.; Ischenko, V.; Woltersdorf, J., Sol–gel derived Si/C/O/N–materials: molecular model compounds, xerogels and porous ceramics. *Appl. Organomet. Chem.* **2011,** *25*, 735-747.

30. Hensen, K.; Kettner, M.; Stumpf, T.; Bolte, M., Syntheses and crystal structure determination of hexacoordinated silicon–complexes with dimethylpyridines. *Z. Naturforsch. B: Chem. Sci.* **2000,** *55*, 901-906.

31. Hensen, K.; Mayr–Stein, R.; Spangenberg, B.; Bolte, M.; Ruhl, S., Complexes of mixed silicon halides with 3,4–lutidine. *Z. Naturforsch. B: Chem. Sci.* **2000,** *55*, 248-252.

32. Bolte, M.; Hensen, K.; Faber, A., Tetrakis(3,5–dimethylpyridine)–dihydridosilicon dibromide bis(acetonitrile) solvate and 3,5–dimethyl–pyridinium bromide. *Acta Crystallogr., Sect. C: Cryst. Struct. Commun.* **2000,** *56*, E524-E525.

33. Besgubenko, L. V.; Pipko, S. E.; Sinitsa, A. D., Complexes of silicon and phosphorus chlorides with nitrogen–containing bases as the condensing agents in the synthesis of amides. *Russ. J. Gen. Chem.* **2012,** *82*, 1382-1390.

34. Lermontov, S. A.; Malkova, A. N.; Lermontova, E. m. K.; Churakov, A. V., Hexafluoropropylene oxide–alcohol: A convenient system for silica dissolution. *Phosphorus, Sulfur Silicon Relat. Elem.* **2011,** *186*, 178-188.

35. Lermontov, S. A.; Malkova, A. N.; Lermontova, E. m. K.; Churakov, A. V., 1–Fluorosilatrane synthesis from SiF_4 complexes and its properties. *J. Organomet. Chem.* **2009,** *694*, 2476-2479.

36. Nakash, M.; Gut, D.; Goldvaser, M., Formation of hypervalent complexes of trifluorosilanes with pyridine and with 4–methoxypyridine, through intermolecular silicon···nitrogen Interactions. *Inorg. Chem.* **2005,** *44*, 1023-1030.

37. Nakash, M.; Goldvaser, M.; Goldberg, I., Formation of hexacoordinate complexes of $PhCCSiF_3$ with 2,2'–bipyridine and with 1,10–phenanthroline through intermolecular silicon···nitrogen interactions. *Inorg. Chem.* **2004,** *43*, 5792-5794.

38. Nakash, M.; Goldvaser, M., Formation of hypervalent complexes of $PhCCSiF_3$ with pyridine through intermolecular silicon···nitrogen interaction. *J. Am. Chem. Soc.* **2004,** *126*, 3436-3437.

39. Song, H. E.; Cissell, J. A.; Vaid, T. P.; Holten, D., Photophysics of reduced silicon tetraphenylporphyrin. *J. Phys. Chem. B* **2007,** *111*, 2138-2142.

40. Cissell, J. A.; Vaid, T. P.; Rheingold, A. L., An antiaromatic porphyrin complex: Tetraphenylporphyrinato(silicon)$(L)_2$ (L = THF or pyridine). *J. Am. Chem. Soc.* **2005,** *127*, 12212-12213.

41. Cissell, J. A.; Vaid, T. P.; DiPasquale, A. G.; Rheingold, A. L., Germanium phthalocyanine, GePc, and the reduced complexes SiPc$(pyridine)_2$ and GePc$(pyridine)_2$ containing antiaromatic π–electron circuits. *Inorg. Chem.* **2007,** *46*, 7713-7715.

42. Waechtler, E.; Gericke, R.; Kutter, S.; Brendler, E.; Wagler, J., Molecular structures of pyridinethiolato complexes of Sn(II), Sn(IV), Ge(IV), and Si(IV). *Main Group Met. Chem.* **2013,** *36*, 181-191.

43. Baus, J. A.; Burschka, C.; Bertermann, R.; Guerra, C. F.; Bickelhaupt, F. M.; Tacke, R., Neutral six–coordinate and cationic five–coordinate silicon(IV) complexes with two bidentate monoanionic N,S–pyridine–2–thiolato(–) ligands. *Inorg. Chem.* **2013,** *52*, 10664-10676.

44. Klebe, G.; Duc, T. Q., Coordinative interactions in chelated complexes of silicon. Part X. Chiral and hexacoordinated chloro(methyl)bis(8–quinolinolato)silicon(IV), $Si(CH_3)(C_9H_6NO)_2Cl$. *Acta Crystallogr., Sect. C: Cryst. Struct. Commun.* **1984,** *40*, 476-9.

45. Bohme, U.; Wagler, J.; Roewer, G., *Private Communication to the Cambridge Structural Database* **2002**, CCDC 194703.

46. Brendler, E.; Waechtler, E.; Wagler, J., Hypercoordinate silacycloalkanes: Step–by–step tuning of N→Si interactions. *Organometallics* **2009,** *28*, 5459-5465.

47. Wagler, J.; Schley, M.; Gerlacha, D.; Boehme, U.; Brendler, E.; Roewer, G., Surprising insights in the various molecular structures of hypercoordinate bis(oxinato)silicon complexes. *Z. Naturforsch. B: Chem. Sci.* **2005,** *60*, 1054-1064.

48. Wagler, J.; Gerlach, D.; Roewer, G., 8–Oxyquinolinate and 8–oxyquinaldinate in silicon complex chemistry – A new face of old ligands. *Chem. Heterocycl. Compd.* **2006,** *42*, 1557-1567.

49. Junold, K.; Burschka, C.; Bertermann, R.; Tacke, R., Novel neutral hexacoordinate benzamidinatosilicon(IV) complexes with SiN_3OF_2, SiN_3OCl_2, SiN_3OBr_2, SiN_5O and SiN_3O_3 skeletons. *Dalton Trans.* **2011,** *40*, 9844-9857.

50. Weiss, J.; Baus, J. A.; Burschka, C.; Tacke, R., Neutral hexacoordinate silicon(IV) complexes with a tridentate dianionic O,N,X ligand (X = O, N, S), bidentate monoanionic X,N ligand (X = O, S), and phenyl ligand: Compounds with a SiO_3N_2C, $SiSO_2N_2C$, SiO_2N_3C, $SiSON_3C$, or SiS_2ON_2C skeleton. *Eur. J. Inorg. Chem.* **2014,** *2014*, 2449-2455.

51. Wagler, J.; Schwarz, D., *Private Communication to the Cambridge Structural Database* **2014**, CCDC 999274.

52. Kawamoto, K.; Akashi, H.; Yamasaki, M.; Shibahara, T., Fluorescent fluoro–silicon(IV) complexes with Schiff base ligands. *Chem. Lett.* **2013,** *42*, 389-391.

53. Wagler, J.; Gerlach, D.; Roewer, G., 2–N–(Quinoline–8–yl)iminomethylphenolate – A (ONN)–tridentate ligand system in silicon complex chemistry. *Inorg. Chim. Acta* **2007,** *360*, 1935-1942.

54. Waechtler, E.; Kaempfe, A.; Krupinski, K.; Gerlach, D.; Kroke, E.; Brendler, E.; Wagler, J., New insights into hexacoordinated silicon complexes with 8–oxyquinolinato ligands: 1,3–shift of Si–bound hydrocarbyl substituents and the influence of Si–bound halides on the 8–oxyquinolinate coordination features. *Z. Naturforsch. B: Chem. Sci.* **2014,** *69*, 1402-1418.

55. Sawitzki, G.; Von Schnering, H. G.; Kummer, D.; Seshadri, T., Chemistry of halosilane adducts. 13. Structure of the octahedral cations cis-$[SiX_2(bipy)_2]^{2+}$; the crystal structure of $[Si(OH)_2(bipy)2]I_2 \cdot 2H_2O$. *Chem. Ber.* **1978,** *111*, 3705-10.

56. Sawitzki, G.; Von Schnering, H. G., The crystal and molecular structure of 1,1,2,2–tetrachloro–1,2–dimethyldisilane–2,2'–bipyridyl. *Chem. Ber.* **1976,** *109*, 3728-34.

57. Fronczek, F. R., *Private Communication to the Cambridge Structural Database* **2015**, CCDC 1411632.

58. Kummer, D.; Chaudhry, S. C.; Thewalt, U.; Debaerdemaeker, T., Contributions to the chemistry of halosilane adducts. XVII. Preparation, crystal and molecular structure of (2,2'–bipyridine)trichloro(trichlorosiloxo)silicon, $Cl_3SiOSiCl_3 \cdot bipy$. *Z. Anorg. Allg. Chem.* **1987,** *553*, 147-55.

59. Kummer, D.; Chaudhry, S. C.; Debaerdemaeker, T.; Thewalt, U., Contributions to the chemistry of halosilane adducts. 20. Hexacoordinated compounds of trichlorosilanes. Preparation, crystal and molecular structure of $RSiCl_3 \cdot bipy$. *Chem. Ber.* **1990,** *123*, 945-51.

60. Hensen, K.; Mayr–Stein, R.; Ruhl, S.; Bolte, M., cis–Bis(2,2'–bipyridyl–N,N')dichlorosilicon diiodide. *Acta Crystallogr., Sect. C: Cryst. Struct. Commun.* **2000,** *56*, 607-609.

61. Breiding, T.; Henker, J.; Fu, C.; Xiang, Y.; Glöckner, S.; Hofmann, P.; Harms, K.; Meggers, E., Synthesis and functionalization of hexacoordinate (arenediolato)bis(polypyridyl)silicon(IV) complexes. *Eur. J. Inorg. Chem.* **2014,** *2014*, 2924-2933.

62. Adley, A. D.; Bird, P. H.; Fraser, A. R.; Onyszchuk, M., Crystal structures of 2,2'–bipyridyltetrafluorosilicon(IV), 2,2'–bipyridyltetrafluorogermanium(IV), and 2,2'–bipyridyltetrafluorotin(VI). *Inorg. Chem.* **1972,** *11*, 1402-9.

63. Portius, P.; Filippou, A. C.; Schnakenburg, G.; Davis, M.; Wehrstedt, K. D., Neutral Lewis base adducts of silicon tetraazide. *Angew. Chem., Int. Ed.* **2010,** *49*, 8013-8016, S8013/1-S8013/41.

64. Maguylo, C.; Chukwu, C.; Aun, M.; Blake Monroe, T.; Ceccarelli, C.; Jones, D. S.; Merkert, J. W.; Donovan–Merkert, B. T.; Schmedake, T. A., Exploring the structure and redox activity of hexacoordinate bis(bipyridyl)silicon(IV) complexes. *Polyhedron* **2015,** *94*, 52-58.

65. Fester, G. W.; Eckstein, J.; Gerlach, D.; Wagler, J.; Brendler, E.; Kroke, E., Reactions of hydridochlorosilanes with 2,2'–bipyridine and 1,10–phenanthroline: Complexation versus dismutation and metal–catalyst–free 1,4–hydrosilylation. *Inorg. Chem.* **2010,** *49*, 2667-2673.

66. Lee, D. A.; Moon, S. K.; Sizeland, A. N.; Gould, N. W.; Gbarbea, E. M.; Owusu, D.; Jones, D. S.; Schmedake, T. A., Synthesis and characterization of a dipyridocatecholate silicon complex. *Inorg. Chem. Commun.* **2013,** *33*, 125-128.

67. Farnham, W. B.; Whitney, J. F., Stereomutation at hexacoordinate silicon by a ligand-dissociation process. *J. Am. Chem. Soc.* **1984,** *106*, 3992-4.

68. Chekhlov, A. N.; Tkachev, V. V.; Lermontov, S. A., Crystal structure of tetrafluoro(1,10–phenanthroline–N,N')silicon acetonitrile semisolvate. *J. Struct. Chem.* **2003,** *44*, 1080-1083.

69. Wagler, J.; Kronstein, M., *Private Communication to the Cambridge Structural Database* **2014**, CCDC 999091.

70. Xiang, Y. G.; Fu, C.; Breiding, T.; Sasmal, P. K.; Liu, H. D.; Shen, Q.; Harms, K.; Zhang, L. L.; Meggers, E., Hydrolytically stable octahedral silicon complexes as bioactive scaffolds: Application to the design of DNA intercalators. *Chem. Commun.* **2012,** *48*, 7131-7133.

71. Fu, C.; Harms, K.; Zhang, L.; Meggers, E., DNA mismatch recognition by a hexacoordinate silicon sandwich–ruthenium hybrid complex. *Organometallics* **2014,** *33*, 3219-3222.

72. Kummer, D.; Chaudhry, S. C.; Depmeier, W.; Mattern, G., Contributions to the chemistry of halogenosilane adducts. 21. Preparation, properties, crystal and molecular structure of dichloro(1,10–phenanthroline)bis(trichlorosilyl)silicon, $(SiCl_3)_2SiCl_2 \cdot phen$. *Chem. Ber.* **1990,** *123*, 2241-5.

73. Portius, P.; Davis, M., A new hexakis(isocyanato)silicate(IV) and the first neutral Lewis–base adducts of silicon tetraisocyanate. *Dalton Trans.* **2010,** *39*, 527-532.

74. Wiberg, E.; Michaud, H., For knowledge on silicontetrazide $Si(N_3)_4$. *Z. Naturforsch. B: Chem. Sci.* **1954,** *9*, 500.

75. Kummer, D.; Gaisser, K. E.; Seshadri, T., Contributions to the chemistry of halosilane adducts, X. Bis(2,2'–bipyridine) complexes of silicon, direct synthesis, structure, and properties. *Chem. Ber.* **1977,** *110*, 1950-62.

76. Kummer, D.; Seshadri, T., Contributions to the chemistry of halosilane adducts. XI. Bis(1,10–phenanthroline) complexes of silicon, synthesis, structure, and properties. *Chem. Ber.* **1977,** *110*, 2355-67.

77. Herzog, S.; Krebs, F., The preparation of tris–2,2'–bipyridine–silicon(0), $SiBipy_3$. *Naturwissenschaften* **1963,** *50*, 330-1.

78. Morancho, R.; Pouvreau, P.; Constant, G.; Jaud, J.; Galy, J., Synthesis and structural study of a new silicon compound: di–2,2'–bipyridinesilicon. *J. Organomet. Chem.* **1979,** *166*, 329-38.

79. Kummer, D.; Gaisser, K. E.; Seifert, J.; Wagner, R., Contributions to the chemistry of halosilane adducts. XIV. Neutral ligand complexes of silicon with six N–donor atoms. *Z. Anorg. Allg. Chem.* **1979,** *459*, 145-56.

80. Suthar, B.; Aldongarov, A.; Irgibaeva, I.; Moazzen, M.; Donovan–Merkert, B.; Merkert, J.; Schmedake, T., Electrochemical and spectral properties of hexacoordinate polypyridyl silicon complexes. *Polyhedron* **2012,** *31*, 754-758.

81. Liu, H. L.; Ohmori, Y.; Kojima, M.; Yoshikawa, Y., Stereochemistry of six–coordinate octahedral silicon(IV) complexes containing 2,2'–bipyridine. *J. Coord. Chem.* **1998,** *44*, 257-268.

82. Ohmori, Y.; Kojima, M.; Kashino, S.; Yoshikawa, Y., Chromatographic resolution mechanism of a tris(1,10–phenanthroline)silicon(IV) complex. *J. Coord. Chem.* **1996,** *39*, 219-230.

83. Ohmori, Y.; Namba, M.; Kuroda, Y.; Kojima, M.; Yoshikawa, Y., Stereochemistry of six–coordinated silicon complexes. 2. Optical resolution of $[Si(\alpha\text{–diimine})_3]^{4+}$ (α–diimine = 2,2'–bipyridine, 1,10–phenanthroline). *Inorg. Chem.* **1992,** *31*, 2299-300.

84. England, J.; Wieghardt, K., 2,2'–Bipyridine compounds of group 14 elements: A density functional theory study. *Inorg. Chem.* **2013,** *52*, 10067-10079.

85. Wulf, E.; Herzog, S., Temperature dependence of the magnetic susceptibilities of [lithium, beryllium, calcium, aluminum, silicon, scandium, vanadium, niobium, chromium, manganese, and cobalt] dipyridyls. *Z. Anorg. Allg. Chem.* **1972,** *387*, 81-90.

86. Samia, A. C.; Chen, X.; Burda, C., Semiconductor quantum dots for photodynamic therapy. *J. Am. Chem. Soc.* **2003,** *125*, 15736-7.

87. Allen, C. M.; Sharman, W. M.; Van Lier, J. E., Current status of phthalocyanines in the photodynamic therapy of cancer. *J. Porphyrins Phthalocyanines* **2001,** *5*, 161-169.

88. Miller, J. D.; Baron, E. D.; Scull, H.; Hsia, A.; Berlin, J. C.; McCormick, T.; Colussi, V.; Kenney, M. E.; Cooper, K. D.; Oleinick, N. L., Photodynamic therapy with the phthalocyanine photosensitizer Pc 4: the case experience with preclinical mechanistic and early clinical–translational studies. *Toxicol. Appl. Pharmacol.* **2007,** *224*, 290-9.

89. Zhao, B.; Yin, J. J.; Bilski, P. J.; Chignell, C. F.; Roberts, J. E.; He, Y. Y., Enhanced photodynamic efficacy towards melanoma cells by encapsulation of Pc4 in silica nanoparticles. *Toxicol. Appl. Pharmacol.* **2009,** *241*, 163-72.

90. Cummins, D.; Boschloo, G.; Ryan, M.; Corr, D.; Rao, S. N.; Fitzmaurice, D., Ultrafast electrochromic windows based on redox–chromophore modified nanostructured semiconducting and conducting films. *J. Phys. Chem. B* **2000,** *104*, 11449-11459.

91. Mortimer, R. J.; Varley, T. S., Novel color–reinforcing electrochromic device based on surface–confined ruthenium purple and solution–phase methyl viologen. *Chem. Mater.* **2011,** *23*, 4077-4082.

92. Deb, S. K., A novel electrophotographic system. *Appl. Opt.* **1969,** *8*, 192-195.

93. Deb, S. K., Optical and photoelectric properties and colour centres in thin films of tungsten oxide. *Philos. Mag.* **1973,** *27*, 801-822.

94. Zheng, H.; Ou, J. Z.; Strano, M. S.; Kaner, R. B.; Mitchell, A.; Kalantar–zadeh, K., Nanostructured tungsten oxide – Properties, synthesis, and applications. *Adv. Funct. Mater.* **2011,** *21*, 2175-2196.

95. Granqvist, C. G., Electrochromics for smart windows: Oxide–based thin films and devices. *Thin Solid Films* **2014,** *564*, 1-38.

96. Liao, C.-C.; Chen, F.-R.; Kai, J.-J., WO_{3-x} nanowires based electrochromic devices. *Sol. Energy Mater. Sol. Cells* **2006,** *90*, 1147-1155.

97. Cheng, W.; Baudrin, E.; Dunn, B.; Zink, J. I., Synthesis and electrochromic properties of mesoporous tungsten oxide. *J. Mater. Chem.* **2001,** *11*, 92-97.

98. Djaoued, Y.; Balaji, S.; Brüning, R., Electrochromic devices based on porous tungsten oxide thin films. *J. Nanomater.* **2012,** *2012*, 9.

99. Ito, S.; Abe, Y.; Kawamura, M.; Kim, K. H., Electrochromic properties of iridium oxide thin films prepared by reactive sputtering in O_2 or H_2O atmosphere. *J. Vac. Sci. Technol., B: Nanotechnol. Microelectron.: Mater., Process., Meas., Phenom.* **2015,** *33*, 041204.

100. Michaelis, L.; Hill, E. S., The viologen indicators. *J. Gen. Physiol.* **1933,** *16*, 859-873.

101. Mortimer, R. J.; Varley, T. S., Electrochromic devices based on surface–confined Prussian blue or Ruthenium purple and aqueous solution–phase di–n–heptyl viologen. *Sol. Energy Mater. Sol. Cells* **2013,** *109*, 275-279.

102. Lu, H. C.; Kao, S. Y.; Chang, T. H.; Kung, C. W.; Ho, K. C., An electrochromic device based on Prussian blue, self–immobilized vinyl benzyl viologen, and ferrocene. *Sol. Energy Mater. Sol. Cells* **2016,** *147*, 75-84.

103. Aristov, N.; Habekost, A., Electrochromism of methylviologen (paraquat). *World J. Chem. Ed.* **2015,** *3*, 82-86.

104. Lin, C. F.; Hsu, C. Y.; Lo, H. C.; Lin, C. L.; Chen, L. C.; Ho, K. C., A complementary electrochromic system based on a Prussian blue thin film and a heptyl viologen solution. *Sol. Energy Mater. Sol. Cells* **2011,** *95*, 3074-3080.

105. Tsai, W. T., A review on environmental exposure and health risks of herbicide paraquat. *Toxicol. Environ. Chem.* **2013,** *95*, 197-206.

106. İçli, M.; Pamuk, M.; Algı, F.; Önal, A. M.; Cihaner, A., A new soluble neutral state black electrochromic copolymer via a donor–acceptor approach. *Org. Electron.* **2010,** *11*, 1255-1260.

107. Algı, F.; Cihaner, A., An ambipolar neutral state green polymeric electrochromic. *Org. Electron.* **2009,** *10*, 704-710.

108. Data, P.; Lapkowski, M.; Motyka, R.; Suwinski, J., Electrochemistry and spectroelectrochemistry of a novel selenophene–based monomer. *Electrochim. Acta* **2012,** *59*, 567-572.

109. Camurlu, P., Polypyrrole derivatives for electrochromic applications. *RSC Adv.* **2014,** *4*, 55832-55845.

110. Beaujuge, P. M.; Amb, C. M.; Reynolds, J. R., Spectral engineering in π–conjugated polymers with intramolecular donor–acceptor interactions. *Acc. Chem. Res.* **2010,** *43*, 1396-1407.

111. Dyer, A. L.; Craig, M. R.; Babiarz, J. E.; Kiyak, K.; Reynolds, J. R., Orange and red to transmissive electrochromic polymers based on electron–rich dioxythiophenes. *Macromolecules* **2010,** *43*, 4460-4467.

112. Vogel, S.; Holze, R., Spectroelectrochemistry of intrinsically conducting aniline–thiophene copolymers. *Electrochim. Acta* **2005,** *50*, 1587-1595.

113. Skotheim, T. A.; Reynolds, J., *Conjugated Polymers: Theory, Synthesis, Properties, and Characterization*. CRC Press: 2006.

114. Somani, P. R.; Radhakrishnan, S., Electrochromic materials and devices: Present and future. *Mater. Chem. Phys.* **2003,** *77*, 117-133.

115. Ak, M.; Gacal, B.; Kiskan, B.; Yagci, Y.; Toppare, L., Enhancing electrochromic properties of polypyrrole by silsesquioxane nanocages. *Polymer* **2008,** *49*, 2202-2210.

116. Data, P.; Lapkowski, M.; Motyka, R.; Suwinski, J., Influence of alkyl chain on electrochemical and spectroscopic properties of polyselenophenes. *Electrochim. Acta* **2013,** *87*, 438-449.

117. Gadgil, B.; Damlin, P.; Ääritalo, T.; Kankare, J.; Kvarnström, C., Electrosynthesis and characterization of viologen cross linked thiophene copolymer. *Electrochim. Acta* **2013,** *97*, 378-385.

118. DeLongchamp, D. M.; Kastantin, M.; Hammond, P. T., High-contrast electrochromism from layer–by–layer polymer films. *Chem. Mater.* **2003,** *15*, 1575-1586.

119. Keshtov, M. L.; Grigor'ev, T. E.; Khokhlov, A. R., New electrochromic polymeric pyridinium salts. *Polym. Sci., Ser. B* **2010,** *51*, 471-482.

120. Bowman, A. C.; England, J.; Sproules, S.; Weyhermüller, T.; Wieghardt, K., Electronic structures of homoleptic [tris(2,2′–bipyridine)M]^n complexes of the early transition metals (M = Sc, Y, Ti, Zr, Hf, V, Nb, Ta; n = 1+, 0, 1–, 2–, 3−): An experimental and density functional theoretical study. *Inorg. Chem.* **2013,** *52*, 2242-2256.

121. England, J.; Scarborough, C. C.; Weyhermüller, T.; Sproules, S.; Wieghardt, K., Electronic structures of the electron transfer series $[\mathrm{M(bpy)_3}]^n$, $[\mathrm{M(tpy)_2}]^n$, and $[\mathrm{Fe(^tbpy)_3}]^n$ (M = Fe, Ru; n = 3+, 2+, 1+, 0, 1–): A Mössbauer spectroscopic and DFT study. *Eur. J. Inorg. Chem.* **2012,** *2012*, 4605-4621.

122. Milko, P.; Iron, M. A., On the innocence of bipyridine ligands: How well do DFT functionals fare for these challenging spin systems? *J. Chem. Theory Comput.* **2014,** *10*, 220-235.

123. Scarborough, C. C.; Sproules, S.; Weyhermüller, T.; DeBeer, S.; Wieghardt, K., Electronic and molecular structures of the members of the electron transfer series $[\mathrm{Cr(^tbpy)_3}]^n$ (n = 3+, 2+, 1+, 0): An X-ray absorption spectroscopic and density functional theoretical study. *Inorg. Chem.* **2011,** *50*, 12446-12462.

124. Wang, M.; England, J.; Weyhermüller, T.; Wieghardt, K., Molecular and electronic structures of the members of the electron transfer series $[\mathrm{Mn(bpy)_3}]^n$ (n = 2+, 1+, 0, 1−) and $[\mathrm{Mn(tpy)_2}]^m$ (m = 4+, 3+, 2+, 1+, 0). An experimental and density functional theory study. *Inorg. Chem.* **2014,** *53*, 2276-2287.

125. Wang, M.; Weyhermüller, T.; Wieghardt, K., The electron transfer series $[\mathrm{Mo^{III}(bpy)_3}]^n$ (n=3+, 2+, 1+, 0, 1–), and the dinuclear species $[\{\mathrm{Mo^{III}Cl(^{Me}bpy)_2}\}_2(\mu_2\text{–}\mathrm{O})]\mathrm{Cl_2}$ and $[\{\mathrm{Mo^{IV}(tpy^{\cdot})_2}\}_2(\mu_2\text{–}\mathrm{MoO_4})](\mathrm{PF_6})_2{\cdot}_4$ MeCN. *Chem. – Eur. J.* **2014,** *20*, 9037-9044.

126. Wang, M.; England, J.; Weyhermüller, T.; Wieghardt, K., Electronic structures of "low-valent" neutral complexes $[\mathrm{NiL_2}]^0$ (S = 0; L = bpy, phen, tpy) – An experimental and DFT computational study. *Eur. J. Inorg. Chem.* **2015,** *2015*, 1511-1523.

127. Wolff, C.; Gottschlich, A.; England, J.; Wieghardt, K.; Saak, W.; Haase, D.; Beckhaus, R., Molecular and electronic structures of mononuclear and dinuclear titanium complexes containing π–radical anions of 2,2′–bipyridine and 1,10–phenanthroline: An experimental and DFT computational study. *Inorg. Chem.* **2015,** *54*, 4811-4820.

128. Irwin, M.; Doyle, L. R.; Krämer, T.; Herchel, R.; McGrady, J. E.; Goicoechea, J. M., A homologous series of first–row transition-metal complexes of 2,2′–bipyridine and their ligand radical derivatives: Trends in structure, magnetism, and bonding. *Inorg. Chem.* **2012,** *51*, 12301-12312.

129. Braterman, P. S.; Song, J. I., Spectroelectrochemistry of aromatic ligands and their derivatives. 1. Reduction products of 4,4'–bipyridine, 2,2'–bipyridine, 2,2'–bipyrimidine, and some quaternized derivatives. *J. Org. Chem.* **1991,** *56*, 4678-4682.

130. König, E.; Kremer, S., The lower excited electronic states of singly and doubly reduced 2,2′–bipyridine. *Chem. Phys. Lett.* **1970,** *5*, 87-90.

131. Torii, Y.; Yazaki, T.; Kaizu, Y.; Murasato, S.; Kobayashi, H., Electronic absorption spectra of the alkali metal complexes with bipyridine. *Bull. Chem. Soc. Jpn.* **1969,** *42*, 2264-2267.

132. Mortimer, R. J., Electrochromic materials. *Annu. Rev. Mater. Res.* **2011,** *41*, 241-268.

133. Heath, G. A.; Yellowlees, L. J.; Braterman, P. S., Spectro–electrochemical studies on tris–bipyridyl ruthenium complexes; Ultra–violet, visible, and near–infrared spectra of the series [Ru(bipyridyl)$_3$]2+/1+/0/1. *J. Chem. Soc., Chem. Commun.* **1981**, 287-289.

134. Pichot, F.; Beck, J. H.; Elliott, C. M., A series of multicolor electrochromic ruthenium(II) trisbipyridine complexes: Synthesis and electrochemistry. *J. Phys. Chem. A* **1999,** *103*, 6263-6267.

135. Gupta, T.; Tartakovsky, E.; Iron, M. A.; van der Boom, M. E., A monolayer–based setup for optical amplification. *ACS Appl. Mater. Interfaces* **2010,** *2*, 7-10.

136. Lombard, J.; Jose, D. A.; Castillo, C. E.; Pansu, R.; Chauvin, J.; Deronzier, A.; Collomb, M. N., Alternated bimetallic [Ru–M] (M = Fe^{2+}, Zn^{2+}) coordination polymers based on $[Ru(bpy)_3]^{2+}$ units connected to bis–terpyridine ligands: Synthesis, electrochemistry and photophysics in solution or in thin film on electrodes. *J. Mater. Chem. C* **2014,** *2*, 9824-9835.

137. Zhong, Y. W.; Vilà, N.; Henderson, J. C.; Abruña, H. D., Transition–metal tris–bipyridines containing three dithienylcyclopentenes: Synthesis, photochromic, and electrochromic properties. *Inorg. Chem.* **2009,** *48*, 7080-7085.

138. Elliott, C. M.; Hershenhart, E. J., Electrochemical and spectral investigations of ring–substituted bipyridine complexes of ruthenium. *J. Am. Chem. Soc.* **1982,** *104*, 7519-7526.

139. Geng, L.; Ewing, A. G.; Jernigan, J. C.; Murray, R. W., Electrochemical reactions of solutes and of electroactive polymer films in low dielectric media: Toluene and heptane. *Anal. Chem.* **1986,** *58*, 852-860.

140. Nie, H. J.; Shao, J. Y.; Wu, J.; Yao, J.; Zhong, Y. W., Synthesis and reductive electropolymerization of metal complexes with 5,5′–divinyl–2,2′–bipyridine. *Organometallics* **2012,** *31*, 6952-6959.

141. The information contained in this section is adapted from Peloquin, D. M.; Dewitt, D. R.; Patel, S. S.; Merkert, J. W.; Donovan-Merkert, B. T.; Schmedake, T. A. Spectroelectrochemistry of tris(bipyridyl)silicon(IV): Ligand localized reductions with potential electrochromic applications. *Dalton Trans.* **2015,** *44*, 18723-18726.

142. Honeycomb spectroelectrochemical cell user guide. Pine Research Instrumentation: Durham, NC, 2013.

143. Sonmez, G.; Shen, C. K. F.; Rubin, Y.; Wudl, F., A red, green, and blue (RGB) polymeric electrochromic device (PECD): The dawning of the PECD era. *Angew. Chem., Int. Ed.* **2004,** *43*, 1498-1502.

144. Argun, A. A.; Aubert, P. H.; Thompson, B. C.; Schwendeman, I.; Gaupp, C. L.; Hwang, J.; Pinto, N. J.; Tanner, D. B.; MacDiarmid, A. G.; Reynolds, J. R., Multicolored electrochromism in polymers: Structures and devices. *Chem. Mater.* **2004,** *16*, 4401-4412.

145. Bulloch, R. H.; Kerszulis, J. A.; Dyer, A. L.; Reynolds, J. R., Mapping the broad CMY subtractive primary color gamut using a dual–active electrochromic device. *ACS Appl. Mater. Interfaces* **2014,** *6*, 6623-6630.

146. Beaujuge, P. M.; Reynolds, J. R., Color control in π–conjugated organic polymers for use in electrochromic devices. *Chem. Rev.* **2010,** *110*, 268-320.

147. Amb, C. M.; Dyer, A. L.; Reynolds, J. R., Navigating the color palette of solution–processable electrochromic polymers. *Chem. Mater.* **2011,** *23*, 397-415.

148. Bernhard, S.; Barron, J. A.; Houston, P. L.; Abruña, H. D.; Ruglovksy, J. L.; Gao, X.; Malliaras, G. G., Electroluminescence in ruthenium(II) complexes. *J. Am. Chem. Soc.* **2002,** *124*, 13624-13628.

149. Beeston, R. F.; Larson, S. L.; Fitzgerald, M. C., Ground– and excited–state properties of a photostable hemicage ruthenium(II) polypyridine complex. *Inorg. Chem.* **1989,** *28*, 4187-4189.

150. Hong, Y. R.; Gorman, C. B., Synthetic approaches to an isostructural series of redox–active, metal tris(bipyridine) core dendrimers. *J. Org. Chem.* **2003,** *68*, 9019-9025.

151. Berger, R. M.; McMillin, D. R., Localized states in reduced and excited–state ruthenium(II) terpyridyls. *Inorg. Chem.* **1988,** *27*, 4245-4249.

152. Thummel, R. P.; Hegde, V.; Jahng, Y., Influence of remote substituents on the properties of bis(terpyridyl)ruthenium(II) complexes. *Inorg. Chem.* **1989,** *28*, 3264-3267.

153. Constable, E. C.; Cargill Thompson, A. M. W., Novel didentate 2,2′:6′,2″–terpyridine complexes of ruthenium(II). *Inorg. Chim. Acta* **1994,** *223*, 177-179.

154. Liu, X.; Xu, J.; Lv, Y.; Wu, W.; Liu, W.; Tang, Y., An ATP–selective, lanthanide complex luminescent probe. *Dalton Trans.* **2013,** *42*, 9840-9846.

155. Helberg, L. E.; Orth, S. D.; Sabat, M.; Harman, W. D., Coordination chemistry of low–valent rhenium polypyridyl complexes: Synthesis, reactivity, and electrochemistry. *Inorg. Chem.* **1996,** *35*, 5584-5594.

156. Jenkins, D. M.; Senn, J. F.; Bernhard, S., Cyclometalated platinum(II) diimine complexes: Synthetically tuning the photophysical and electrochemical properties. *Dalton Trans.* **2012,** *41*, 8077-8085.

157. Wing–WahYam, V.; Pui, Y. L.; Cheung, K. K., Synthesis, structure, luminescence, and electrochemical properties of polynuclear mercury(II) chalcogenolate complexes. *J. Chem. Soc., Dalton Trans.* **2000**, 3658-3662.

158. Yang, P.; Sun, P.; Mai, W., Electrochromic energy storage devices. *Mater. Today* **2015**.

159. Zheng–Fei, G.; Kun, P.; Xue–Jin, W., Electrochromic & magnetic properties of electrode materials for lithium ion batteries. *Chin. Phys. B* **2016,** *25*, 017801.

160. Giannuzzi, R.; Manca, M.; De Marco, L.; Belviso, M. R.; Cannavale, A.; Sibillano, T.; Giannini, C.; Cozzoli, P. D.; Gigli, G., Ultrathin TiO_2(B) nanorods with superior lithium–ion storage performance. *ACS Appl. Mater. Interfaces* **2014,** *6*, 1933-1943.

161. Moon, H. C.; Lodge, T. P.; Frisbie, C. D., Solution processable, electrochromic ion gels for sub–1 V, flexible displays on plastic. *Chem. Mater.* **2015,** *27*, 1420-1425.

162. Moon, H. C.; Kim, C. H.; Lodge, T. P.; Frisbie, C. D., Multicolored, low–power, flexible electrochromic devices based on ion gels. *ACS Appl. Mater. Interfaces* **2016,** *8*, 6252-6260.

163. Wen, R. T.; Arvizu, M. A.; Niklasson, G. A.; Granqvist, C. G., Electrochromics for energy efficient buildings: Towards long–term durability and materials rejuvenation. *Surf. Coat. Technol.* **2015,** *278*, 121-125.

164. Thakur, V. K.; Ding, G.; Ma, J.; Lee, P. S.; Lu, X., Hybrid materials and polymer electrolytes for electrochromic device applications. *Adv. Mater.* **2012,** *24*, 4071-4096.

165. Du, Y.; Peng, H. Y.; Mao, H.; Jin, K. X.; Wang, H.; Li, F.; Gao, X. Y.; Chen, W.; Wu, T., Evolution of the $SrTiO_3$–MoO_3 interface electronic structure: An in situ photoelectron spectroscopy study. *ACS Appl. Mater. Interfaces* **2015,** *7*, 11309-11314.

166. Chen, B. H.; Kao, S. Y.; Hu, C. W.; Higuchi, M.; Ho, K. C.; Liao, Y. C., Printed multicolor high–contrast electrochromic devices. *ACS Appl. Mater. Interfaces* **2015,** *7*, 25069-25076.

167. Cui, B. B.; Zhong, Y. W.; Yao, J., Three–state near–infrared electrochromism at the molecular scale. *J. Am. Chem. Soc.* **2015,** *137*, 4058-4061.

168. de Ruiter, G.; Lahav, M.; Evmenenko, G.; Dutta, P.; Cristaldi, D. A.; Gulino, A.; van der Boom, M. E., Composite molecular assemblies: Nanoscale structural control and spectroelectrochemical diversity. *J. Am. Chem. Soc.* **2013,** *135*, 16533-16544.

169. Abe, M.; Futagawa, H.; Ono, T.; Yamada, T.; Kimizuka, N.; Hisaeda, Y., An electropolymerized crystalline film incorporating axially–bound metalloporphycenes: Remarkable reversibility, reproducibility, and coloration efficiency of ruthenium(II/III)–based electrochromism. *Inorg. Chem.* **2015,** *54*, 11061-11063.

170. Pehlivan, İ. B.; Marsal, R.; Pehlivan, E.; Runnerstrom, E. L.; Milliron, D. J.; Granqvist, C. G.; Niklasson, G. A., Electrochromic devices with polymer electrolytes functionalized by SiO_2 and In_2O_3:Sn nanoparticles: Rapid coloring/bleaching dynamics and strong near–infrared absorption. *Sol. Energy Mater. Sol. Cells* **2014,** *126*, 241-247.

171. Schwab, P. F. H.; Fleischer, F.; Michl, J., Preparation of 5–brominated and 5,5‘–dibrominated 2,2‘–bipyridines and 2,2‘–bipyrimidines. *J. Org. Chem.* **2002,** *67*, 443-449.

172. D'Souza, D. M.; Leigh, D. A.; Papmeyer, M.; Woltering, S. L., A scalable synthesis of 5,5'–dibromo–2,2'–bipyridine and its stepwise functionalization via Stille couplings. *Nat. Protoc.* **2012,** *7*, 2022+.

173. Nie, H. J.; Yao, J.; Zhong, Y.-W., Synthesis of vinyl–substituted polypyridyl ligands through Suzuki–Miyaura cross-coupling of potassium vinyltrifluoroborate with bromopolypyridines. *J. Org. Chem.* **2011,** *76*, 4771-4775.

APPENDIX A: CYCLIC VOLTAMMETRY OF [Si(5dmbpy)$_3$](PF$_6$)$_4$

When reducing the [Si(5dmbpy)$_3$](PF$_6$)$_4$ complex by four electrons in acetonitrile/0.100 M TBAPF$_6$, possible adsorption to the electrode was noticed above -1.200 V vs. Fc/Fc$^+$. This fourth reduction wave was only partially chemically reversible because of this possible adsorption.

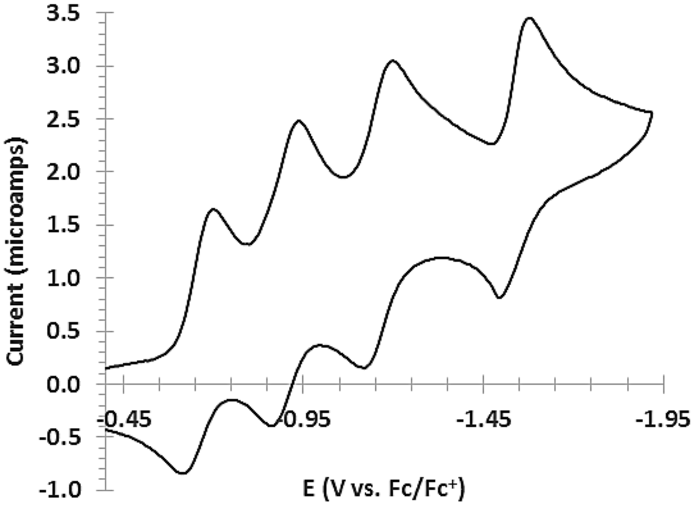

FIGURE 51: Cyclic voltammagram of [Si(5dmbpy)$_3$](PF$_6$)$_4$ in acetonitrile/0.100 M TBAPF$_6$ vs. Fc/Fc$^+$ with a platinum disk working electrode. Scan rate = 0.200 V/s with iR compensation.

APPENDIX B: UV–VIS SPECTRA OBTAINED WHEN REDUCING THE BIPYRIDINE COMPLEXES TO THE NEUTRAL SPECIES

Spectra for the neutral species of the 4dtbbpy and 5dmbpy complexes could not be obtained. Although on the fast time scale of cyclic voltammetry the neutral state could be observed with 5dmbpy, on the longer time scale used for equilibrium of each state before spectra were measured, precipitation/adsorption of the neutral species was observed, indicating that the neutral species must not be particularly soluble in acetonitrile. The UV–Vis spectra obtained indicating the irreversible reactions of the 4dtbbpy complex (FIGURE 52) and the 5dmbpy complex (FIGURE 53) are reported below.

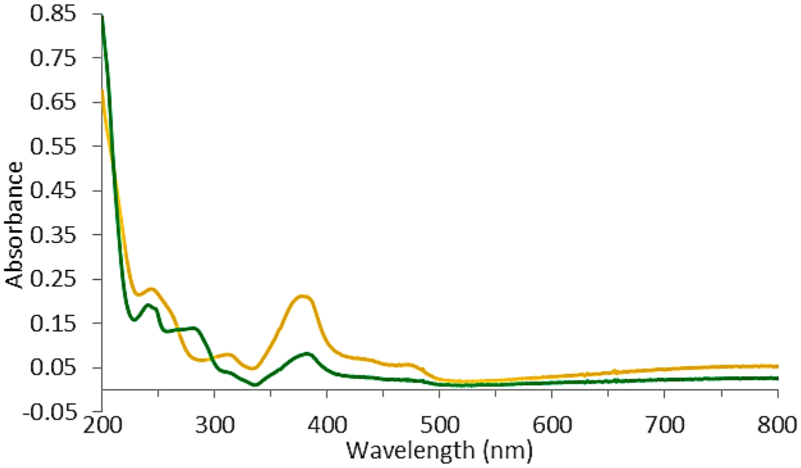

FIGURE 52: UV–Vis spectra of plating out observed during electrochemical reduction of [Si(4dtbbpy)$_3$](PF$_6$)$_4$ in acetonitrile/0.100 M TBAPF$_6$ vs. Fc/Fc$^+$. The colored lines indicate the spectra taken just before (yellow line, -1.270 V) and just after (green line, -1.295 V) precipitation occurred.

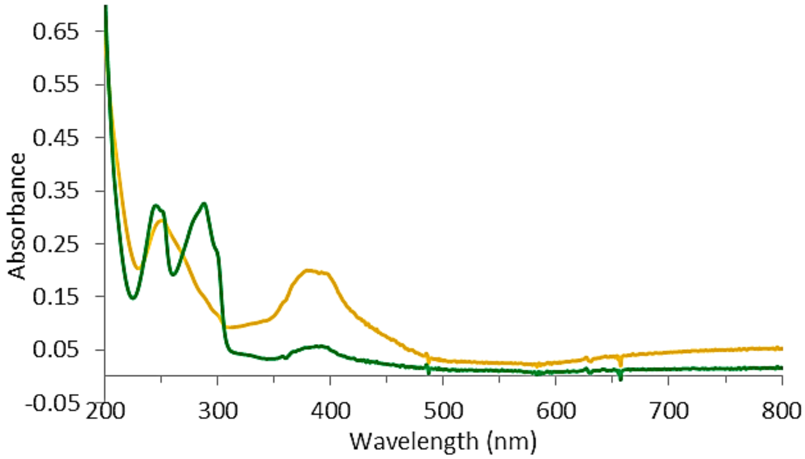

FIGURE 53: UV–Vis spectra of plating out observed during electrochemical reduction of $[Si(5dmbpy)_3](PF_6)_4$ in acetonitrile/0.100 M $TBAPF_6$ vs. Fc/Fc^+. The colored lines indicate the spectra taken just before (yellow line, -1.195 V) and just after (green line, -1.220 V) precipitation occurred.

APPENDIX C: UV–VIS SPECTRA OF SIDE PRODUCTS WHEN SAMPLES WERE NOT FULLY DEGASSED

It was found that in the presence of oxygen, when the cell was not properly degassed due to the lack of diffusion caused by the electrode card and tapered cell pathlength, an irreversible reaction appeared to occur with all four of the polypyridine complexes for which spectroelectrochemical characterization was performed. These species were not observed when degassing was thoroughly performed by sliding the electrode card up and down.

For the bpy complex, the unidentified species absorbs around 425 nm and does not absorb in the region from 600-1000 nm, and disappearance of the initial peaks also occurred (FIGURE 54).

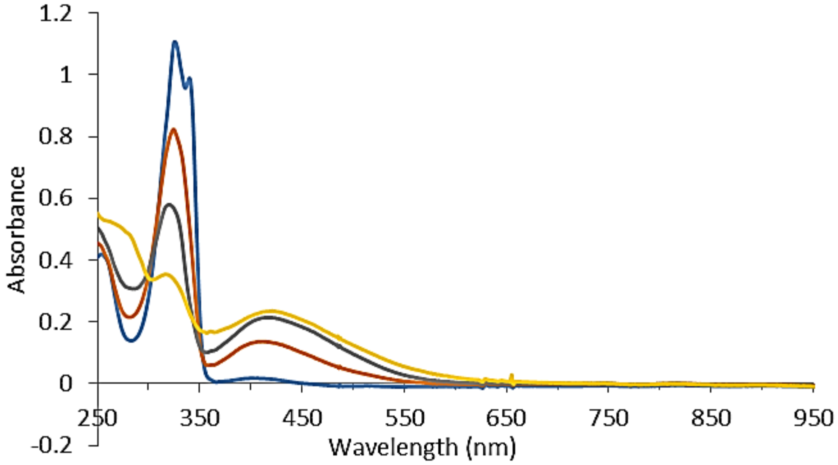

FIGURE 54: UV–Vis spectra of side products to $[Si(bpy)_3]^{+4}$ generated electrochemically at -0.445 V (blue line), -0.645 V (red line), -0.895 V (gray line), and -1.095 V (yellow line) vs. Fc/Fc^+ without proper degassing.

For the 4dtbbpy complex, a broad peak around 421 nm emerged with no absorbance above 700 nm and disappearance of the initial overlapping 321/334 nm peaks occurred concurrently (FIGURE 55).

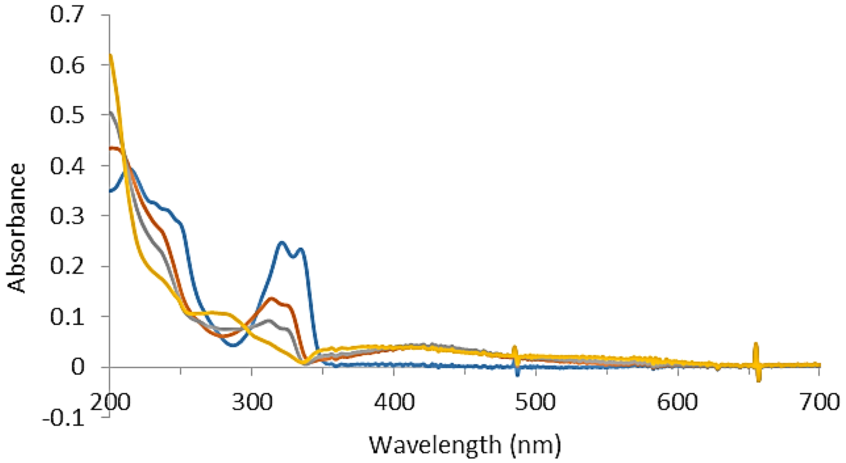

FIGURE 55: UV–Vis spectra of side products to $[Si(4dtbbpy)_3]^{+4}$ generated electrochemically at -0.445 V (blue line), -0.845 V (red line), -1.045 V (gray line), and -1.245 V (yellow line) vs Fc/Fc$^+$ without proper degassing.

For the 5dmbpy complex, a broad peak around 435 nm emerged with no absorbance above 700 nm and the initial overlapping 340/356 nm peaks disappeared (FIGURE 56).

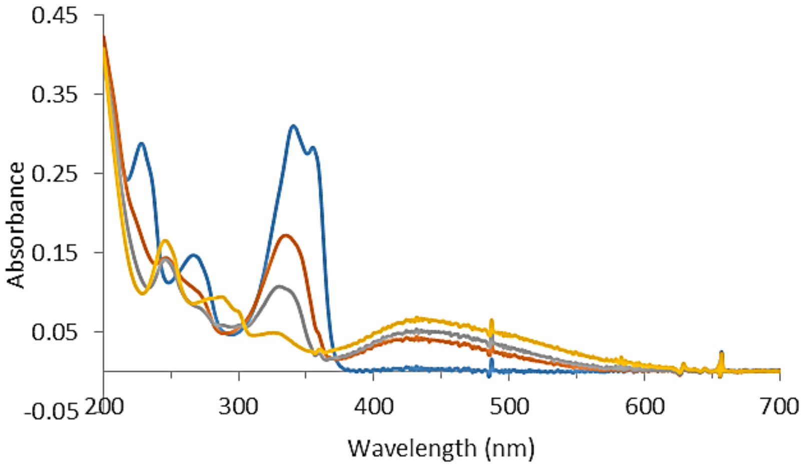

FIGURE 56: UV–Vis spectra of side products to $[Si(5dmbpy)_3]^{+4}$ generated electrochemically at -0.445 V (blue line), -0.745 V (red line), -0.945 V (gray line), and -1.145 V (yellow line) vs Fc/Fc$^+$ without proper degassing.

For the ttpy complex, a long–tailed broad peak initially appeared centered at 544 nm which then shifted and stayed centered at 485 nm, and the initial overlapping 378/407 nm peaks disappeared (FIGURE 57).

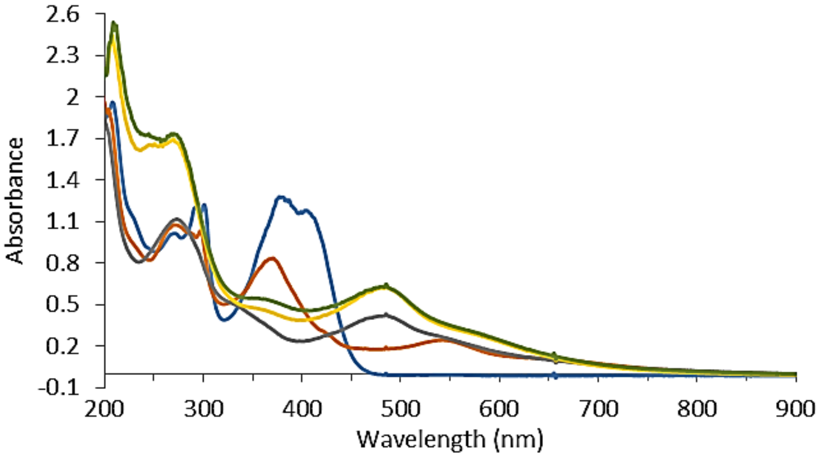

FIGURE 57: UV–Vis spectra of side products to $[Si(ttpy)_2]^{+4}$ generated electrochemically at -0.245 V (blue line), -0.520 V (red line), -0.945 V (gray line), -1.370 V (yellow line), and -1.695 V (green line) vs Fc/Fc^+ without proper degassing.

APPENDIX D: NMR SPECTRA OF HOMOLEPTIC POLYPYRIDINE SILICON(IV) COMPLEXES

This appendix contains all of the NMR spectra (^1H, $^{13}C\{^1H\}$, and ^{29}Si) of the complexes prepared in Chapter 3. Spectra of the iodide salts of each complex were measured in D_2O and spectra of the hexafluorophosphate salts were measured in CD_3CN. Often minor impurity peaks of water (in CD_3CN), acetone, methanol, THF, or ether can be observed in the NMR from incomplete drying of the solids.

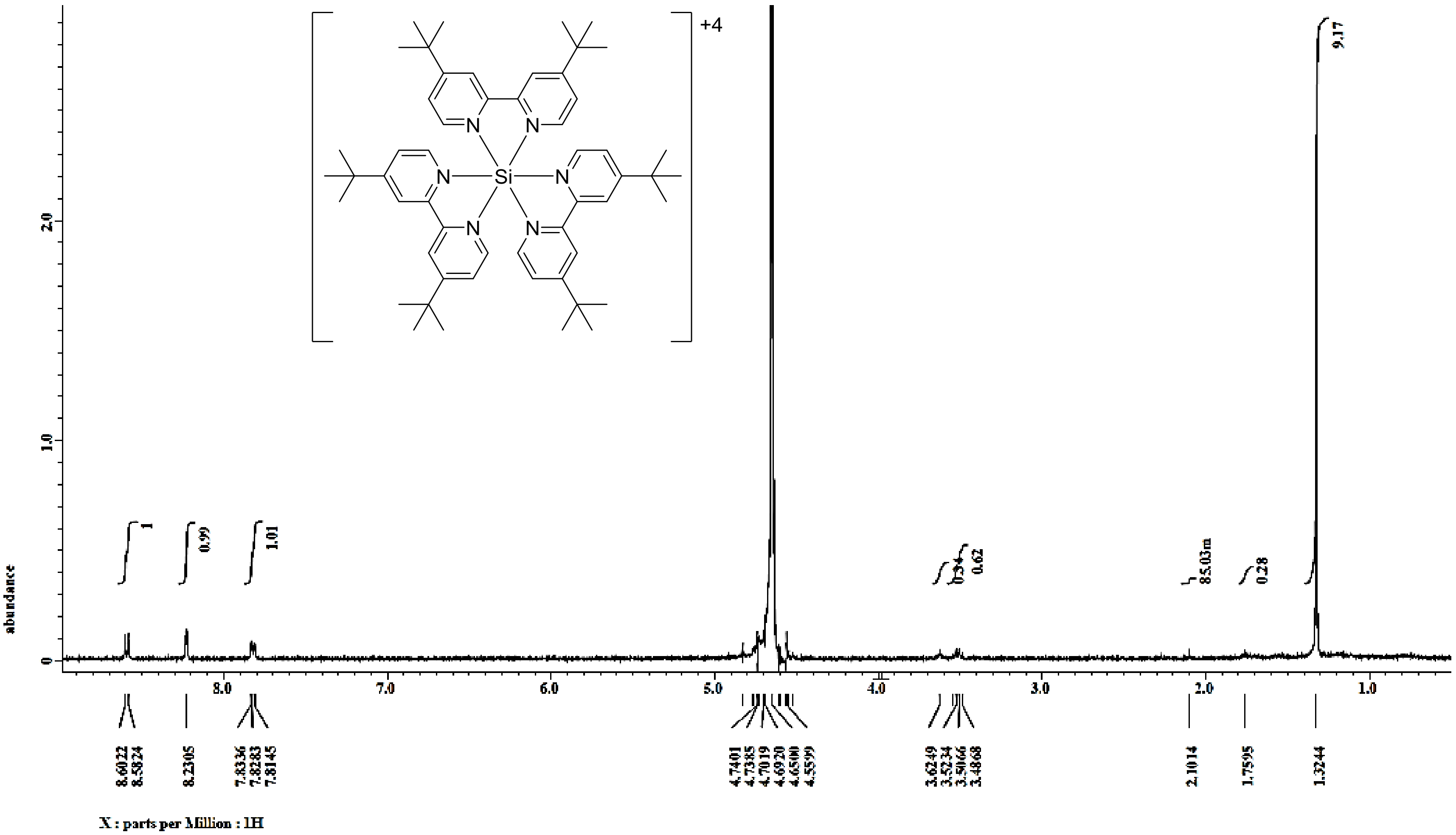

FIGURE 58: ^{1}H NMR spectrum of $[Si(4dtbbpy)_3]I_4$ in D_2O.

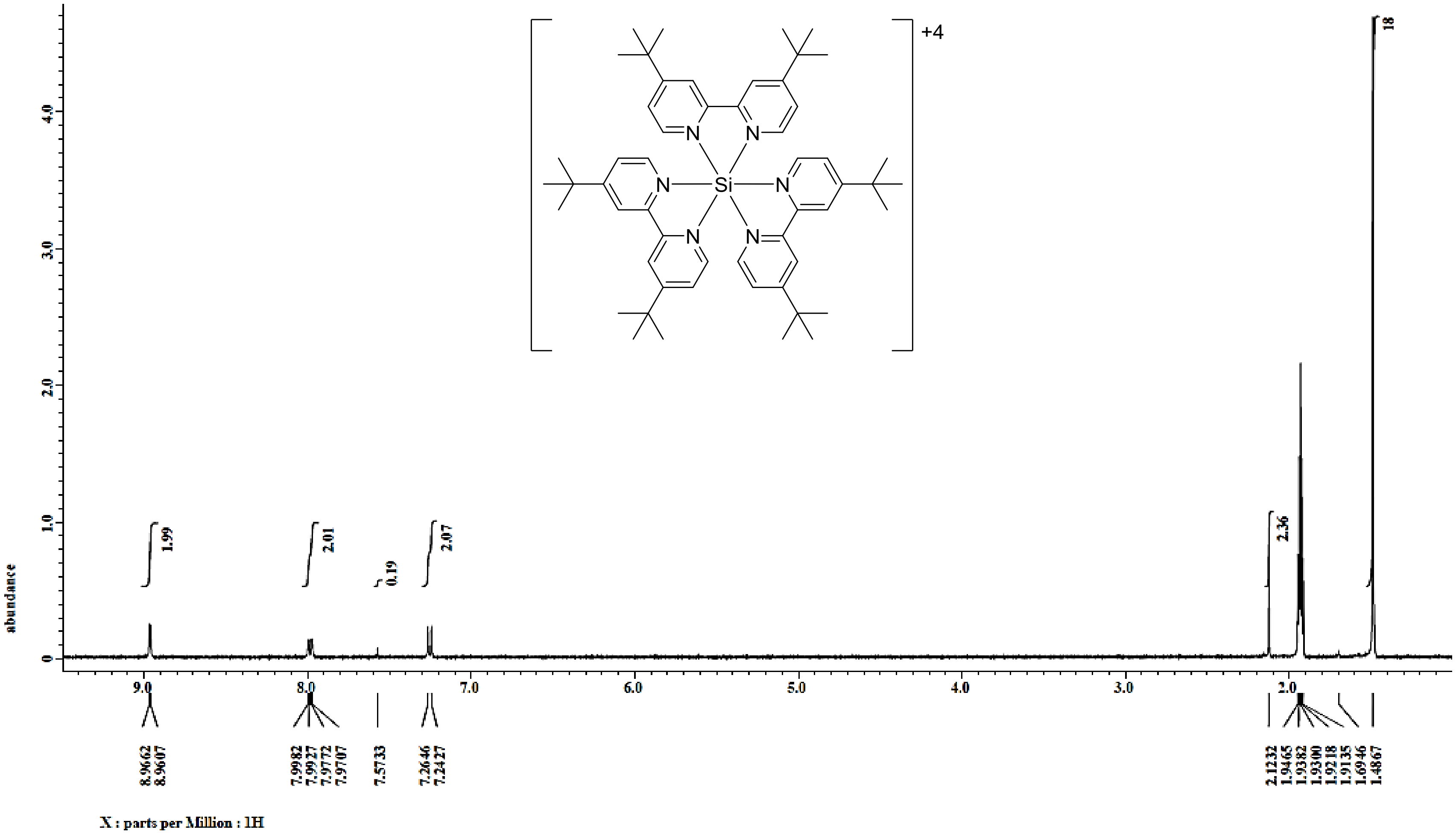

FIGURE 59: ^{1}H NMR spectrum of $[Si(4dtbbpy)_3](PF_6)_4$ in CD_3CN.

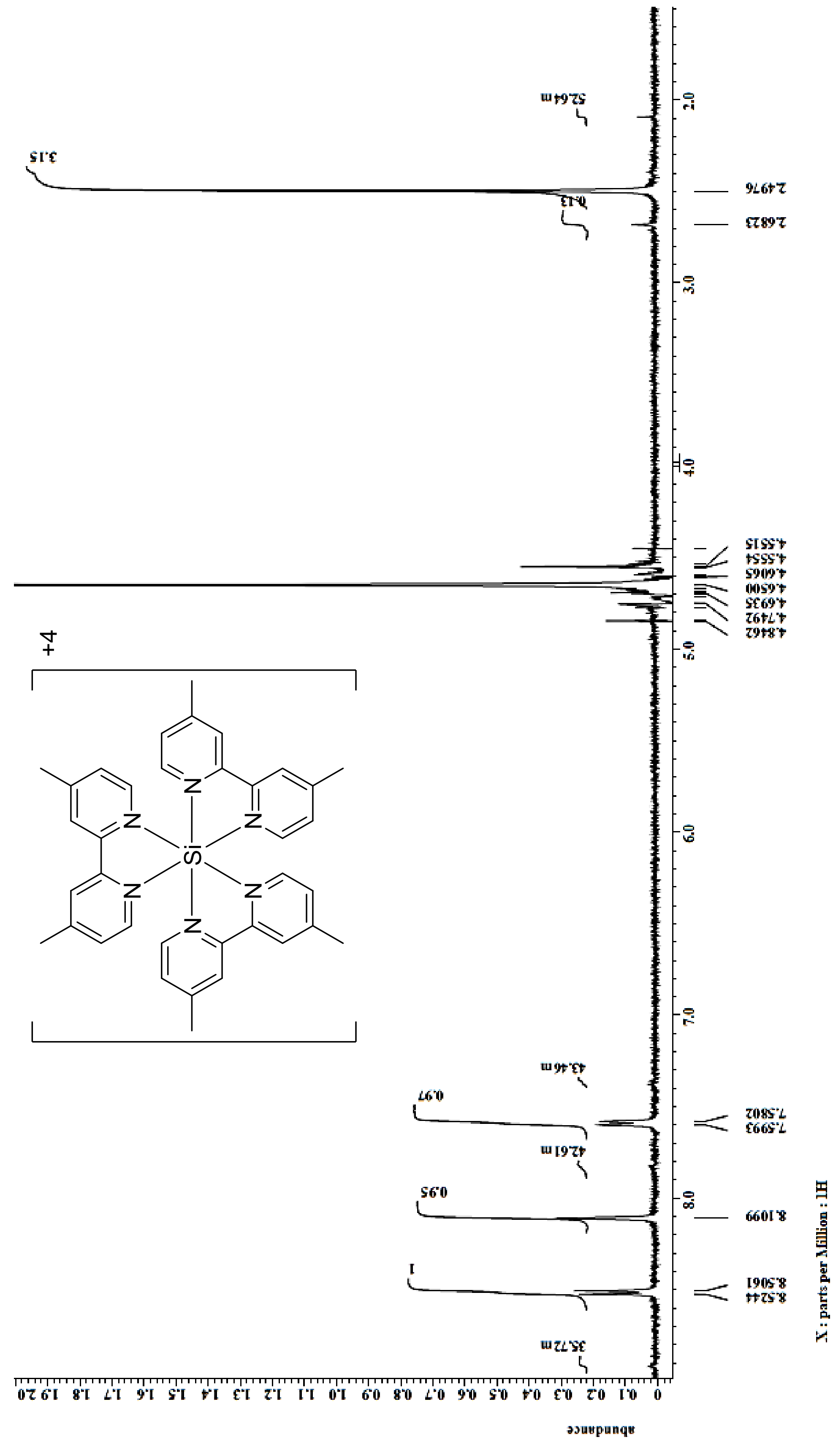

FIGURE 60: ^{1}H NMR spectrum of $[Si(4dmbpy)_3]I_4$ in D_2O.

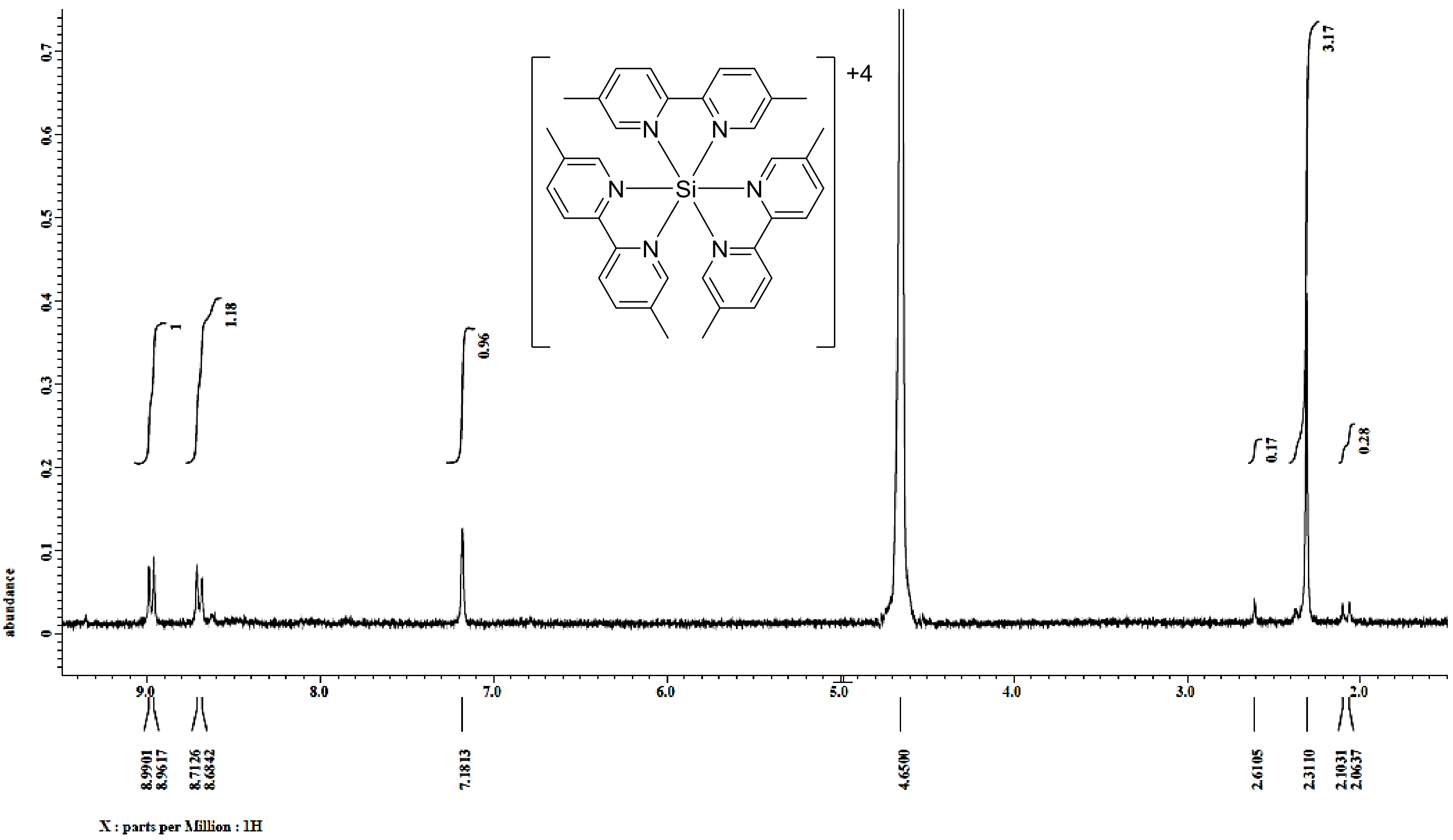

FIGURE 61: ^{1}H NMR spectrum of $[Si(5dmbpy)_3]I_4$ in D_2O.

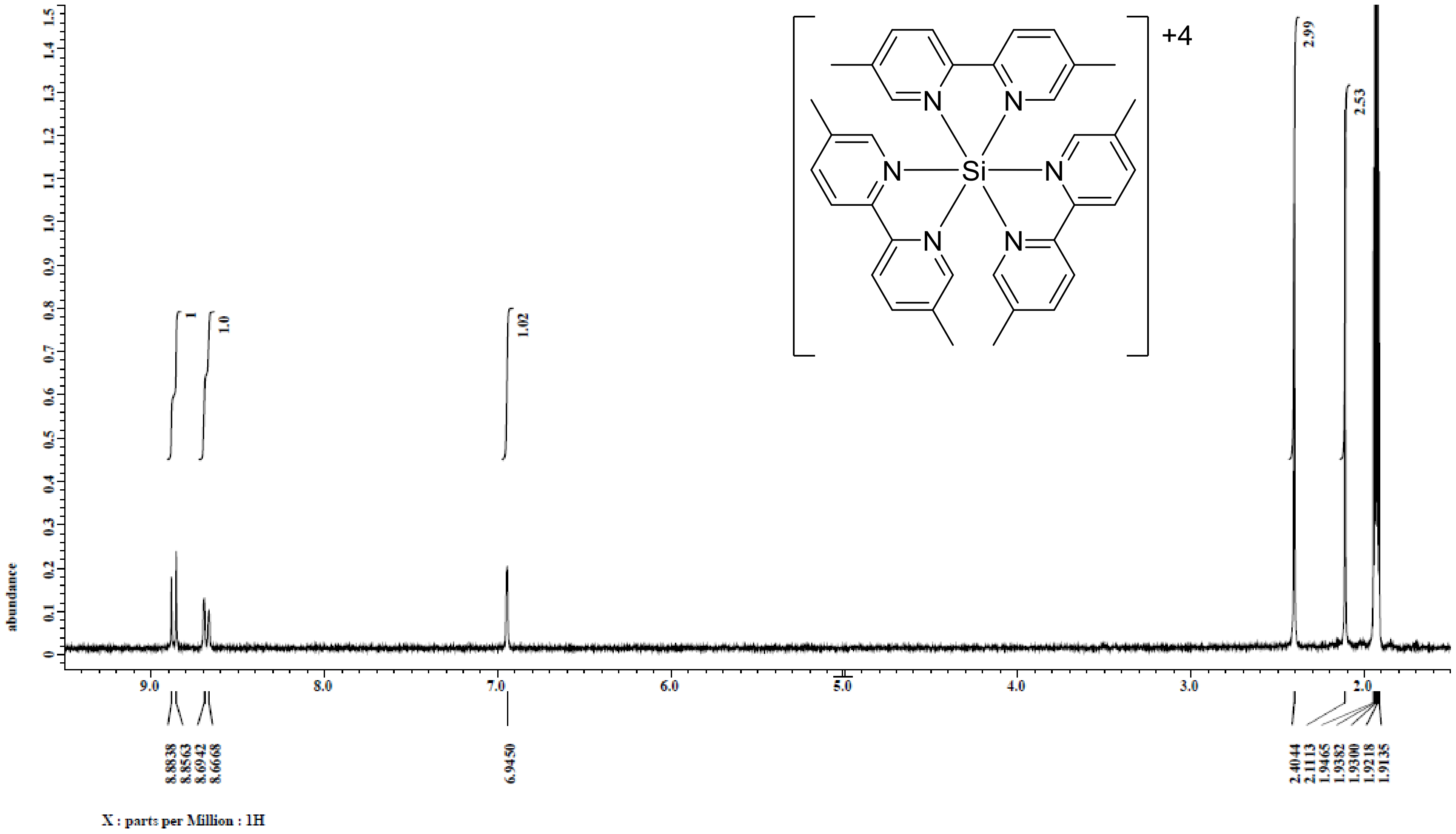

FIGURE 62: ^{1}H NMR spectrum of $[Si(5dmbpy)_3](PF_6)_4$ in CD_3CN.

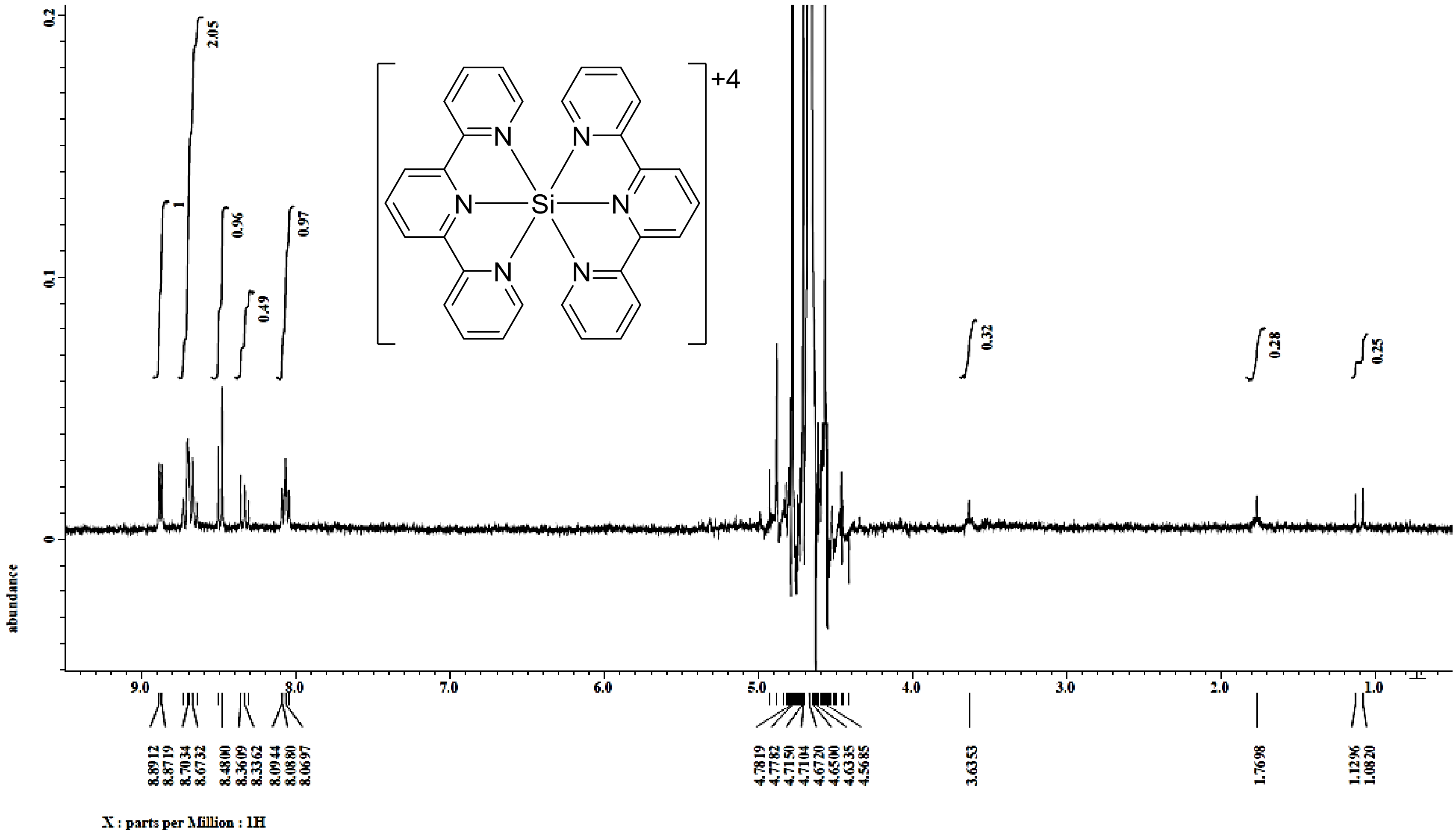

FIGURE 63: ^{1}H NMR spectrum of $[Si(tpy)_2]I_4$ in D_2O.

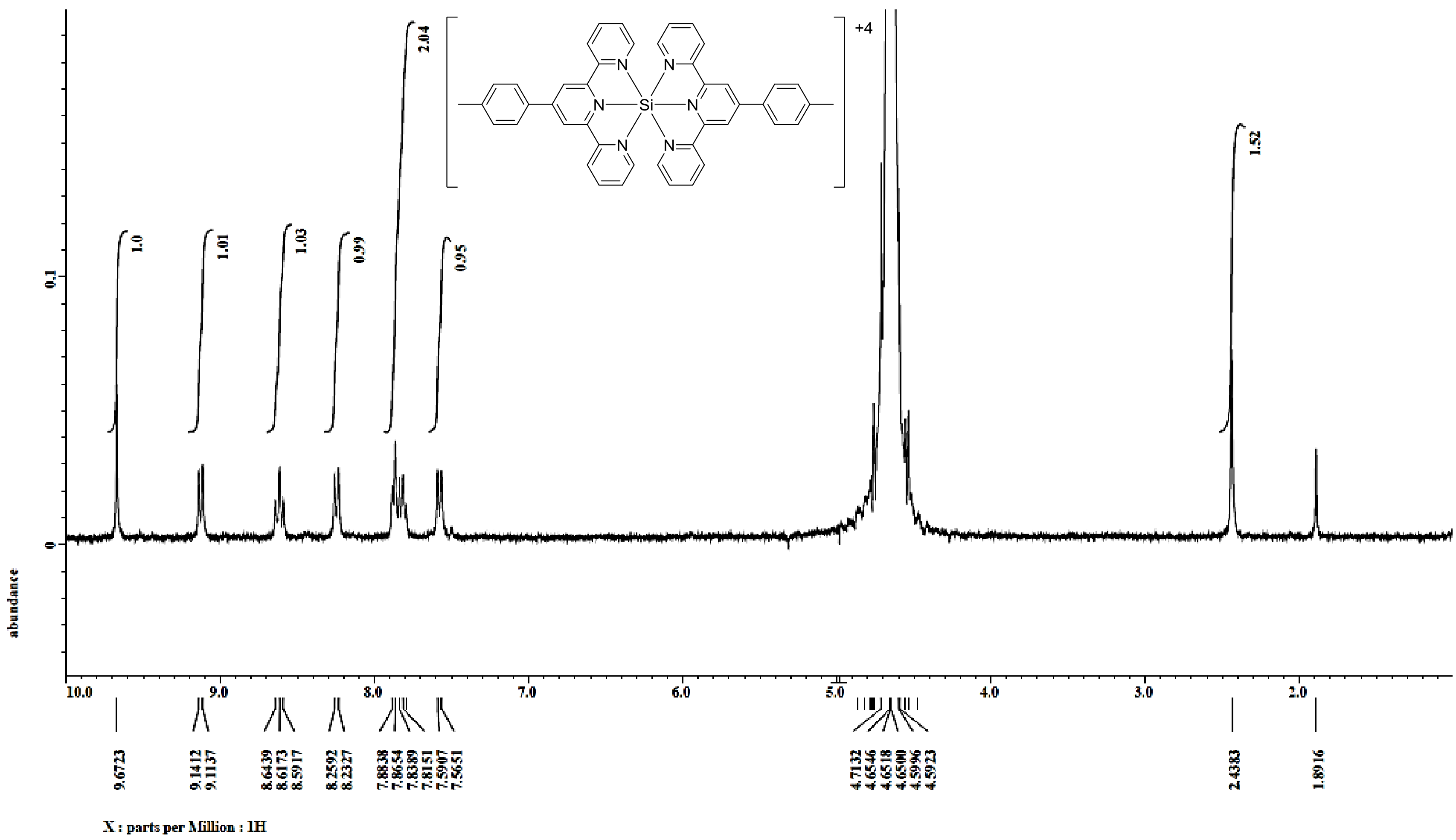

FIGURE 64: ^{1}H NMR spectrum of $[Si(ttpy)_2]I_4$ in D_2O.

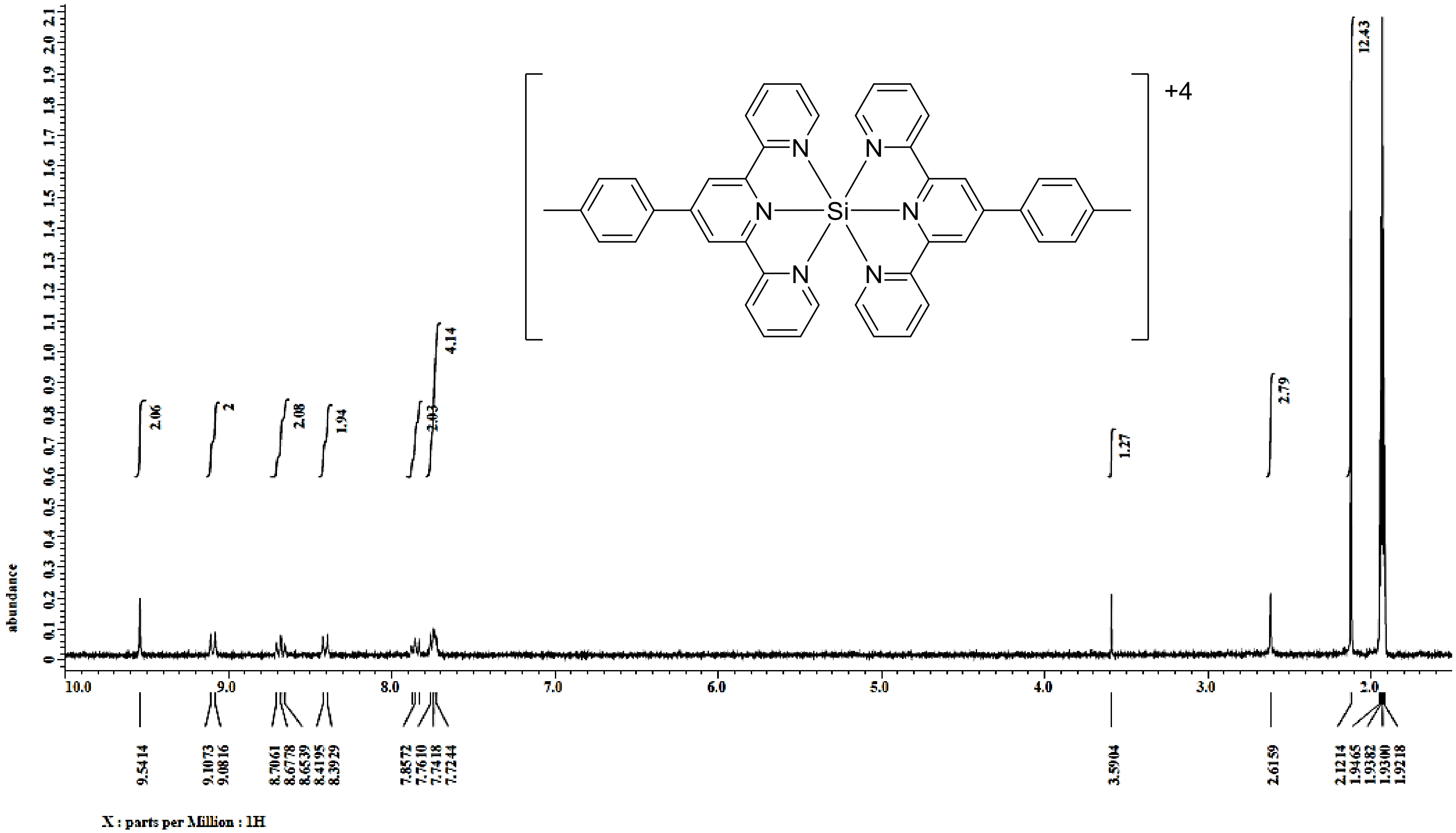

FIGURE 65: ^{1}H NMR spectrum of $[Si(ttpy)_2](PF_6)_4$ in CD_3CN.

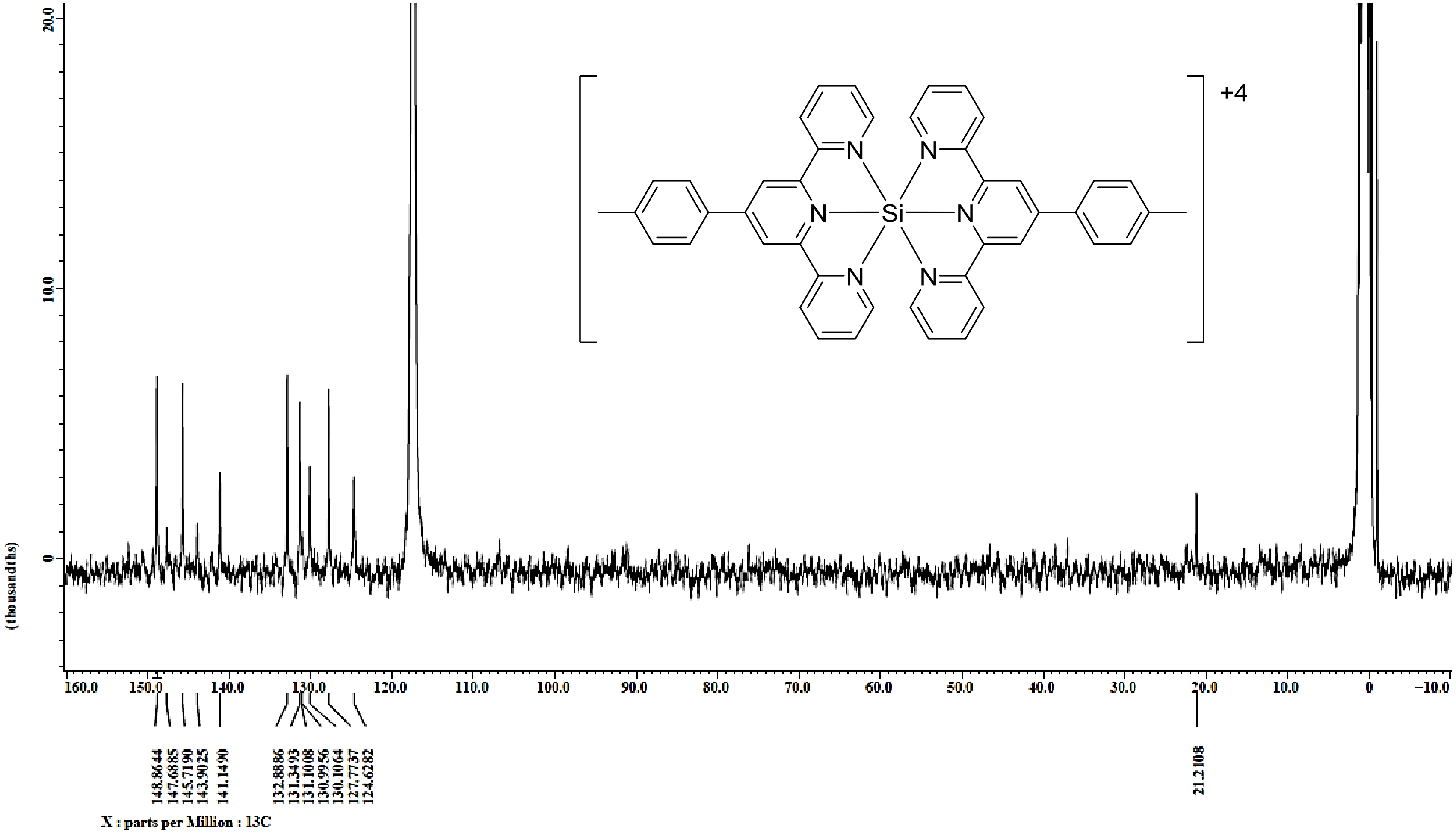

FIGURE 66: $^{13}C\{^1H\}$ NMR spectrum of $[Si(ttpy)_2](PF_6)_4$ in CD_3CN.

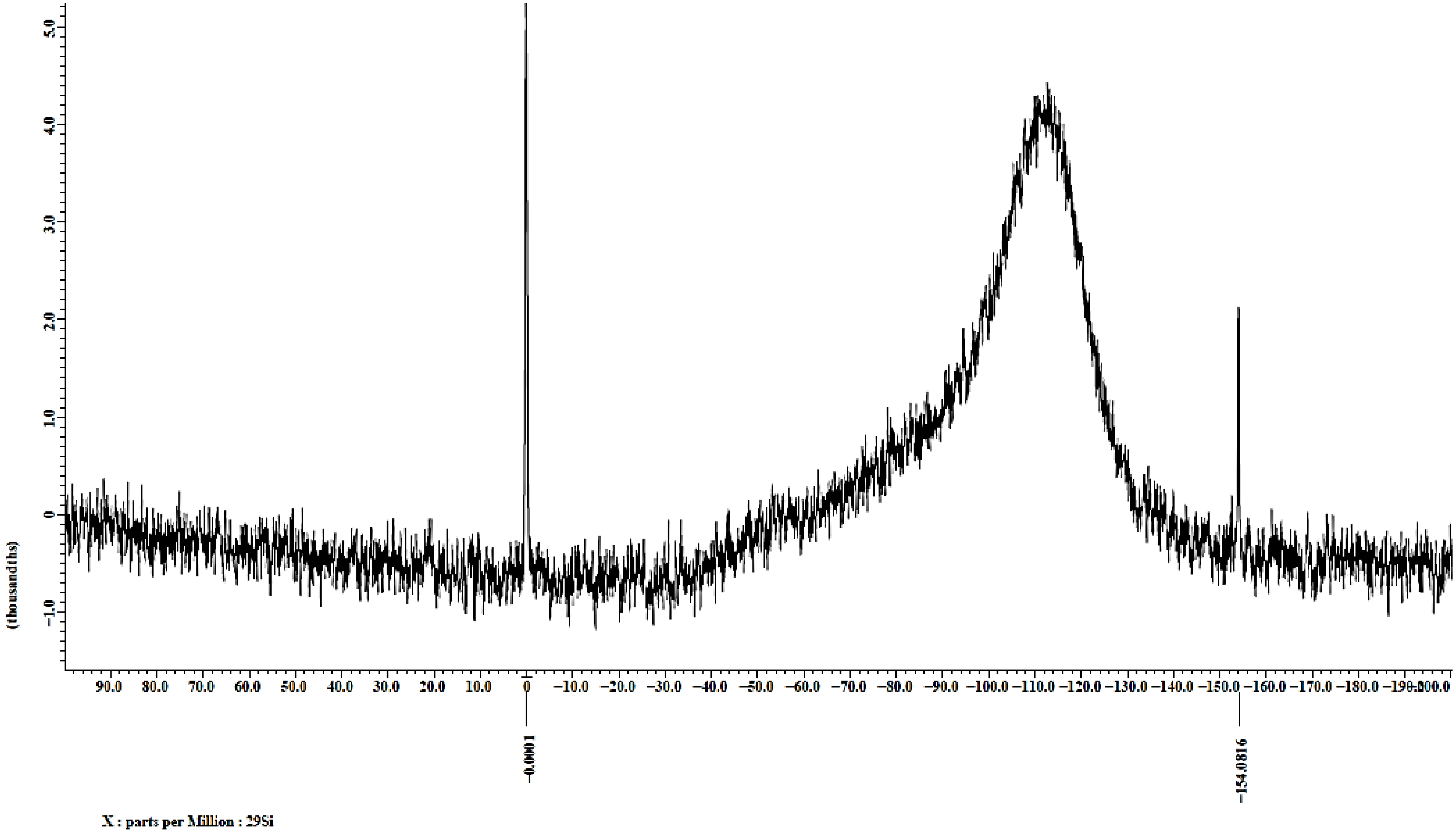

FIGURE 67: ^{29}Si NMR spectrum of [Si(ttpy)$_2$](PF$_6$)$_4$ with 0.05 M Cr(acac)$_3$ as a relaxation agent and tetramethylsilane as a standard in CD$_3$CN.

APPENDIX E: ^{1}H NMR SPECTRA FOR POLYMERIZABLE SILICON COMPLEXES

This appendix provides the ^{1}H NMR spectra in CD_3OD of the diiodo bis–bipyridine silicon complexes using bpy, 4dmbpy, and 4dtbbpy and the crude ^{1}H NMR spectra of the reaction products between $[Si(bpy)_2I_2]I_2$ and both Br_2bpy and 5dvbpy.

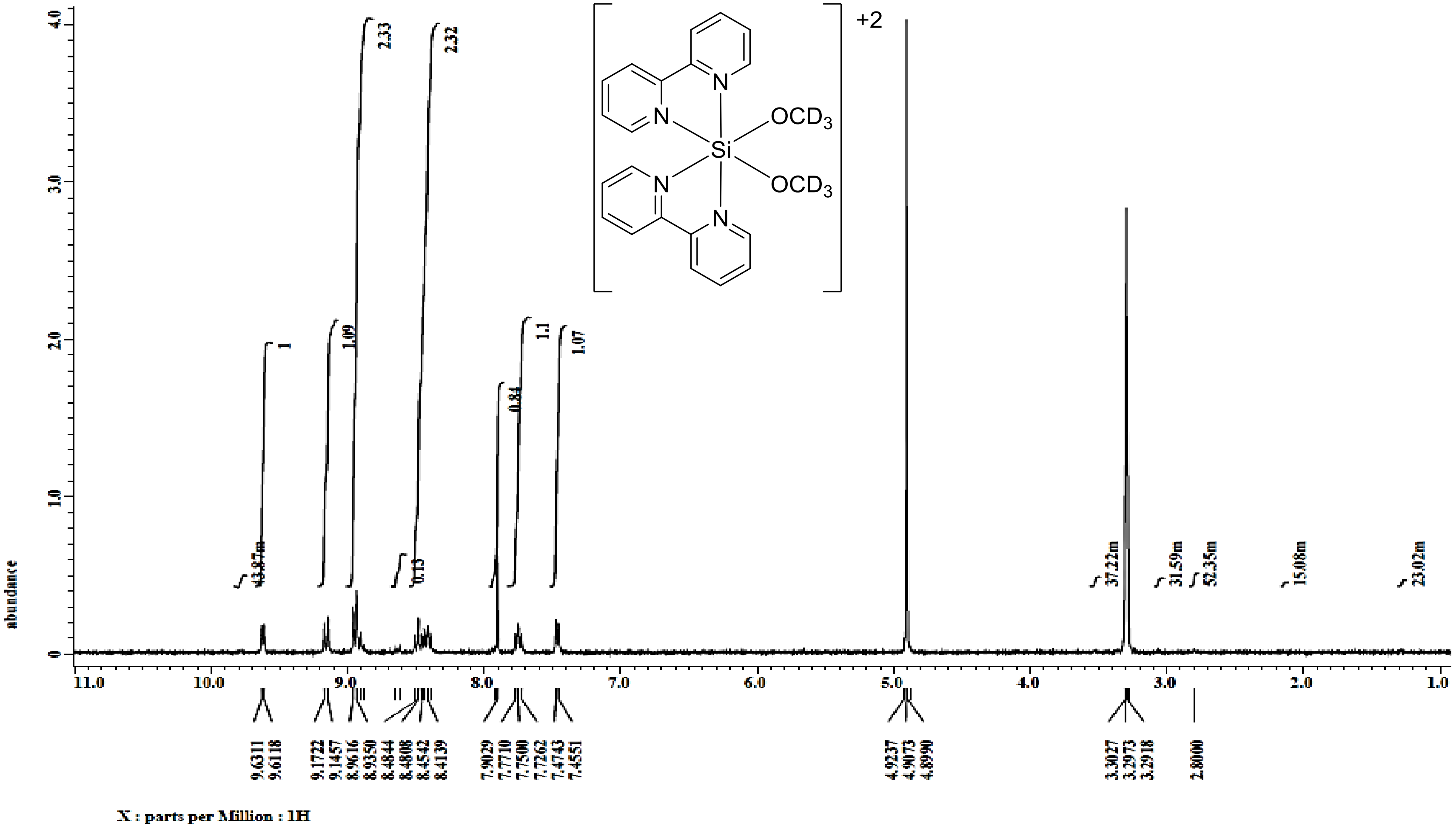

FIGURE 68: ^{1}H NMR spectrum of $[Si(bpy)_2I_2]I_2$ after reaction in CD_3OD.

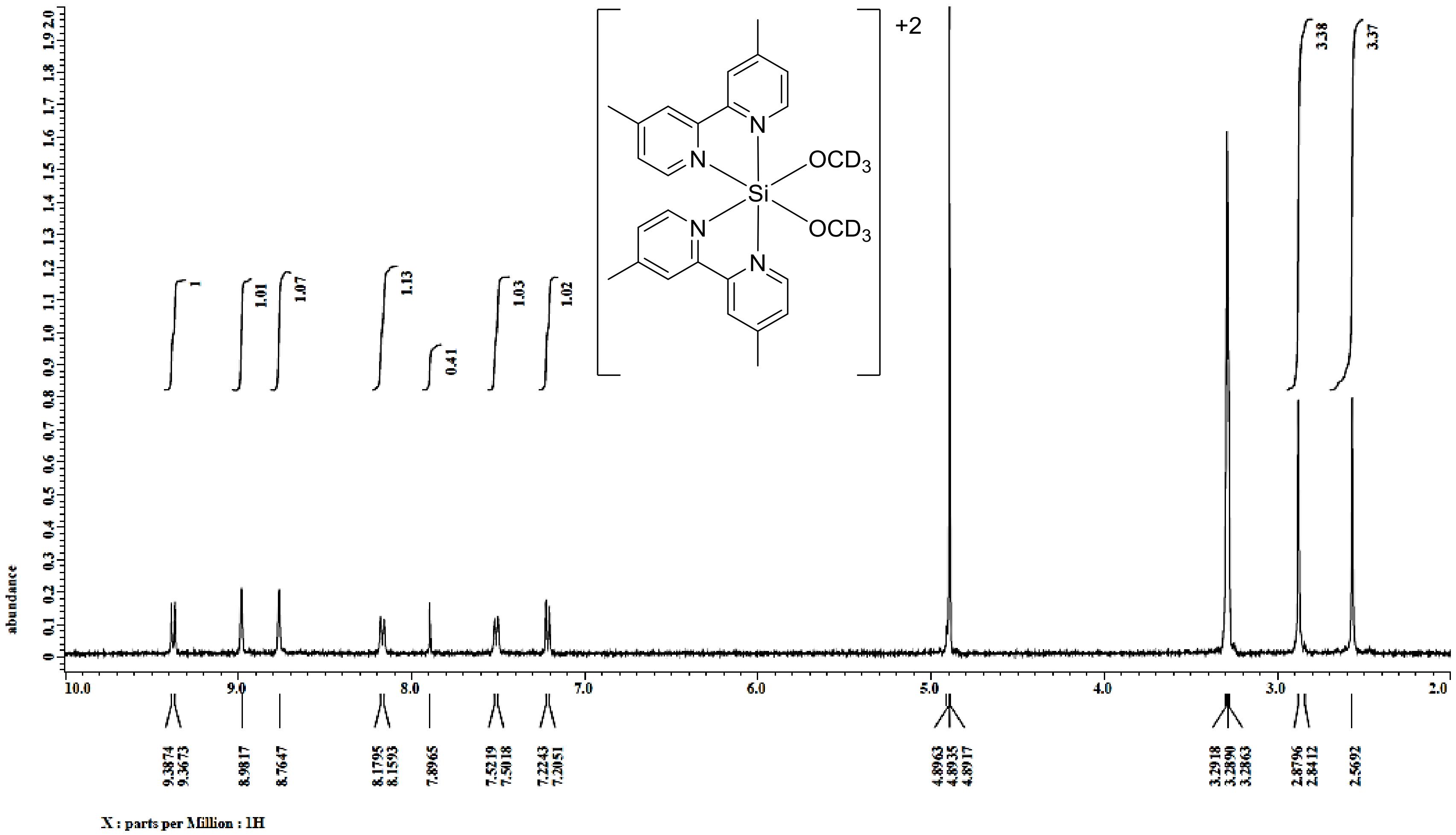

FIGURE 69: ^{1}H NMR spectrum of $[Si(4dmbpy)_2I_2]I_2$ after reaction in CD_3OD.

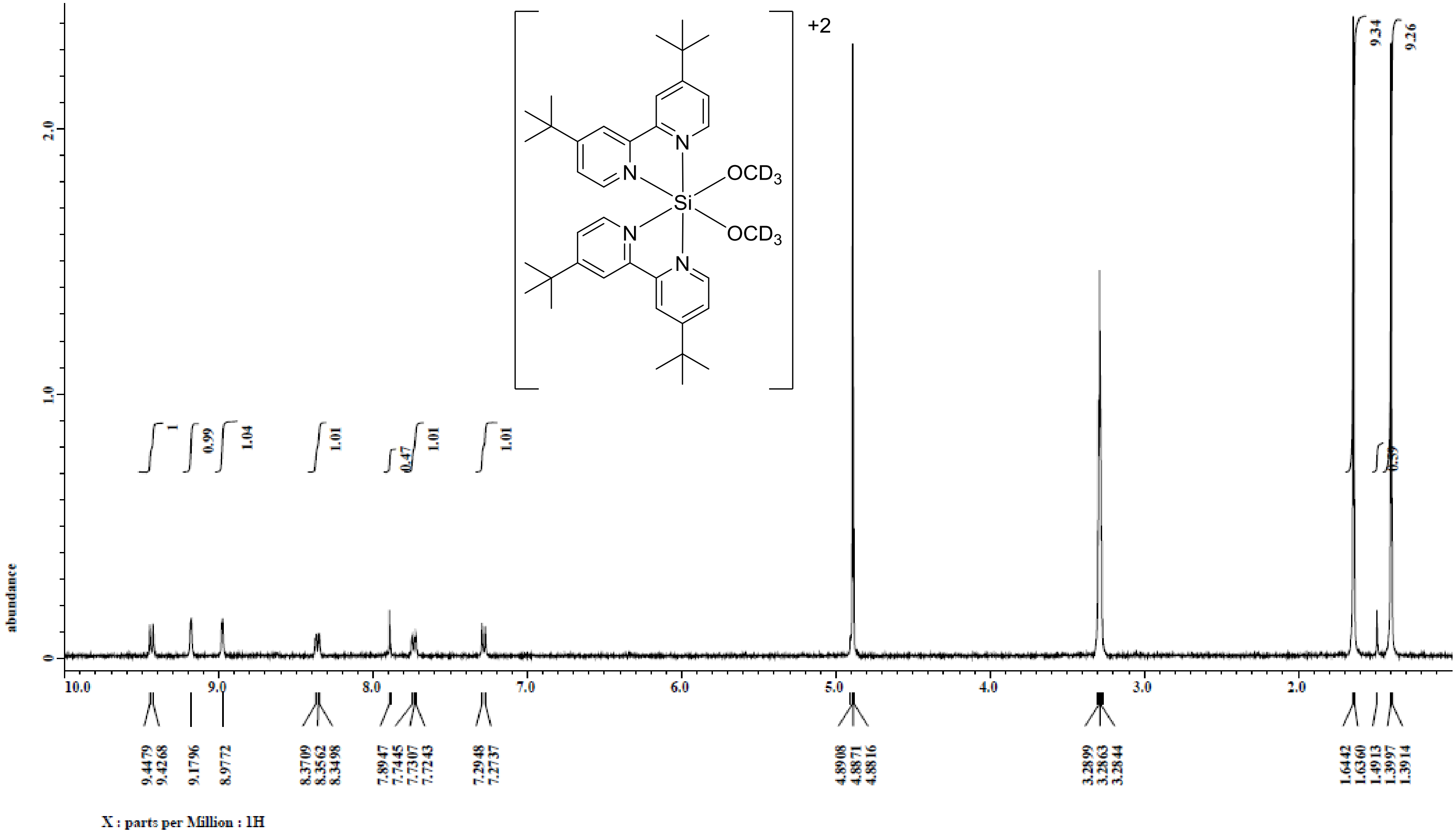

FIGURE 70: ^{1}H NMR spectrum of [Si(4dtbbpy)$_2$I$_2$]I$_2$ after reaction in CD$_3$OD.

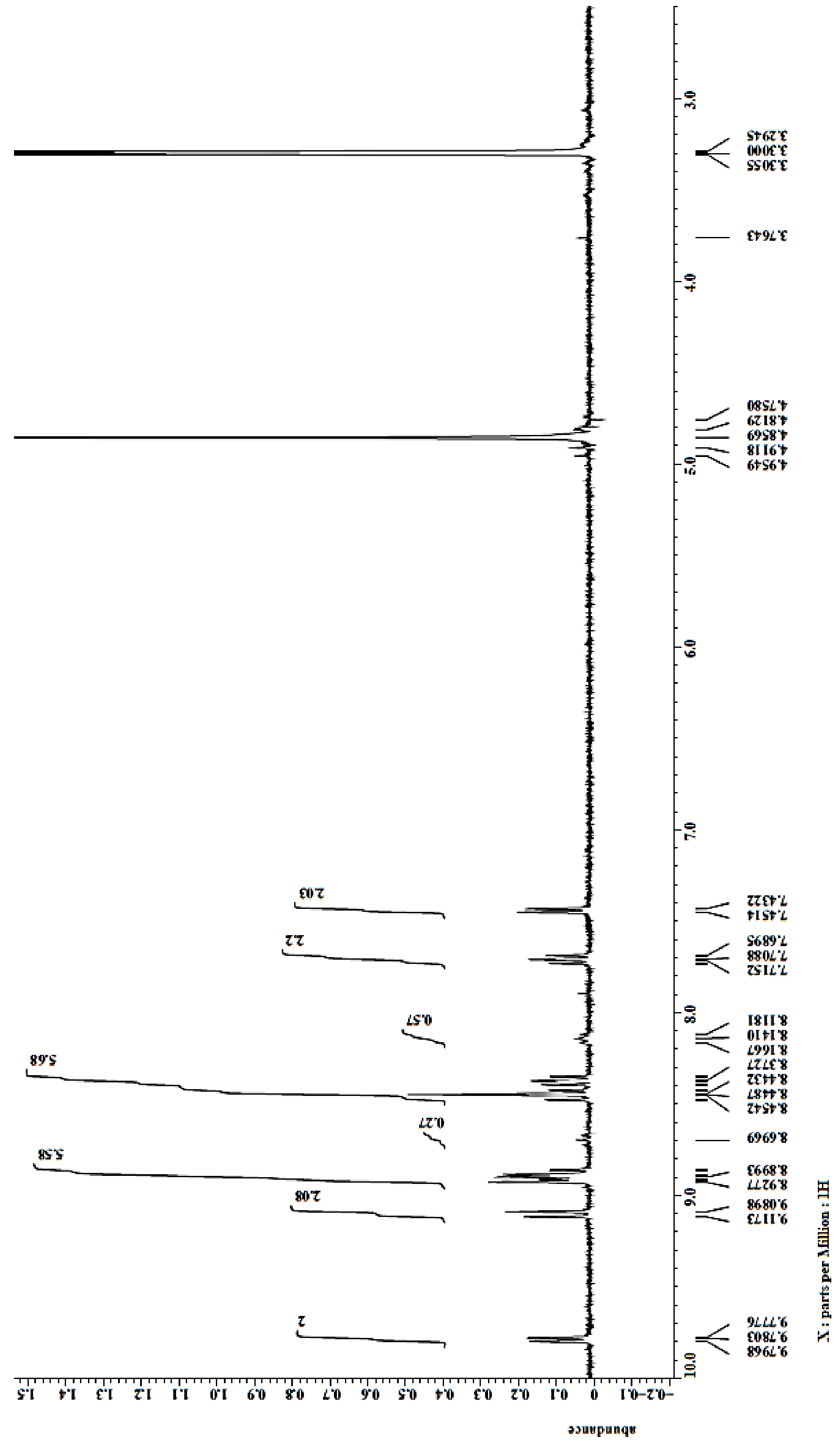

FIGURE 71: ^{1}H NMR spectrum of reaction product between $[Si(bpy)_2I_2]I_2$ and Br_2bpy in CD_3OD.

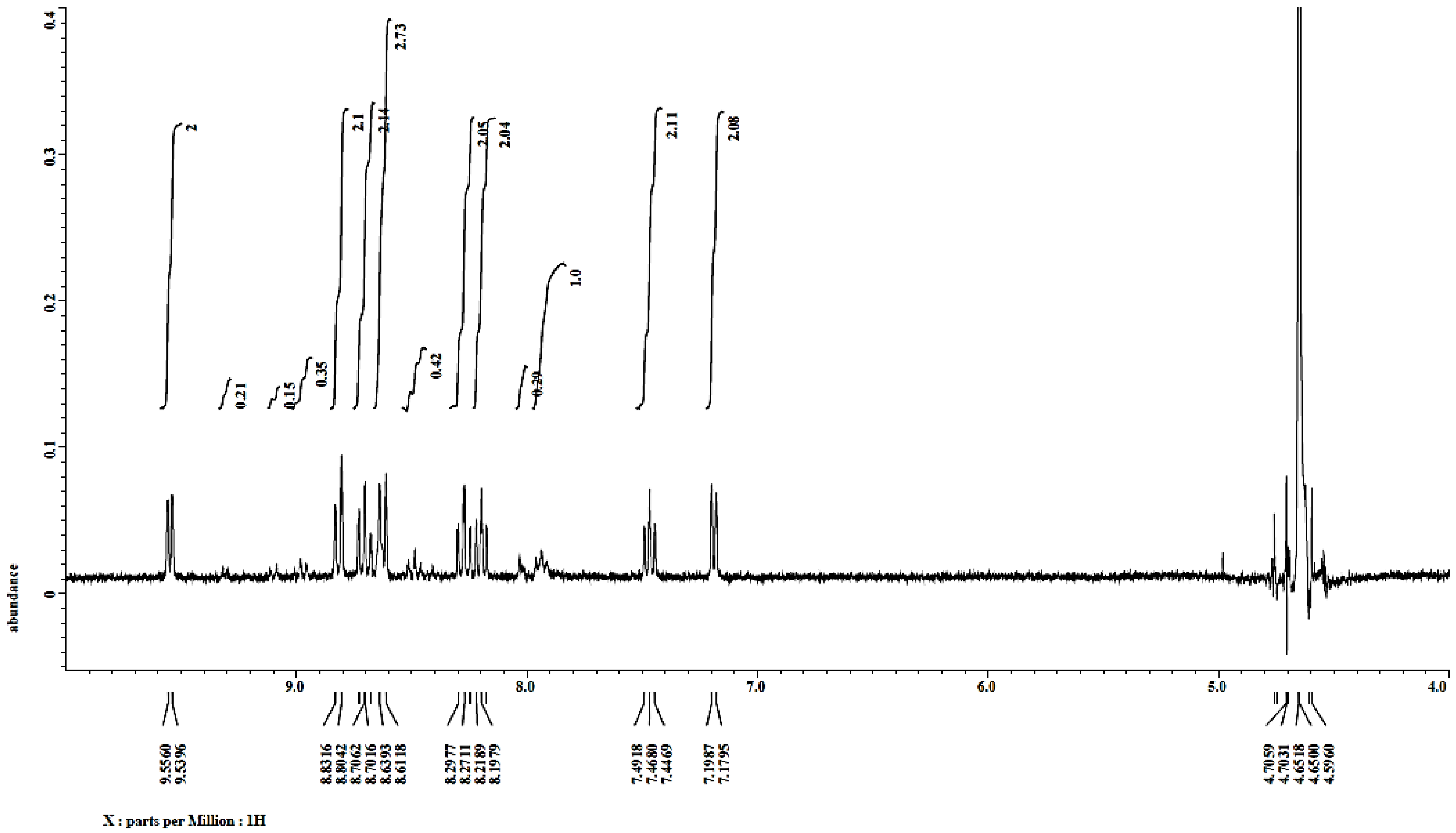

FIGURE 72: ^{1}H NMR spectra of reaction product between $[Si(bpy)_2I_2]I_2$ and 5dvbpy in D_2O.